ITUPublications
Recommendations

International Telecommunication Union
Radiocommunication Sector

Recommendation ITU-R P.372-17

(08/2024)

P Series: Radiowave propagation

Radio noise

Foreword

The role of the Radiocommunication Sector is to ensure the rational, equitable, efficient and economical use of the radio-frequency spectrum by all radiocommunication services, including satellite services, and carry out studies without limit of frequency range on the basis of which Recommendations are adopted.

The regulatory and policy functions of the Radiocommunication Sector are performed by World and Regional Radiocommunication Conferences and Radiocommunication Assemblies supported by Study Groups.

Policy on Intellectual Property Right (IPR)

ITU-R policy on IPR is described in the Common Patent Policy for ITU-T/ITU-R/ISO/IEC referenced in Resolution ITU-R 1. Forms to be used for the submission of patent statements and licensing declarations by patent holders are available from http://www.itu.int/ITU-R/go/patents/en where the Guidelines for Implementation of the Common Patent Policy for ITU-T/ITU-R/ISO/IEC and the ITU-R patent information database can also be found.

Series of ITU-R Recommendations

(Also available online at https://www.itu.int/publ/R-REC/en)

Series	Title
BO	Satellite delivery
BR	Recording for production, archival and play-out; film for television
BS	Broadcasting service (sound)
BT	Broadcasting service (television)
F	Fixed service
M	Mobile, radiodetermination, amateur and related satellite services
P	**Radiowave propagation**
RA	Radio astronomy
RS	Remote sensing systems
S	Fixed-satellite service
SA	Space applications and meteorology
SF	Frequency sharing and coordination between fixed-satellite and fixed service systems
SM	Spectrum management
SNG	Satellite news gathering
TF	Time signals and frequency standards emissions
V	Vocabulary and related subjects

Note: *This ITU-R Recommendation was approved in English under the procedure detailed in Resolution ITU-R 1.*

Electronic Publication
Geneva, 2024

RECOMMENDATION ITU-R P.372-17

Radio noise*

(Question ITU-R 214/3)

(1951-1953-1956-1959-1963-1974-1978-1982-1986-1990-1994-2001-2003-2007-2009-2013-2015-2016-2019-2021-2022-2024)

Scope

Recommendation ITU-R P.372 provides information on the background levels of radio noise[1] in the frequency range from 0.1 Hz to 100 GHz. It takes account of noise emitted by lightning, atmospheric gases, clouds, rain, the Earth's surface, the galaxy, and man-made sources. Noise figures or temperatures are given to provide a basis for the estimation of system performance.

Keywords

Radio noise, noise factor, noise temperature, sky brightness temperature

Abbreviations/Glossary

Amsl	Above mean sea level
IDWM	ITU Digitized World Map
LoS	Line-of-sight

The ITU Radiocommunication Assembly,

considering

a) that radio noise sets a limit to the performance of radio systems;

b) that the effective antenna noise figure, or antenna noise temperature, together with the amplitude probability distribution of the received noise envelope, are suitable parameters (almost always necessary, but sometimes not sufficient) for use in system performance analysis and design;

c) that knowledge of radio emission from natural sources is required in:

– evaluation of the effects of the atmosphere on radiowaves;

– allocation of frequencies to remote sensing of the Earth's environment;

d) that radio noise from man-made sources is significant in setting the limit for some radio applications;

e) methods for measurements of radio noise are given in Recommendation ITU-R SM.1753;

f) methods for indoor noise environment measurements are given in Recommendation ITU-R SM.2093,

recommends

that the following information on the background levels of external radio noise should be used where appropriate in radio system design and analysis:

---

* A supplemental computer program associated with the calculation of atmospheric noise due to lightning, man-made noise, and galactic noise (at frequencies below about 100 MHz), described in this Recommendation, is available at: https://github.com/ITU-R-Study-Group-3/ITU-R-HF/releases/tag/v14.3

1 The terms 'radio noise', 'radio-frequency noise' and 'RF noise' are synonymous.

TABLE OF CONTENTS

Page

PART 1

General

1.1 Sources of radio noise

Radio noise is defined as follows:

radio noise;

A time-varying electromagnetic phenomenon having components in the radio-frequency range, apparently not conveying information and which may be superimposed on, or combined with, a wanted signal.

NOTE 1 – In certain cases a radio-frequency noise may convey information on some characteristics of its source, for example its nature and location.

NOTE 2 – An aggregate of signals may appear as radio-frequency noise, when they are not separately identifiable.

This Recommendation provides data on radiated radio noise emanating from sources external to the radio receiving system and received through the reference antenna which derives from the following causes:

– natural noise:
  - emissions from atmospheric gases and hydrometeors;
  - the Earth's surface; e.g. emissivity of land, ocean, and other obstructions within the antenna beam;
  - radiation from celestial radio sources;
  - radiation from lightning and other static electrical discharges (atmospheric noise);
– man-made noise:
  - particularly for outdoor antennas, aggregated unintended radiation from electrical machinery, electrical and electronic equipment and networks, power transmission lines, powerline communication, wireless power transfer, industrial, scientific, and medical (ISM) equipment, or from internal combustion engine ignition, as well as electromagnetic radiation from imperfectly shielded enclosures, transmission lines, and cables;
  - indoors or for antennas near to obstructions, aggregated unintended radiation, as above, to the extent possible, but also including typical radiation levels from individual or small numbers of sources, in defined typical environments.

NOTE 3 – The estimates of radio noise levels given here do not include signals associated with radio services that are also present. Spurious emissions from individual transmitting or receiving systems may be part of the accumulated noise level received.

NOTE 4 – This Recommendation provides information only on radio noise which reaches the receiver through the antenna and the feeder cable or waveguide. It does not include noise which may reach the receiver through other conducting cables or structures, nor noise which may be received due to inadequate screening or balance of the feeder cable and the connections, etc.

NOTE 5 – In the case of man-made noise, the data provided are intended to be representative of the environmental category, with typical levels of electrical and electronic activity operating normally, at typical distances for that environment.

1.2 Terms for the specification of noise intensity and their interrelationship

The noise for a receiving system is composed of a number of noise sources at the receiving terminal of the system. Both external noise and the internal noise generated within the receiver must be considered. The only appropriate reference point for the overall operating noise for a radio receiving system is the input of an equivalent loss-free receiving antenna. (The terminals of this lossless antenna do not exist physically.)

This noise may be expressed as a noise factor, *f*, relative to thermal noise, as an effective noise temperature, or as an electric field strength.

1.2.1 Noise factor

For receivers free from spurious responses, the system noise factor is given by:

$$f = f_a + (f_c - 1) + l_c\,(f_t - 1) + l_c\,l_t\,(f_r - 1) \tag{1}$$

where:

f_a: the external noise factor defined as:

$$f_a = \frac{p_n}{k\,T_0\,b} \tag{2}$$

NOTE 1 – F_a is the external noise figure defined as:

$$F_a = 10 \log f_a \quad \text{dB}$$

p_n: available noise power from an equivalent lossless antenna

k: Boltzmann's constant = 1.38×10^{-23} J/K

T_0: reference temperature (K) taken as 290 K

b: noise power bandwidth of the receiving system (Hz)

l_c: antenna circuit loss (available input power/available output power)

l_t: transmission line loss (available input power/available output power)

f_r: internal noise factor of the receiver.

NOTE 2 – F_r is the receiver noise figure defined as:

$$F_r = 10 \log f_r \quad \text{dB}$$

f_c is the noise factor associated with the antenna circuit losses,

$$f_c = 1 + (l_c - 1)\left(\frac{T_c}{T_0}\right) \tag{3}$$

f_t is the noise factor associated with the transmission line losses,

$$f_t = 1 + (l_t - 1)\left(\frac{T_t}{T_0}\right) \tag{4}$$

where:

T_c: actual temperature (K) of the antenna and nearby ground

and

T_t: actual temperature (K) of the transmission line.

If $T_c = T_t = T_0$, equation (1) becomes

$$f = f_a - 1 + f_c\,f_t\,f_r \tag{5}$$

Equation (2) can be written:

$$P_n = F_a + B - 204 \qquad \text{dBW} \tag{6}$$

where:

P_n = 10 log p_n: available power (W)

B = 10 log b, and $-204 = 10 \log k T_0$.

1.2.2 r.m.s noise field strength

From estimates of F_a the corresponding values of E_n may be determined using equations such as (7) and (8) appropriate to the type of antenna employed.

For a short ($h << \lambda$) vertical monopole above a perfectly conducting ground plane, the vertical component of the r.m.s. field strength is given by:

$$E_n = F_a + 20 \log f_{\text{MHz}} + B - 95.5 \qquad \text{dB}(\mu\text{V/m}) \tag{7}$$

where:

E_n: field strength in bandwidth b, and

f_{MHz}: centre frequency (MHz).

Similarly for a reference isotropic antenna in free space:

$$E_n = F_a + 20 \log f_{\text{MHz}} + B - 96.8 \qquad \text{dB}(\mu\text{V/m}) \tag{8}$$

1.2.3 Noise temperature

The external noise factor is also commonly expressed as a temperature, T_a, where, by definition of f_a:

$$f_a = \frac{T_a}{T_0} \tag{9}$$

T_a is the effective antenna temperature due to external noise.

1.2.4 Noise variability

The noise power, while needed in determining the signal-to-noise ratio, for example, is seldom sufficient to determine system performance (white Gaussian background noise being the only exception). Appropriate probabilistic descriptions of the received random noise waveform are required. Since for the types of noise of concern in this Recommendation, the phase of the received envelope is usually uniformly distributed, the amplitude probability distribution (APD) (exceedance probability) of the received envelope is specified.

For impulsive noise processes at the higher frequencies (i.e. > about 1 GHz), F_a values are quite low and only the higher magnitude pulses appear above the receiver's noise threshold. Impulsive noise can be described by its peak value for a given time period, exceedance probabilities at these higher levels, and the pulse count at a specified level.

PART 2

Noise levels as a function of frequency

The following three Figures and related discussion specify the expected values of F_a in the frequency range 0.1 Hz to 100 GHz along with other noise levels of interest. The three Figures display the relative magnitude of the noise types specified in § 1. Additional details for the various noise types are given in later sections of this Recommendation.

Figure 1 covers the frequency range 0.1 Hz to 10 kHz. The solid curve is the minimum expected hourly median values of F_a based on measurements (taking into account the entire Earth's surface, all seasons and times of day) and the dashed curve gives the maximum expected values. Note that in this frequency range there is very little seasonal, diurnal, or geographic variation. The larger variability in the 100-10 000 Hz range is due to the variability of the Earth-ionosphere wave-guide cutoff.

FIGURE 1

F_a minimum and maximum versus frequency (10^{-1} to 10^4 Hz)

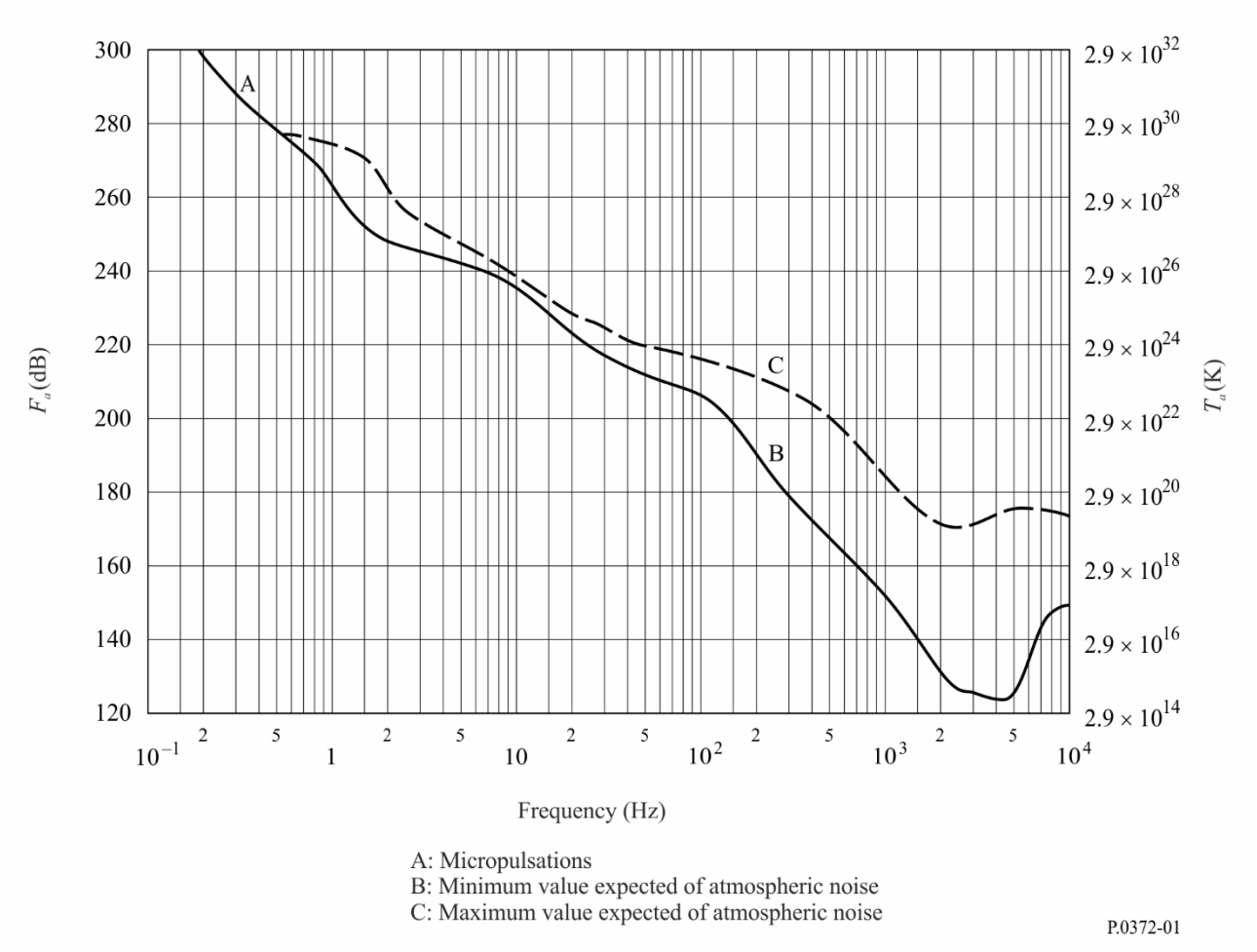

A: Micropulsations
B: Minimum value expected of atmospheric noise
C: Maximum value expected of atmospheric noise

P.0372-01

Figure 2 covers the frequency range 10^4 to 10^8 Hz, i.e. 10 kHz to 100 MHz, for various categories of noise. The minimum expected noise is shown by the solid curves. For atmospheric noise due to lightning, the minimum values of the hourly medians expected are taken to be those values exceeded 99.5% of the hours and the maximum values are those exceeded 0.5% of the hours. All times of day, seasons, and the entire Earth's surface have been taken into account.

FIGURE 2

F_a versus frequency (10^4 to 10^8 Hz)

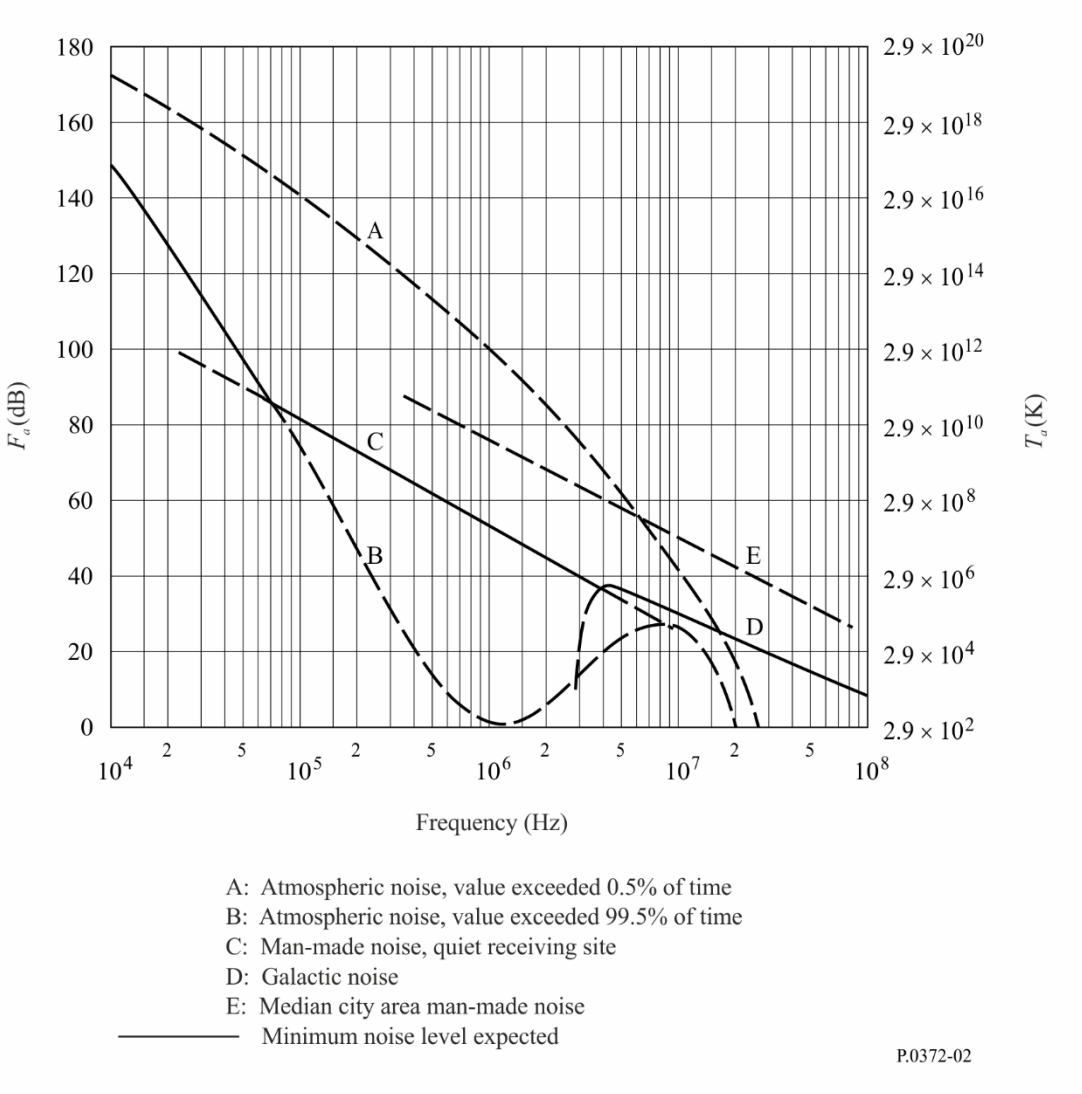

Figure 3 covers the frequency range 10^8 to 10^{11} Hz, i.e. 100 MHz to 100 GHz. Again the minimum noise is given by solid curves, while some other noise of interest are given by dashed curves.

The majority of the results shown in the three Figures are for omni-directional antennas (except as noted on the Figures). For directional antennas, however, studies have indicated that at HF (for example), for atmospheric noise from lightning for very narrow beam antennas, there can be as much as 10 dB variation (5 dB above to 5 dB below the average Fa value shown) depending on antenna pointing direction, frequency and geographical location.

For galactic noise, the average value (over the entire sky) is given by the solid curve labelled galactic noise (Figs 2 and 3). Measurements indicate a ±2 dB variation about this curve, neglecting

ionospheric shielding. The minimum galactic noise (narrow beam antenna towards galactic pole) is 3 dB below the solid galactic noise curve shown on Fig. 3. The maximum galactic noise for narrow beam antennas is shown via a dashed curve in Fig. 3.

FIGURE 3

F_a versus frequency (10^8 to 10^{11} Hz)

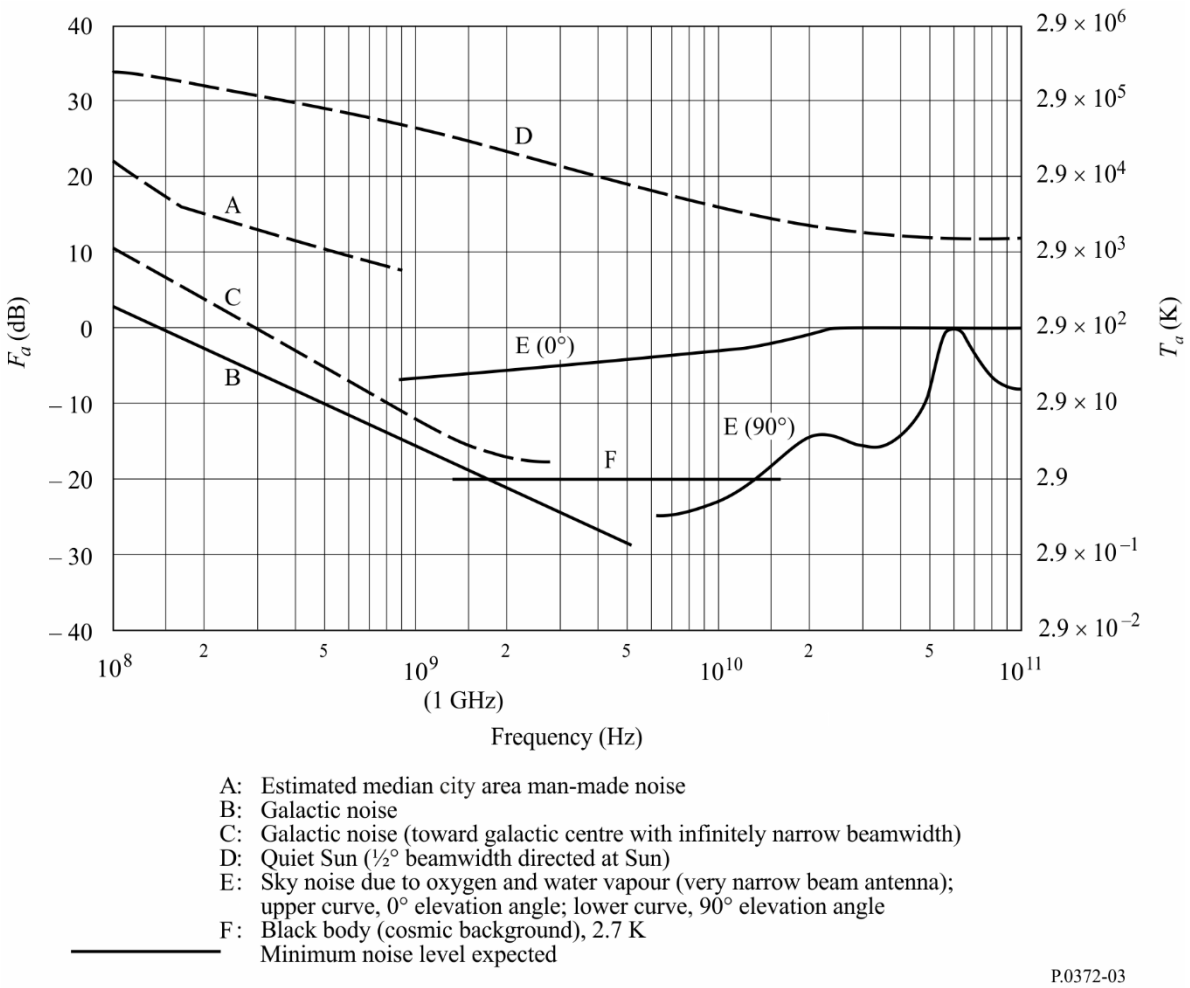

A: Estimated median city area man-made noise
B: Galactic noise
C: Galactic noise (toward galactic centre with infinitely narrow beamwidth)
D: Quiet Sun (½° beamwidth directed at Sun)
E: Sky noise due to oxygen and water vapour (very narrow beam antenna); upper curve, 0° elevation angle; lower curve, 90° elevation angle
F: Black body (cosmic background), 2.7 K
Minimum noise level expected

P.0372-03

PART 3

Noise from atmospheric gases and the Earth's surface

Noise from individual sources such as the Sun, atmospheric gases, the Earth's surface, etc., are usually given in terms of a brightness temperature, T_b. The antenna temperature, T_a, is the convolution of the antenna pattern and the brightness temperature of the sky and ground. For antennas whose patterns encompass a single source, the antenna temperature and brightness temperature are the same (curves C, D and E of Fig. 3, for example).

Figures 4 and 5 show the brightness temperature of the atmosphere for a ground-based receiver excluding the cosmic noise contribution of 2.7 K or other extra-terrestrial sources for frequencies between 1 and 340 GHz in the first instance and 1 and 60 GHz in the second. The curves are calculated using a radiative transfer program for seven different elevation angles and an average atmosphere (7.5 g surface water vapour density, surface temperature of 288 K, and a scale height of 2 km for water vapour). The "U.S. Standard Atmosphere, 1976" is used for the dry atmosphere. A typical water vapour contribution is added above the tropopause.

FIGURE 4

Brightness temperature (clear air) for 7.5 g/m^3 water vapour concentration (surface temperature and pressure equal to 15°C and 1 023 mb); θ is the elevation angle

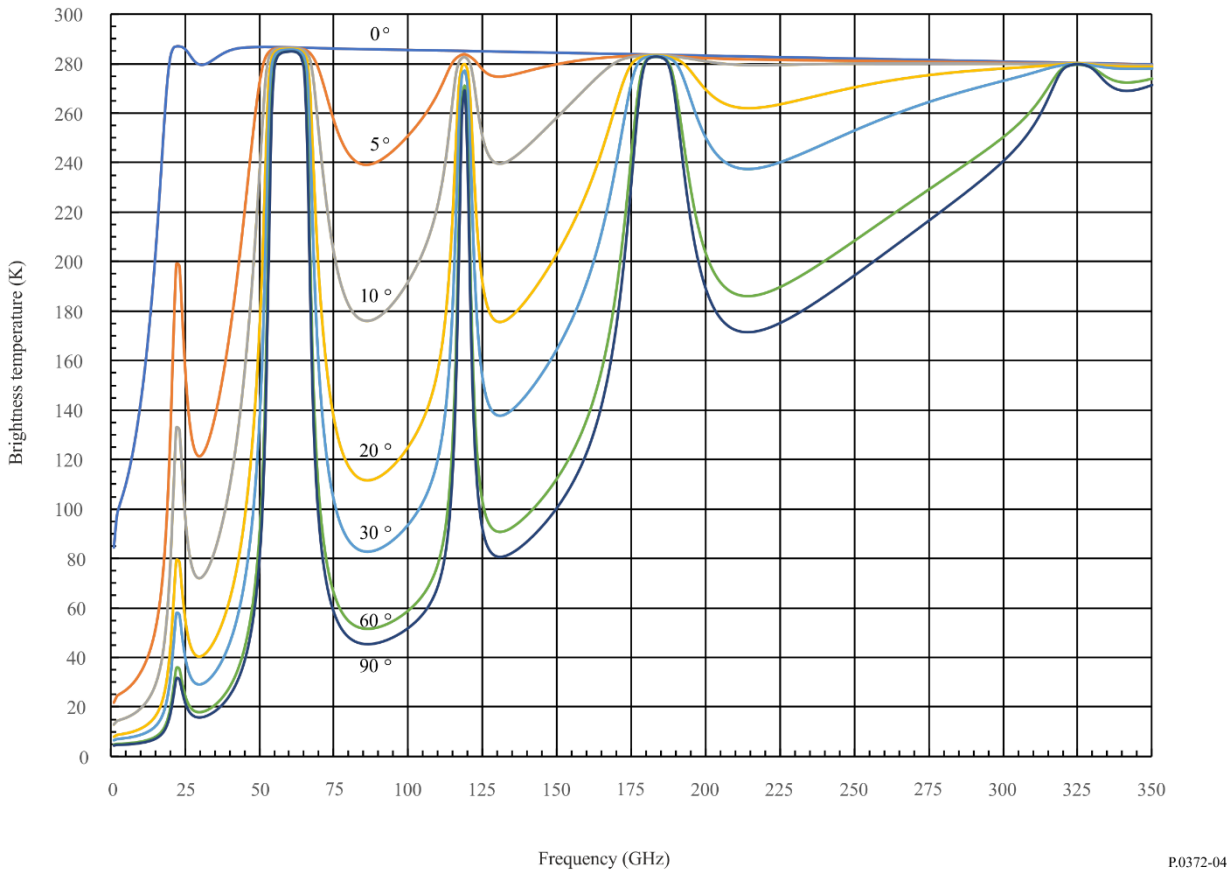

FIGURE 5

Brightness temperature for clear air for 7.5 g/m³ of water vapour concentration (expansion of abscissa scale of Fig. 4); θ is the elevation angle

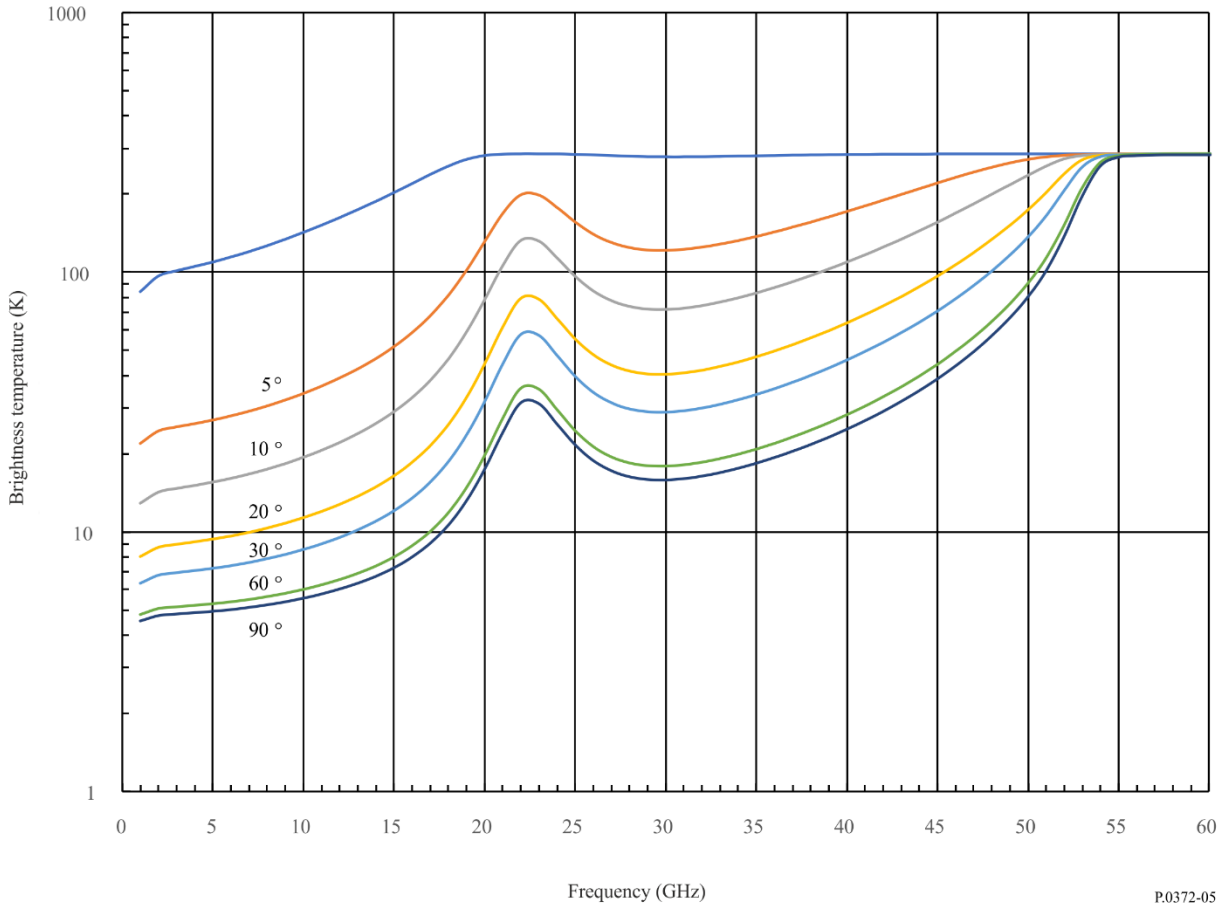

3.1 Radio noise due to the Earth's atmosphere for earth stations

3.1.1 Instantaneous brightness temperature prediction method

The instantaneous sky brightness temperature, $T_B(f)$, K, at any desired frequency, elevation angle, and location on the surface of the Earth can be predicted from the concurrent instantaneous total attenuation (excluding scintillation fading); and the surface values of total (barometric) pressure, temperature, and water vapour density at the location of interest as follows:

$$T_B(f) = 2.73 \cdot 10^{-\frac{A_T(f,\theta)}{10}} + T_{mr}\left(f, T_s, P_s, \rho_{w_s}\right) \cdot \left(1 - 10^{-\frac{A_T(f,\theta)}{10}}\right) \quad \text{(K)} \quad (10)$$

where:

$$T_{mr}\left(f, P_s, T_s, \rho_{w_s}\right) = \begin{cases} a_t(f) + b_t(f) \cdot T_s + c_t(f) \cdot P_s + d_t(f) \cdot \rho_{w_s}, & \text{for no rain} \\ 275, & \text{for rain} \end{cases} \quad \text{(K)} \quad (11)$$

and:

f : frequency, in GHz, for no rain: $1 \le f \le 200$ GHz; for rain: $1 \le f \le 55$ GHz

P_s : instantaneous total (barometric) surface pressure, in hPa, at the desired location

T_s : instantaneous surface temperature, in K, at the desired location

ρ_{w_s} : instantaneous surface water vapour density, in g/m^3, at the desired location

θ : elevation angle at the surface of the Earth at the location of interest

$A_T(f,\theta)$: instantaneous total atmospheric attenuation excluding scintillation, in dB, for the desired space-to-Earth slant path.

The coefficients a_t, b_t, c_t and d_t at the frequency of interest should be linearly interpolated between the frequencies in the data file Tmr_approx.txt, which is an integral part of this Recommendation. The data file contains the coefficients a_t, b_t, c_t and d_t in columns 2, 3, 4 and 5, respectively, for frequencies between 1 GHz and 200 GHz in 0.5 GHz increments in column 1.

Tmr_approx.txt

3.1.2 Statistical brightness temperature prediction method

Sky brightness temperature statistics, $T_B(f,p)$, K, for at any desired frequency, elevation angle, location on the surface of the Earth, and exceedance probability (CCDF), p, %, can be predicted from the total attenuation (excluding scintillation fading) vs. exceedance probability; and the mean surface values of total (barometric) pressure, temperature, and water vapour density at the location of interest as follows:

$$T_B(f,p) = 2.73 \cdot 10^{-\frac{A_T(f,p,\theta)}{10}} + T_{mr}\left(f,\overline{P_s},\overline{T_s},\overline{\rho_{w_s}}\right)\cdot\left(1-10^{-\frac{A_T(f,p,\theta)}{10}}\right) \quad \text{(K)} \quad (12)$$

where:

$$T_{mr}\left(f,\overline{P_s},\overline{T_s},\overline{\rho_{w_s}}\right) = \begin{cases} a_t(f) + b_t(f)\cdot\overline{T_s} + c_t(f)\cdot\overline{P_s} + d_t(f)\cdot\overline{\rho_{w_s}}, & \text{for no rain} \\ 275, & \text{for rain} \end{cases} \quad \text{(K)} \quad (13)$$

and:

f : frequency, in GHz, for no rain: $1 \le f \le 200$ GHz; for rain: $1 \le f \le 55$ GHz

$\overline{P_s}$: mean total (barometric) surface pressure, in hPa, at the desired location

$\overline{T_s}$: mean surface temperature, in K, at the desired location

$\overline{\rho_{w_s}}$: mean surface water vapour density, in g/m^3, at the desired location

θ : elevation angle at the surface of the Earth at the location of interest

$A_T(f,p,\theta)$: total atmospheric attenuation, in dB, excluding scintillation at the exceedance probability, p, for the desired space-to-Earth slant path.

The coefficients a_t, b_t, c_t and d_t at the frequency of interest should be linearly interpolated between the frequencies in the data file Tmr_approx.txt, which is an integral part of this Recommendation. The data file contains the coefficients a_t, b_t, c_t and d_t in columns 2, 3, 4 and 5, respectively, for frequencies between 1 GHz and 200 GHz in 0.5 GHz increments in column 1.

Tmr_approx.txt

3.2 Radio noise due to the Earth's atmosphere and the Earth's surface for space stations

The brightness temperature of the Earth's surface as seen from a particular nadir angle may be calculated using the radiative transfer equation describing the reflection of downwelling atmospheric radiation and the emission of radiation by the Earth's surface.

This calculation involves integration of downwelling radiation over all angles and includes atmospheric attenuation.

It may be simplified as:

$$T = \varepsilon \cdot T_{surf} + \rho\, T_{atm} \tag{14}$$

where:

ε : effective emissivity of the surface

ρ : effective reflection coefficient

T_{surf} : physical temperature (K) of the Earth's surface

T_{atm} : weighted average of the sky brightness temperature.

Up to about 100 GHz, but particularly below 10 GHz, the reflection coefficient ρ is generally high and the emissivity ε, low.

In Fig. 7a), the emissivity and the brightness temperature of a smooth water surface are given for vertical and horizontal polarizations and for two angles of incidence. It should be noted that fresh and salted water are indistinguishable for frequencies greater than 5 GHz.

Figure 7b) shows the nadir brightness temperature of the sea surface at three frequencies as a function of the sea surface physical temperature, for a salinity of 36 parts per thousand.

The increase in brightness temperature of the sea surface with wind speed is given in Figs 7c) and 7d), which also provides a useful tool for storm detection.

The emissivities (and hence the brightness temperatures) of land surfaces are higher than those of water surfaces due to the lower dielectric constants of land. In Fig. 8a), the brightness temperature of a smooth field for different moisture contents is shown; in Fig. 8b), the brightness temperature for different degrees of roughness is presented. The curves are given for vertical, horizontal and circular polarization. If the moisture content increases, the brightness temperature decreases; if the roughness is higher, the brightness temperature increases.

Figure 9 shows calculations of brightness temperature as seen from geostationary orbit by a satellite using an Earth-coverage beam (Earth fills the main beam between 3 dB points). As the satellite moves around its orbit, one can see the effect of the African land mass (hot) at 30º E longitude and of the Pacific Ocean (cold) at 180º W to 150º W longitude. Brightness temperature increases with increasing frequency, largely due to gaseous absorption. Curves are for US Standard Atmosphere with 2.5 g/m^3 water vapour and 50% cloud cover. The Earth-coverage antenna pattern is given by $G(\varphi) = -3 \times (\varphi/8.715)^2$ dB for $0 \le \varphi \le 8.715$ where φ is the angle off boresight.

FIGURE 6

Fraction of the time the zenith sky noise (brightness) temperature is equal to or less than the abscissa value for a typical year

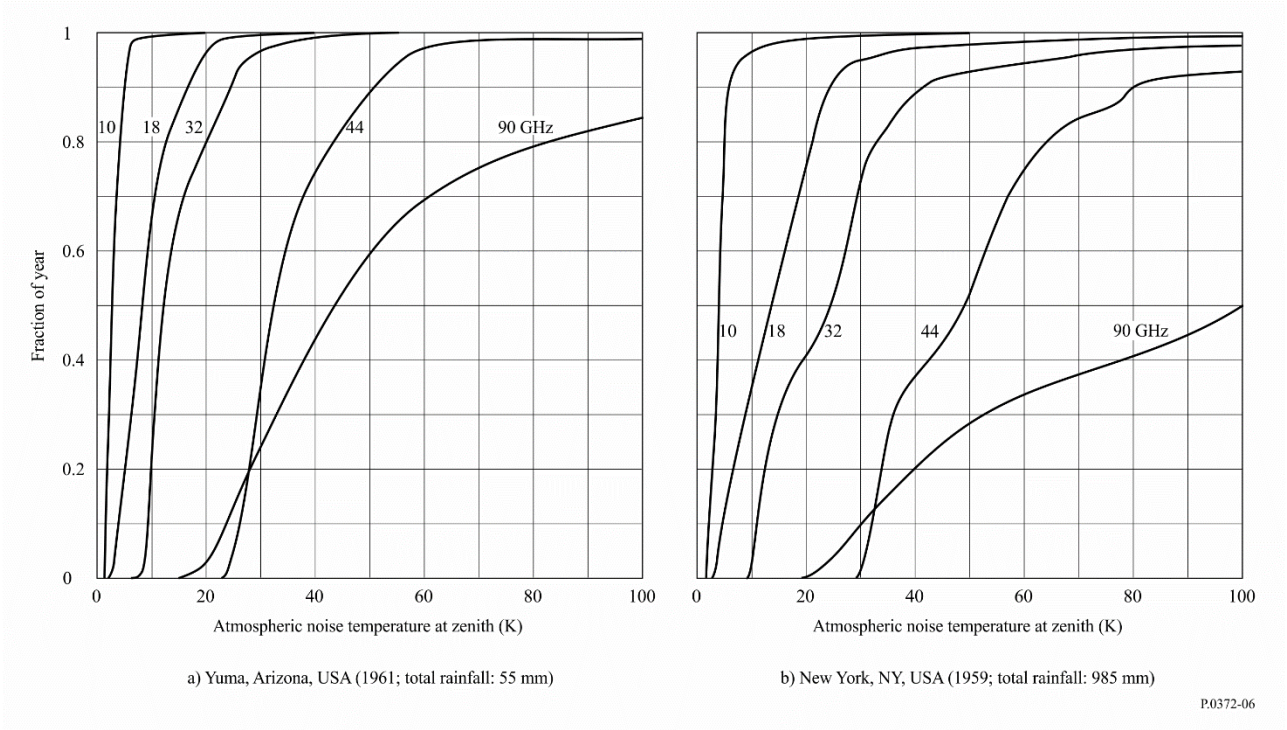

a) Yuma, Arizona, USA (1961; total rainfall: 55 mm)

b) New York, NY, USA (1959; total rainfall: 985 mm)

FIGURE 7

Emissivity and brightness temperature variations of the sea surface

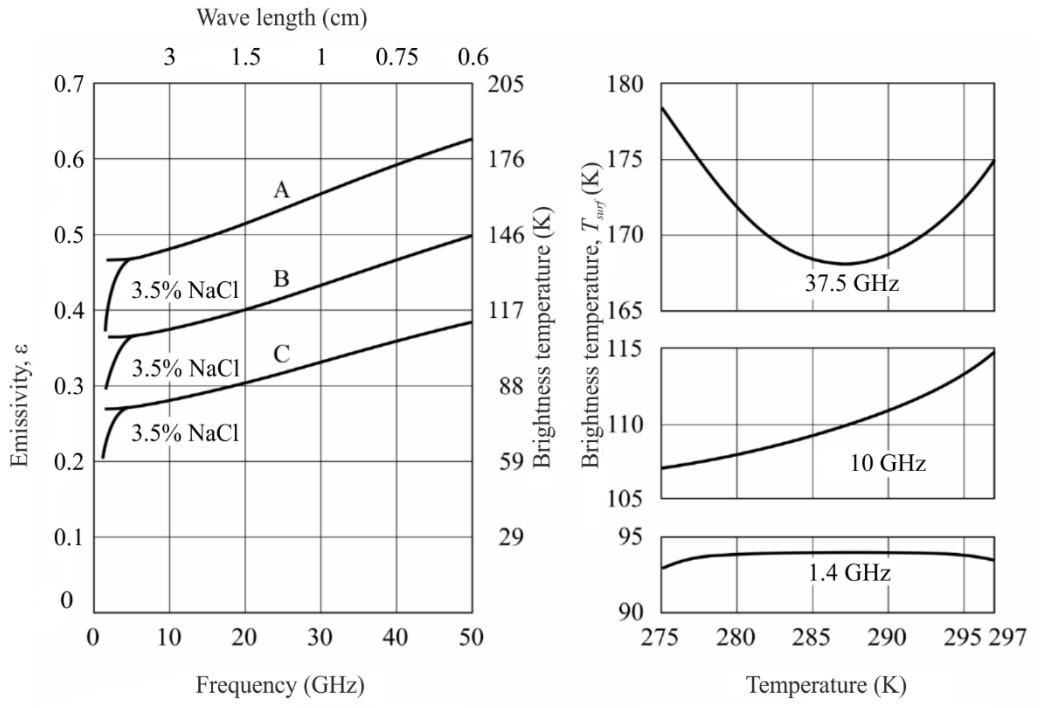

a) Emissivity of a smooth water surface

A: Vertical polarization
B: Incidence angles of 45° and 0°
C: Horizontal polarization

b) Brightness temperature of the sea surface as a function of sea surface temperature (nadir)for a salinity of 36 parts per thousand

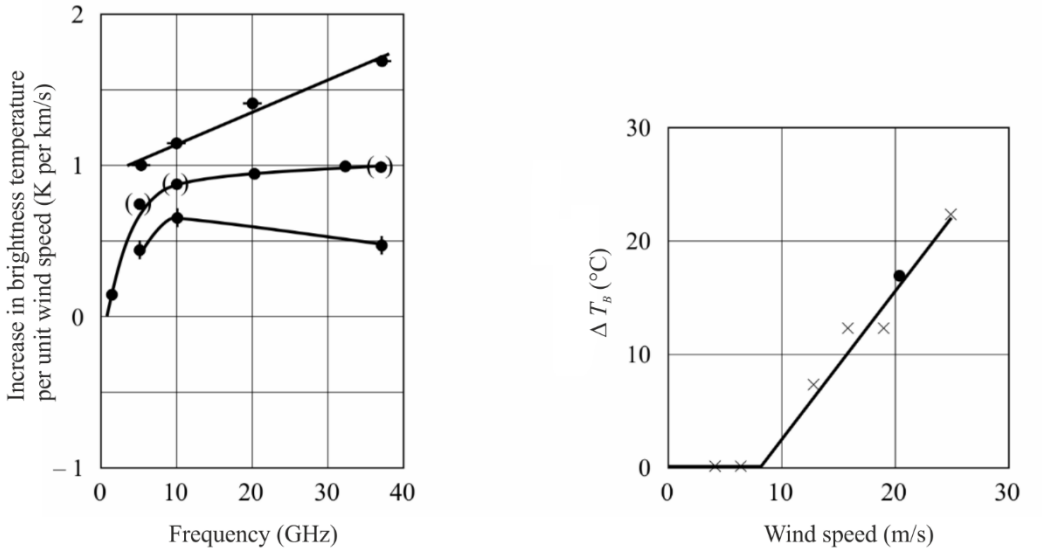

c) Spectrum of increase in brightness temperature caused by wind at the ocean surface

● Nadir
Vertical polarization (38°)
Horizontal polarization (38°)
(●) Inferred

d) Increase in brightness temperature of the ocean surface at 19.35 GHz due to wind speed

× Atlantic, North Sea
● Salton Sea

P.0372-07

FIGURE 8

Brightness temperature at 1 430 MHz of the ground as a function of elevation angle

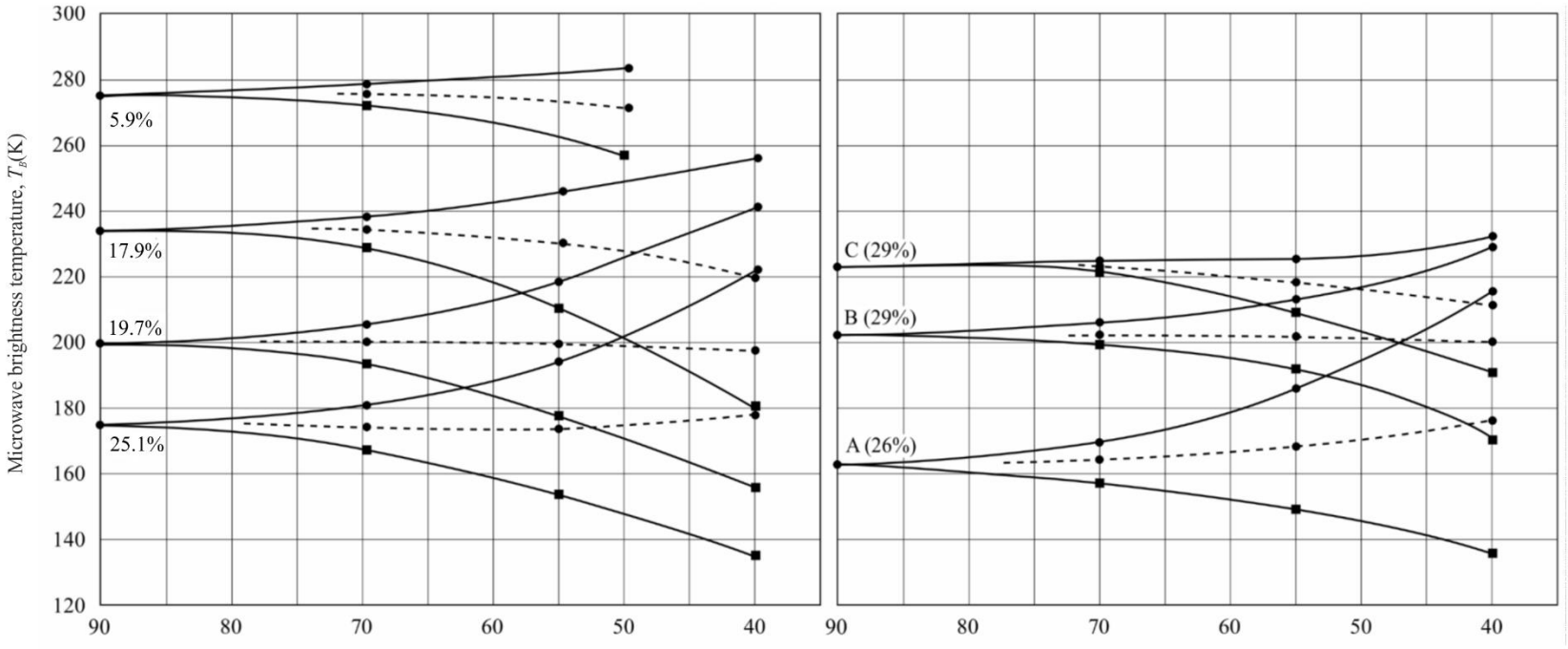

a) Moisture content from 5.9% to 25.1% for a bare, smooth field

b) For (A) smooth field (B) medium roughness and (C) rough (deeply ploughed) field with percentage water content as indicated

FIGURE 9

Weighted brightness temperature of the Earth as a function of longitude viewed from geostationary orbit at frequencies between 1 and 51 GHz

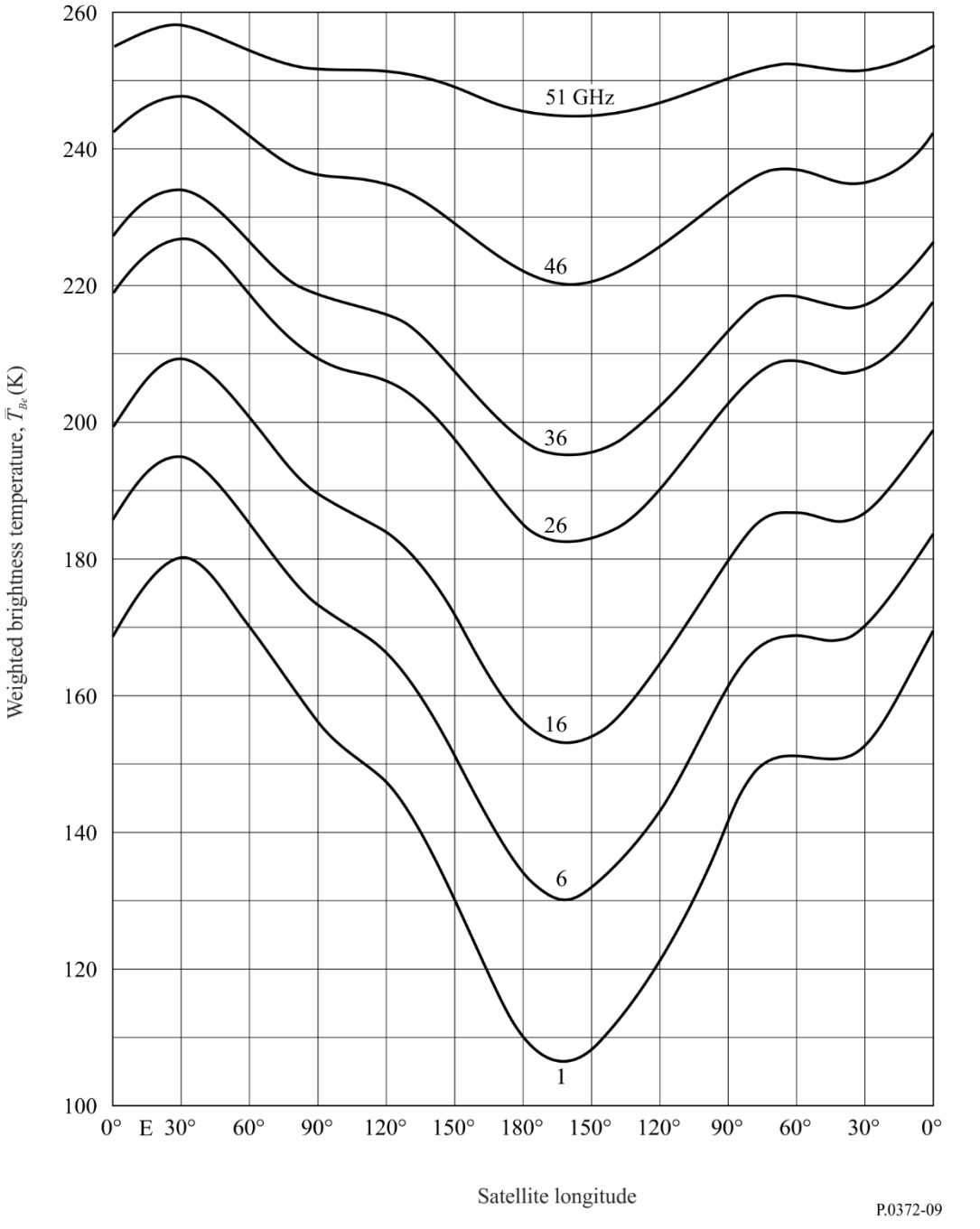

PART 4

Brightness temperature due to extra-terrestrial sources

4.1 Brightness temperature due to extra-terrestrial sources

As a general rule, for communications below 2 GHz, one needs to be concerned with the Sun and the galaxy (the Milky Way), which appears as a broad belt of strong emission. For frequencies up to about 100 MHz, the median noise figure for galactic noise for a vertical antenna, neglecting ionospheric shielding, is given by:

$$F_{am} = 52 - 23 \log f \qquad \text{(dB)} \tag{15}$$

where:

f: frequency (MHz).

The decile deviations of the mean galactic noise power are ±2 dB.

For these circumstances, the decile variation of both the upper and lower deciles for galactic noise is 2 dB.

Galactic noise will not be observed at frequencies lower than foF2 and will be less than given by equation (16) for frequencies up to about three times foF2.

Above 2 GHz, one need to consider only the Sun and a few very strong non-thermal sources such as Cassiopeia A, Cygnus A and X and the Crab nebula since the cosmic background contributes 2.7 K only and the Milky Way appears as a narrow zone of somewhat enhanced intensity. The brightness temperature range for the common extra-terrestrial noise sources in the frequency range 0.1 to 100 GHz is illustrated in Fig. 10.

Figures 11a, 11b, 11c and 11d plot the total radio sky temperature at 408 MHz smoothed to 5º angular resolution. Figures 11 are given in equatorial coordinates, declination δ (latitude) and right ascension α (hours eastward around equator from vernal equinox). The contours are directly in K above 2.7 K. The accuracy is 1 K. The contour intervals are:

– 2 K below 60 K,

– 4 K from 60 K to 100 K,

– 10 K from 100 K to 200 K,

– 20 K above 200 K.

Arrows on unlabelled contour lines point clockwise around a minimum in the brightness distribution.

The dashed sinusoidal curve between ±23.5º in Figs 11a and 11d defines the ecliptic which crosses the Milky Way close to the galactic centre. This means that, if one observes a spacecraft in interplanetary space, it might be necessary to take this into account. The strongest point sources are indicated by narrow peaks of the temperature distribution, while weaker sources are less apparent owing to the limited angular resolution.

The radiation of the galactic background varies with frequency. To obtain brightness temperatures at other frequencies f_i for background radiation use

$$T_b(f_i) = T_b(f_0)\,(f_i/f_0)^{-2.75} + 2.7 \qquad \text{K} \tag{16}$$

Thus, for T_b = 200 K, f_0 = 408 MHz and f_i = 1 GHz, this extrapolation would yield:

$$T_b = 19.7 \qquad \text{K}$$

More precise extrapolation using this formula needs to take into account variations of the exponent over the frequency range and over the sky. For point sources, the variation of the intensity with frequency depends on their different physical conditions.

For telecommunication using satellites in geostationary orbit, a limited part of the sky is of special interest, as illustrated in Fig. 12a). The corresponding range of declinations (±8.7º) is shown in Fig. 12b), indicating the strongest sources.

The Sun is a strong variable noise source with a noise temperature of about 10^6 K at 50 to 200 MHz and at least 10^4 K at 10 GHz under quiet Sun conditions. Large increases occur when the Sun is disturbed. The brightness temperature of the Moon is almost independent of frequency above 1 GHz; it varies from about 140 K at new Moon up to 280 K at full Moon. The Sun's path is in the plane of ecliptic (dashed line in Fig. 11). The Moon is observed within ±5º in declination of the plane of the ecliptic.

FIGURE 10

Extra-terrestrial noise sources

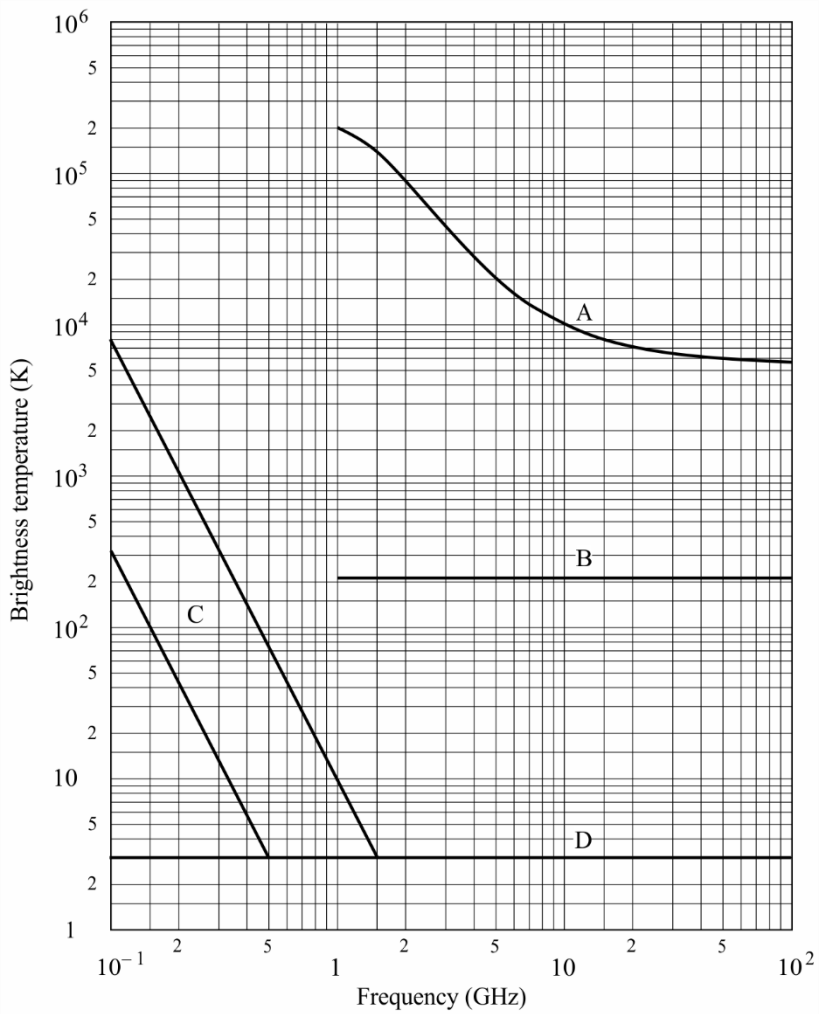

FIGURE 11a

Radio sky temperature at 408 MHz

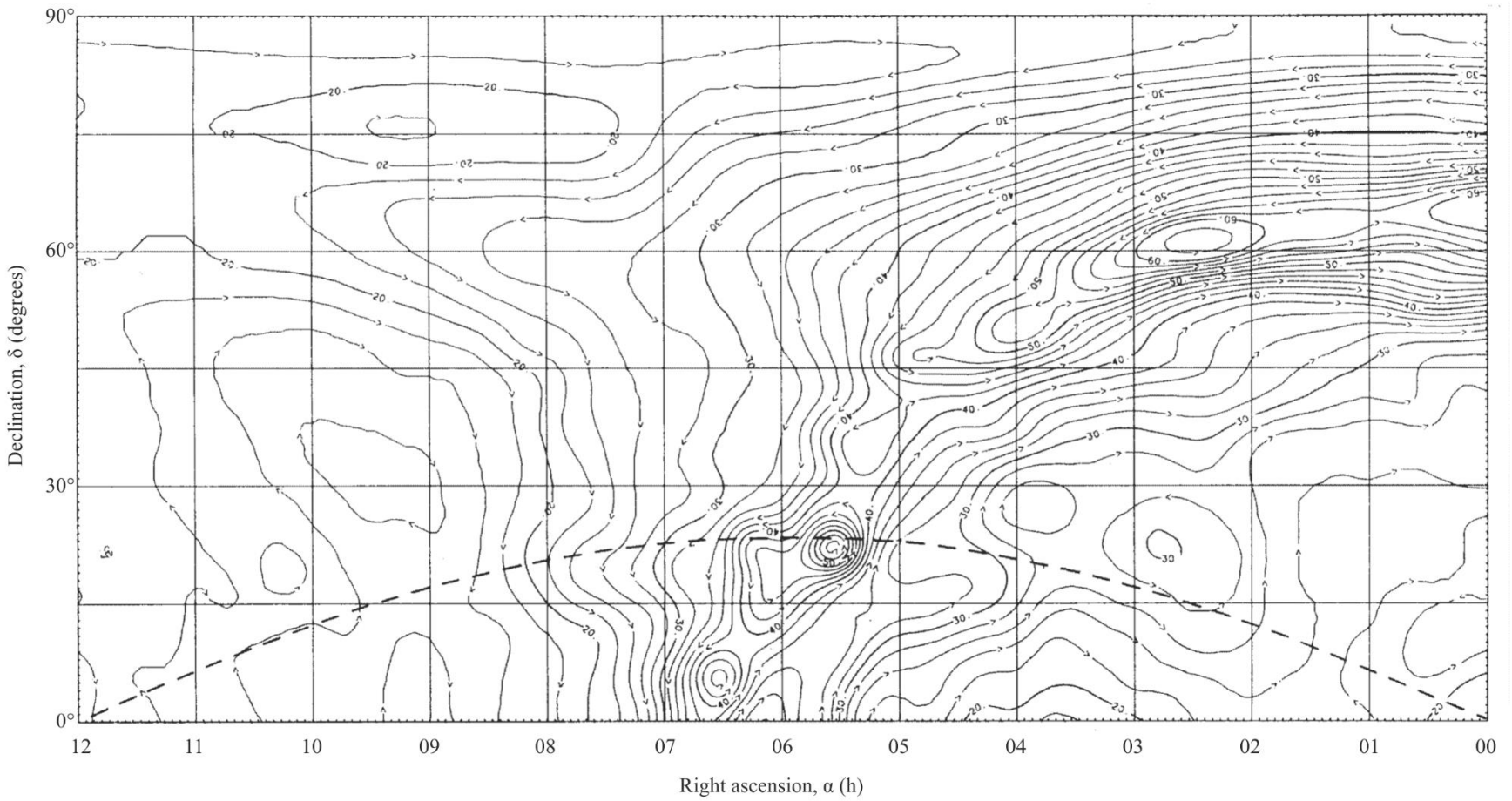

Right ascension 0000 h to 1200 h, declination 0° to +90°, dashed curve; ecliptic

P.0372-11a

FIGURE 11b

Radio sky temperature at 408 MHz

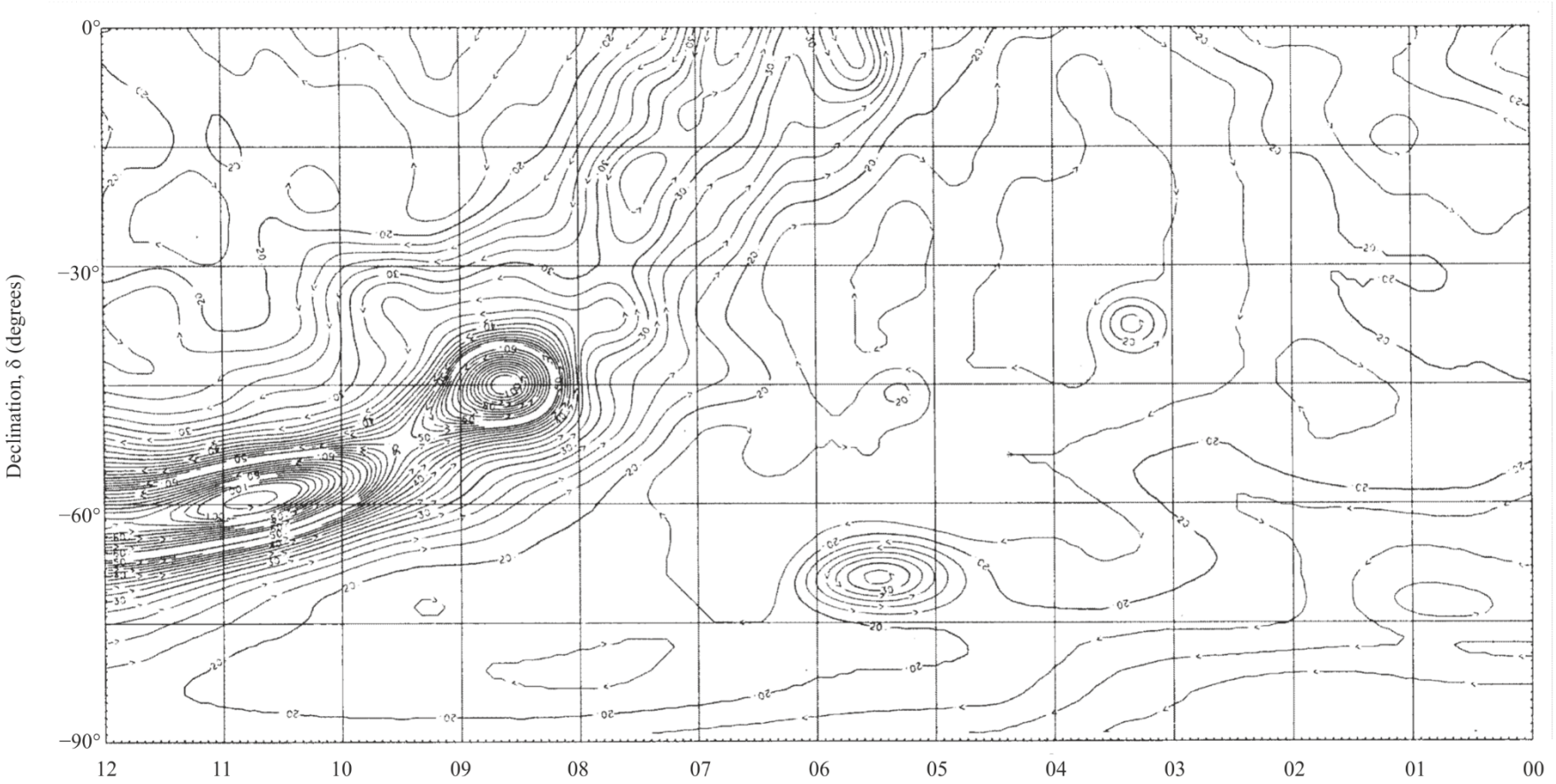

Right ascension 0000 h to 1200 h, declination 0° to −90°

P.0372-11b

FIGURE 11c

Radio sky temperature at 408 MHz

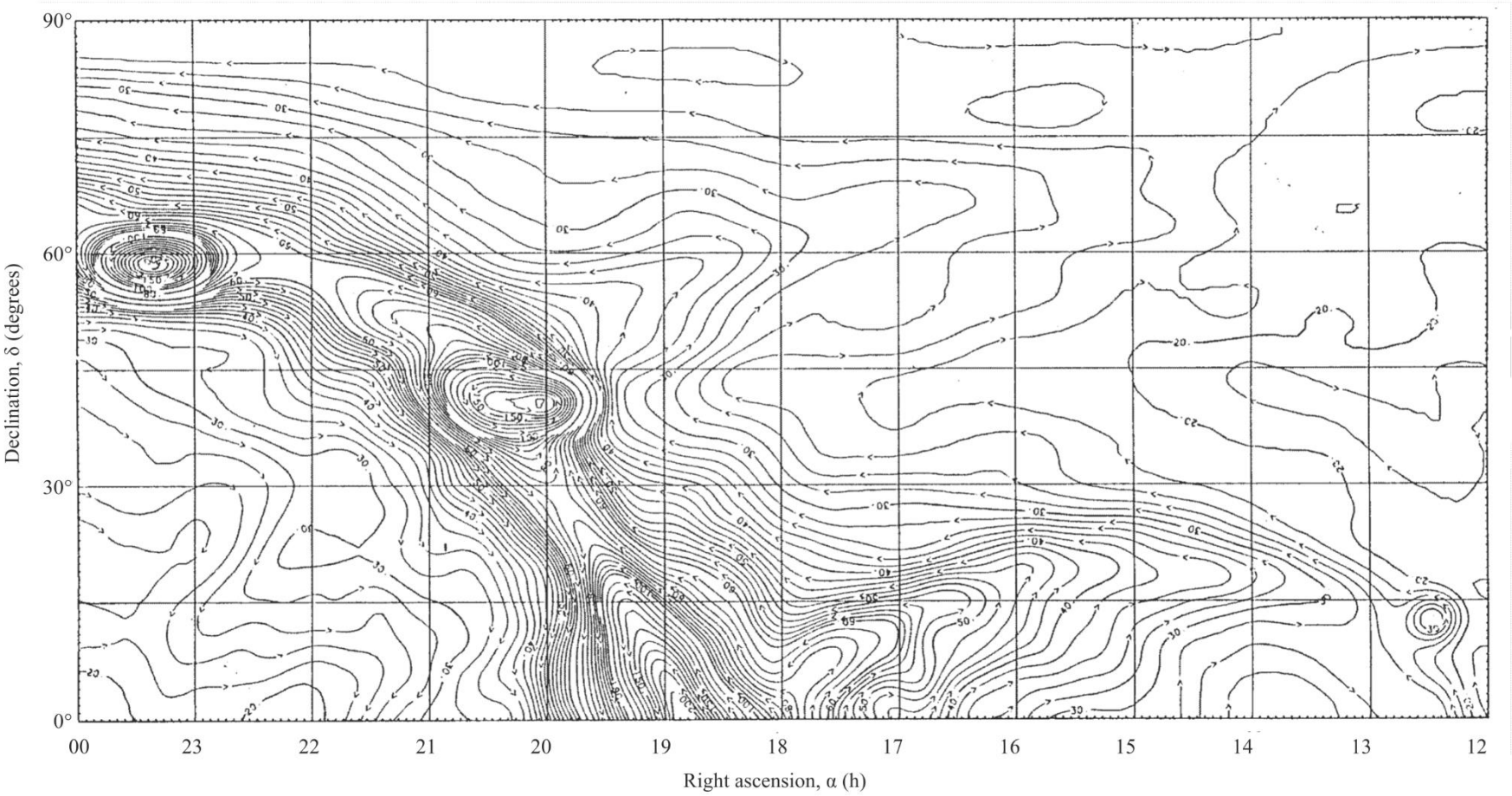

Right ascension 1200 h to 2400 h, declination 0° to +90°

P.0372-11c

FIGURE 11d

Radio sky temperature at 408 MHz

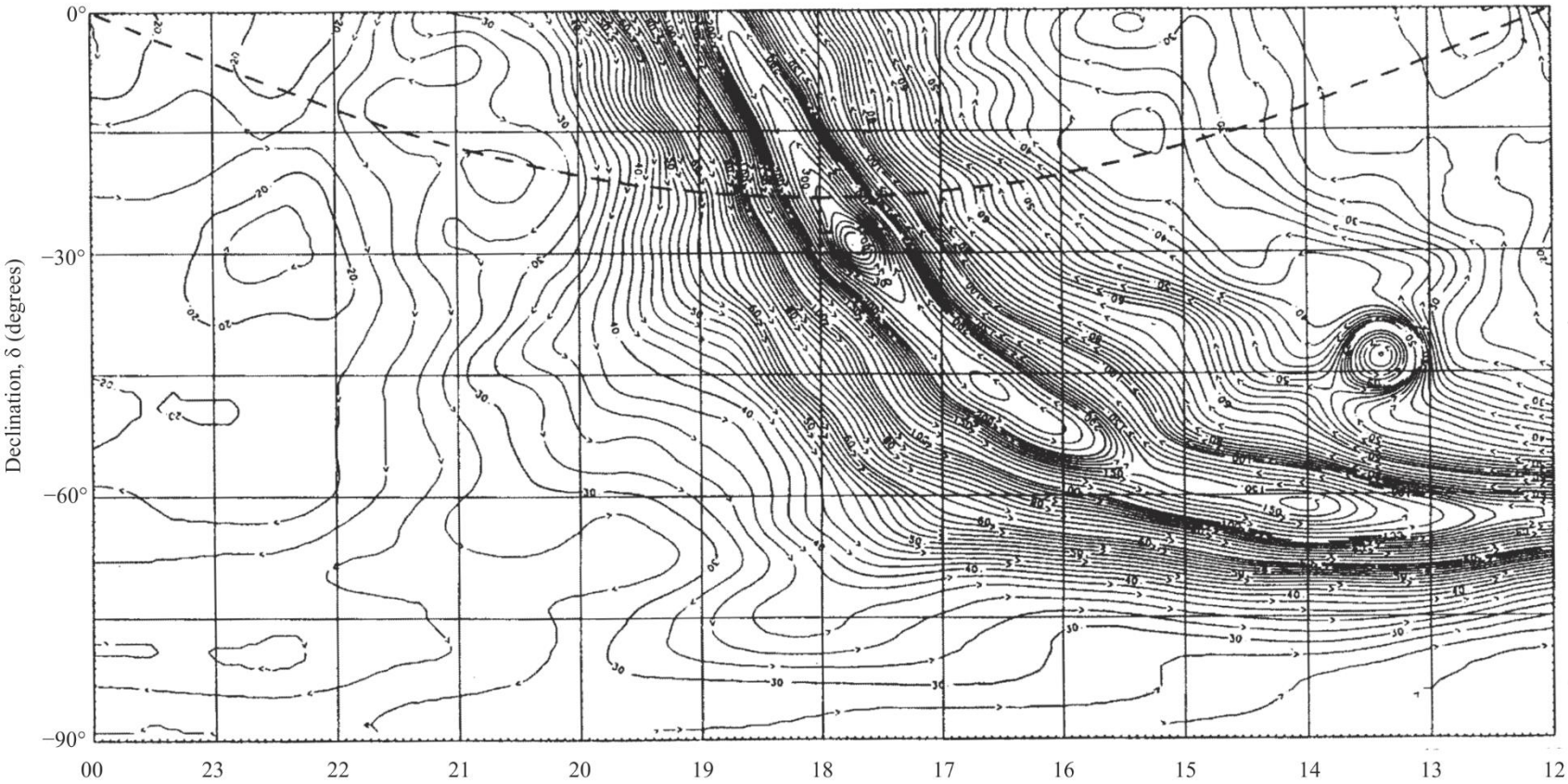

Right ascension 1200 h to 2400 h, declination 0° to −90°, dashed curve; ecliptic

P.0372-11d

FIGURE 12

Part of the sky which is relevant for telecommunication with satellites in geostationary orbit

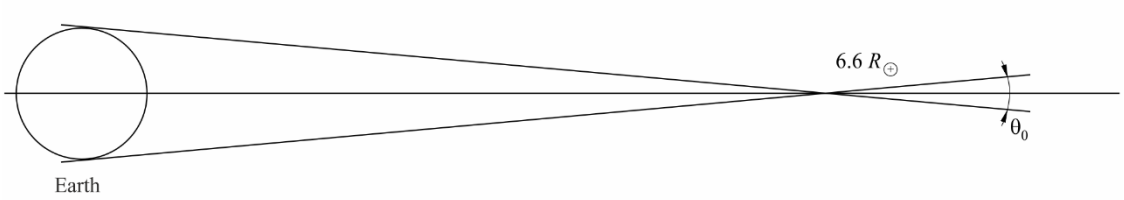

a) The geostationary orbit viewed from Earth showing θ_0 ($R_\oplus$: mean Earth radius)

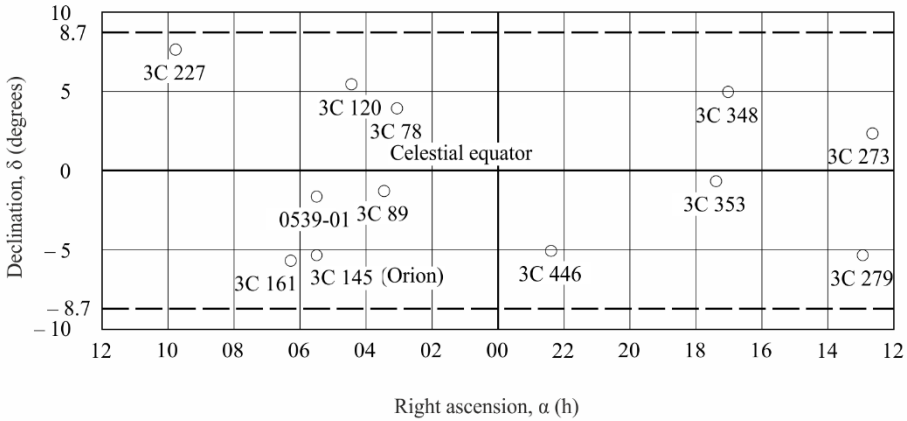

b) Locations of strongest radio sources (○) for a band of ± 8.7° about the celestial equator. The numbers refer to catalogue designations, e.g. 3C indicates third Cambridge

P.0372-12

PART 5

Atmospheric noise due to lightning

5.1 Atmospheric noise due to lightning

World charts of the background atmospheric radio noise, showing the expected median values of the mean noise power, F_{am} (dB) above $k\,T_0\,b$, at 1 MHz for each three-month time block, 4-hour-time block, in local time, are shown in Figs 13a to 36a. The three-month time blocks are 1) December, January, February 2) March, April, May 3) June, July, August 4) September, October, November. The 4-hour-time blocks are in terms of local time which are the same local times in different 15° longitude regions. The variation of F_{am} with frequency for each season-time block is given in Figs 13b to 36b and the variation with frequency of the other noise parameters is given in Figs 13c to 36c. The reference antenna for these atmospheric noise estimates is a short vertical monopole over a perfectly conducting ground plane (the influence of a perfectly conducting ground plane is discussed in Recommendation ITU-R P.341, Annex 2). The estimates are those for the atmospheric noise aggregated from all directions and it is not appropriate to take the directivity of practical antennas into account. The incident field strength can be obtained, see § 2.

It will be observed that values of atmospheric noise are indicated that are below the expected levels of man-made noise and galactic noise. These values should be used with caution, as they represent only estimates of what atmospheric noise levels would be recorded if the other types of noise were not present. An examination of the data, however, shows that such low levels were, on rare occasions, actually measured.

Atmospheric noise due to lightning is generally not Gaussian in character and its probability density function may be important in determining the performance of digital systems. The amplitude probability distribution (APD) of this type of noise is described in terms of the voltage deviation, V_d, the ratio of the root mean square to the average of the noise envelope voltage.

APD curves corresponding to various values of V_d, are given in Fig. 37, in which the r.m.s. envelope voltage A_{rms}, is taken as the reference. The measured values of V_d vary about the predicted median value, V_{dm}, and their variation is given by σV_d. The APD curves can be used for a wide range of bandwidths. The estimates of V_d given (Figs 13c-36c) are for a 200 Hz bandwidth and Fig. 39 gives a means to convert the 200 Hz V_d to the corresponding V_d in other bandwidths. Figure 39 is strictly valid only at MF and HF frequencies, so care should be exercised when applying these results to lower frequencies (i.e. LF, VLF, ELF).

The Figures are used in the following way. The value of F_{am} for 1 MHz is found from the noise charts (Figs 13a-36a) for the season under consideration. Using this value as the noise grade, the value of F_{am} for the required frequency is determined from the frequency curves (Figs 13b-36b). The variability parameters σ_{Fam}, D_u, σ_{Du}, etc., are obtained for the required frequency from Figs 13c to 36c. Values of D and σ_D for other percentages of time may be obtained assuming log-normal half distributions each side of the median values.

FIGURE 13a

Expected values of atmospheric radio noise, F_{am} (dB above kT_0b at 1 MHz) (Dec-Jan-Feb; 0000-0400 LT)

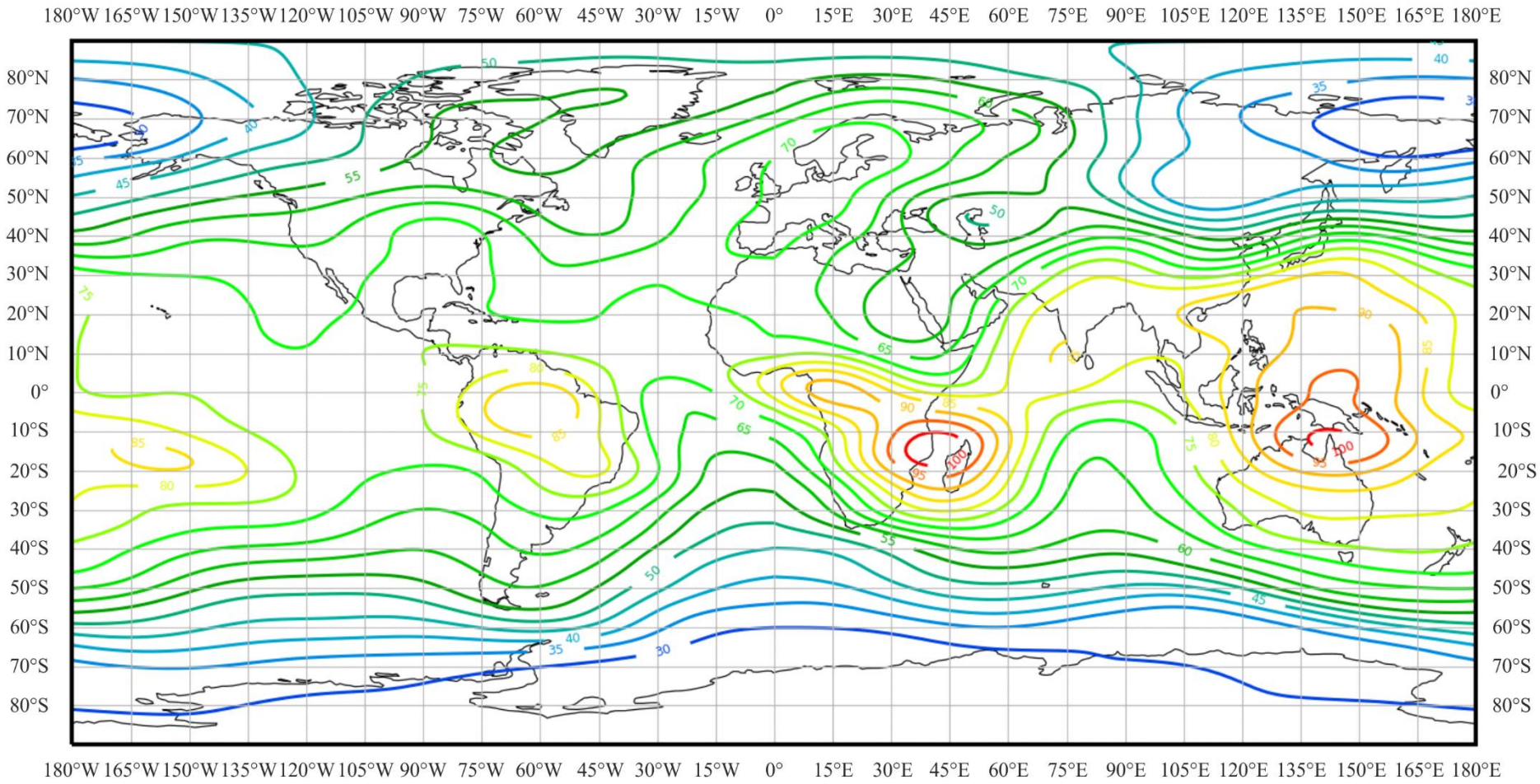

FIGURE 13b

Variation of radio noise with frequency (Northern hemisphere: Dec-Jan-Feb; Southern hemisphere: Jun-Jul-Aug; 0000-0400 LT)

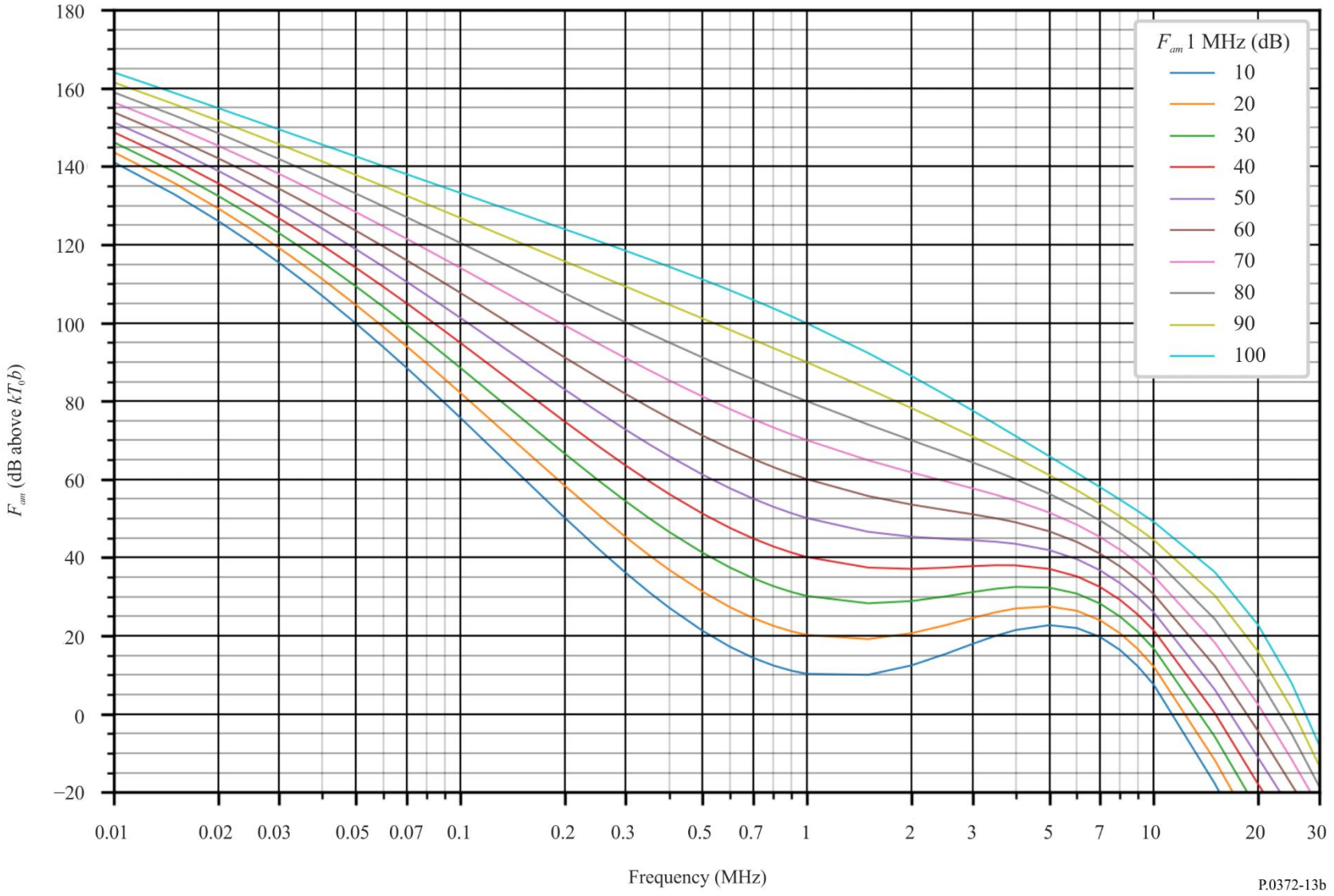

FIGURE 13c

Data on noise variability and character (Northern hemisphere: Dec-Jan-Feb; Southern hemisphere: Jun-Jul-Aug; 0000-0400 LT)

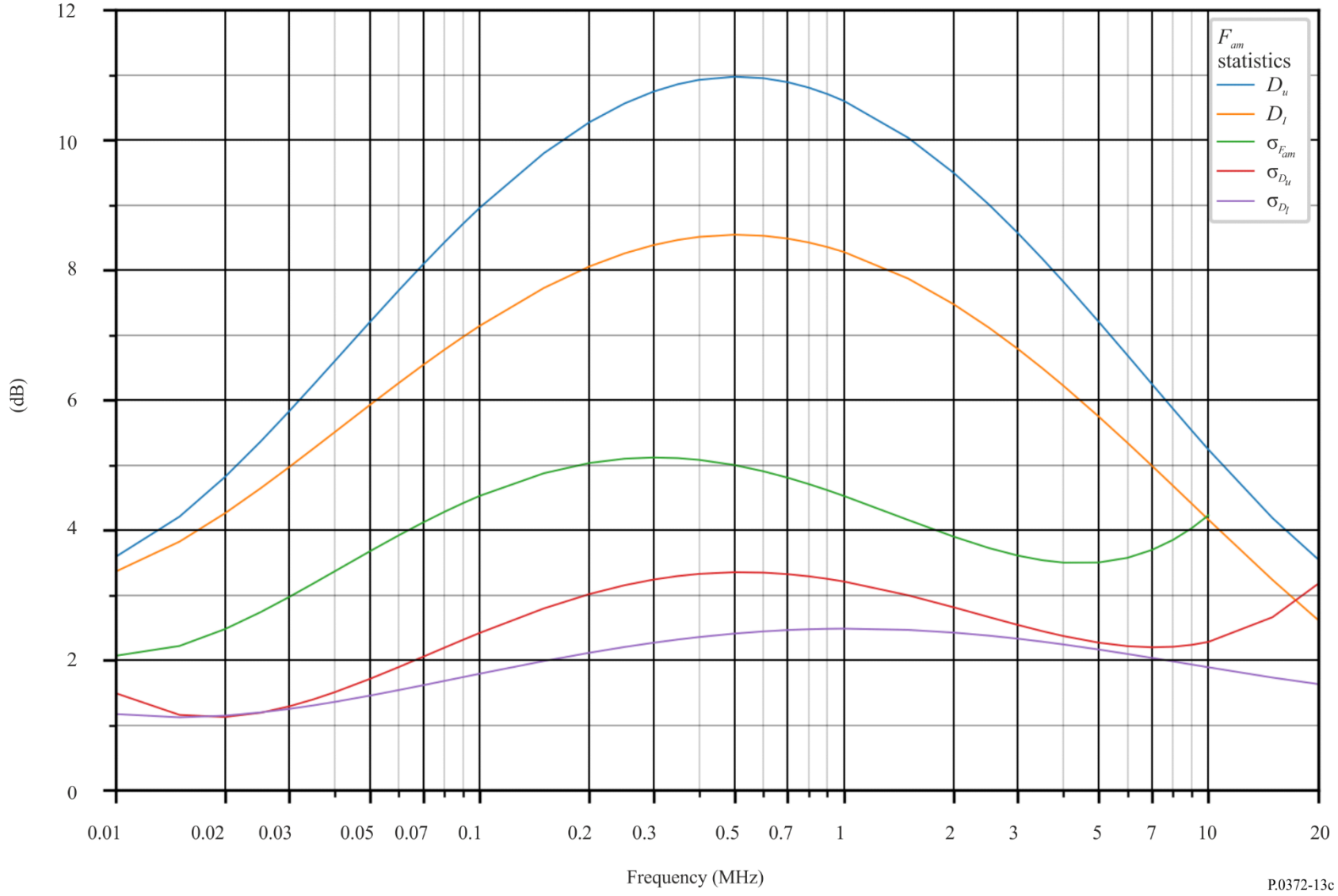

FIGURE 14a

Expected values of atmospheric radio noise, F_{am} (dB above kT_0b at 1 MHz) (Dec-Jan-Feb; 0400-0800 LT)

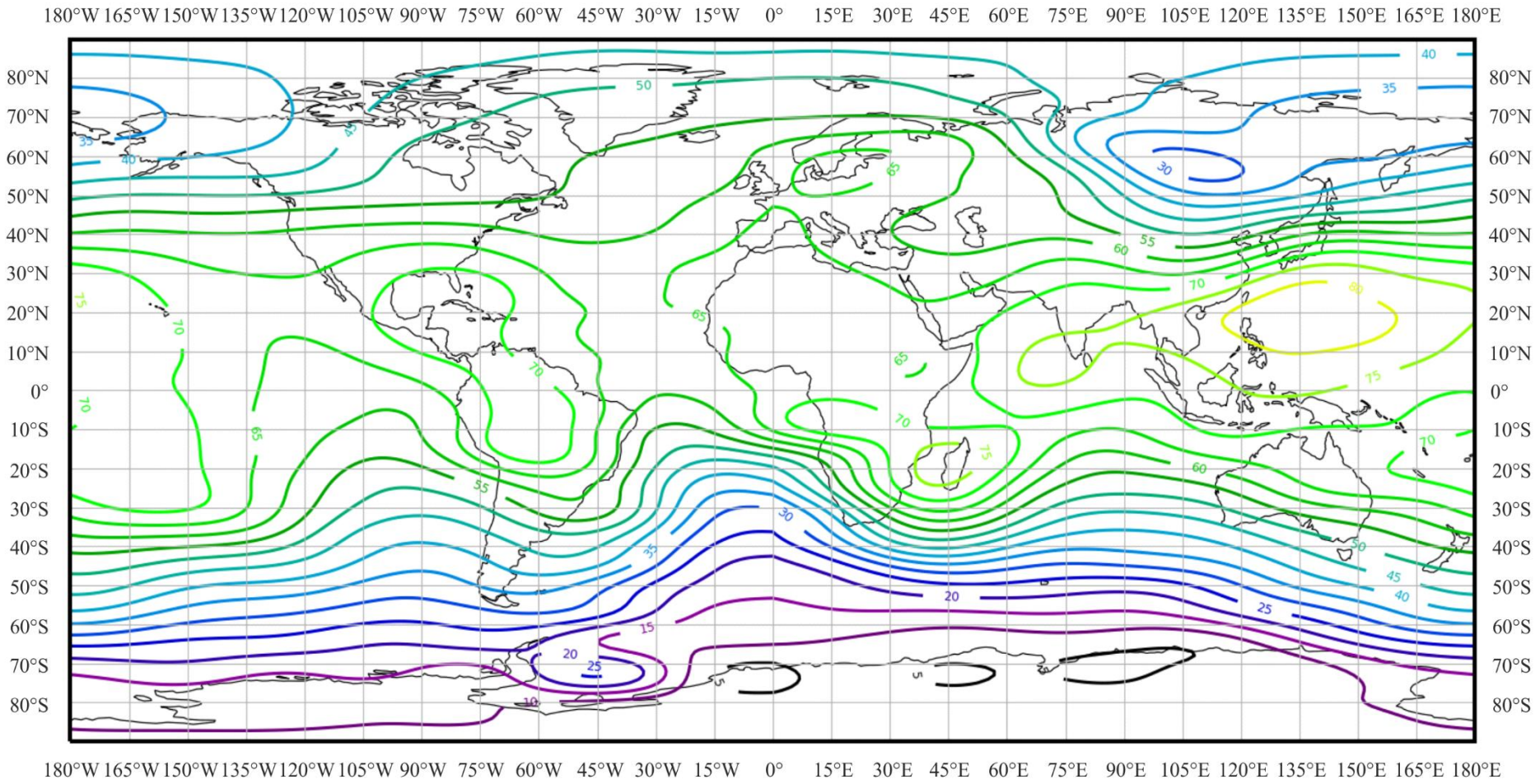

P.0372-14a

FIGURE 14b

Variation of radio noise with frequency (Northern hemisphere: Dec-Jan-Feb; Southern hemisphere: Jun-Jul-Aug; 0400-0800 LT)

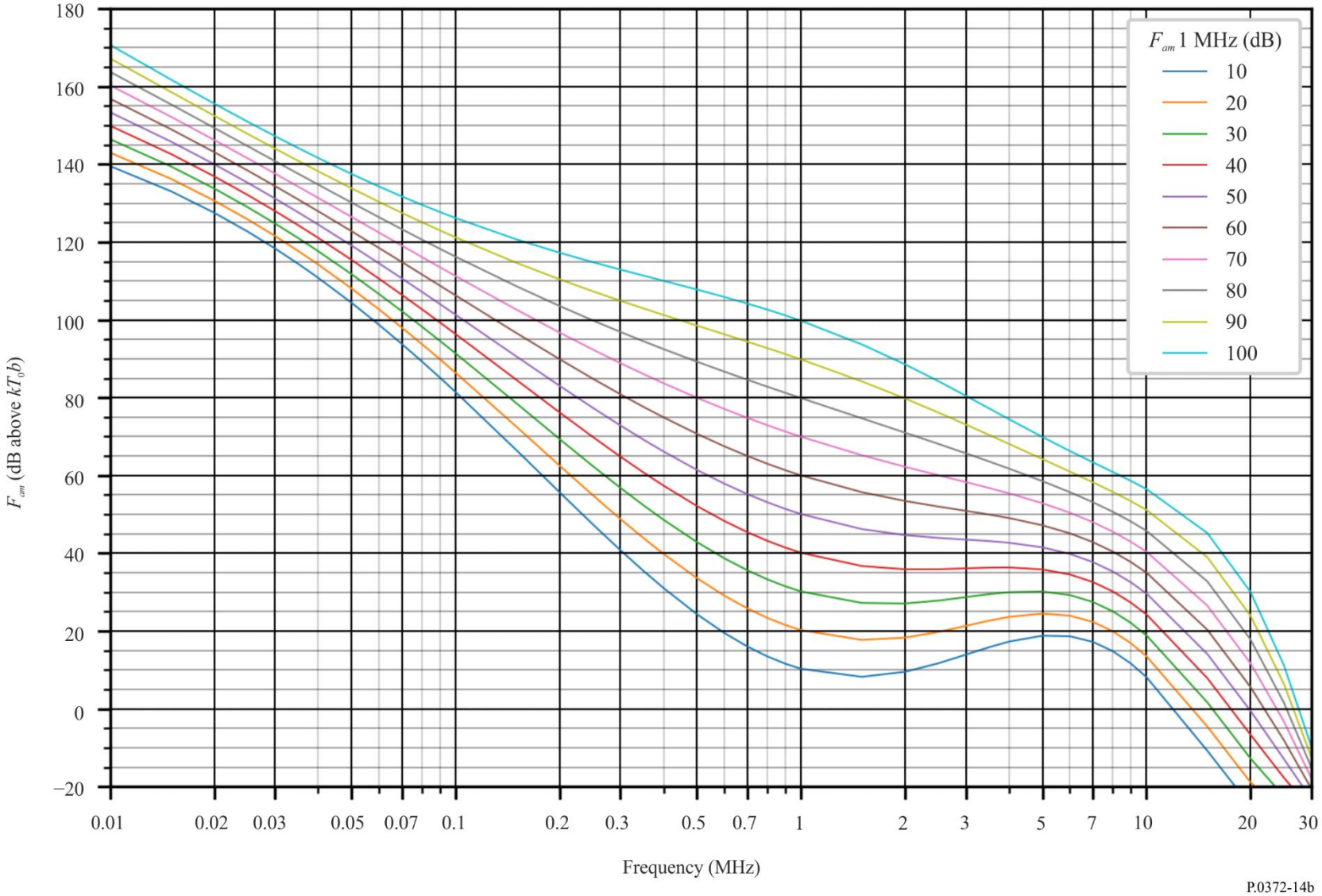

FIGURE 14c

Data on noise variability and character (Northern hemisphere: Dec-Jan-Feb; Southern hemisphere: Jun-Jul-Aug; 0400-0800 LT)

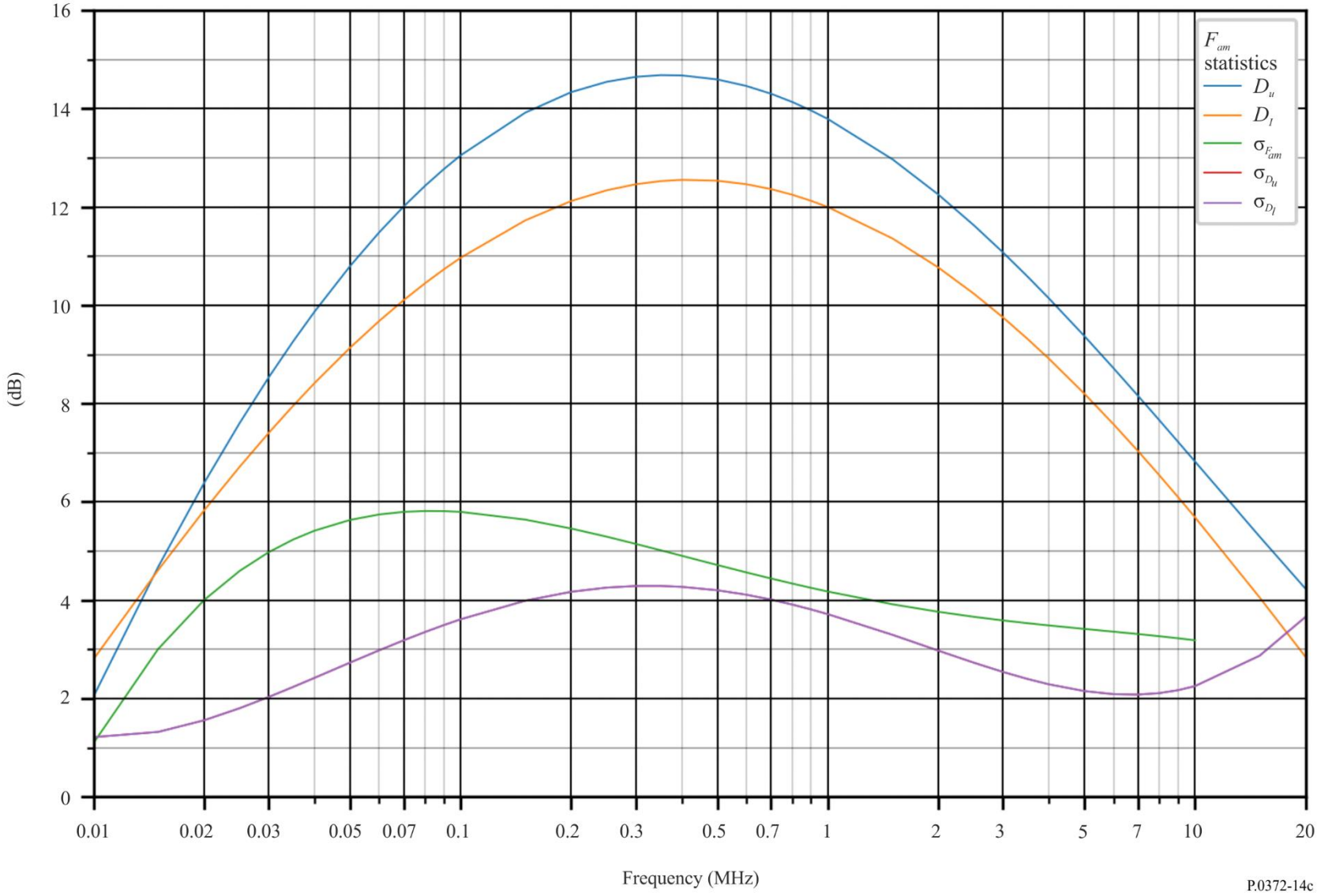

FIGURE 15a

Expected values of atmospheric radio noise, F_{am} (dB above kT_0b at 1 MHz) (Dec-Jan-Feb; 0800-1200 LT)

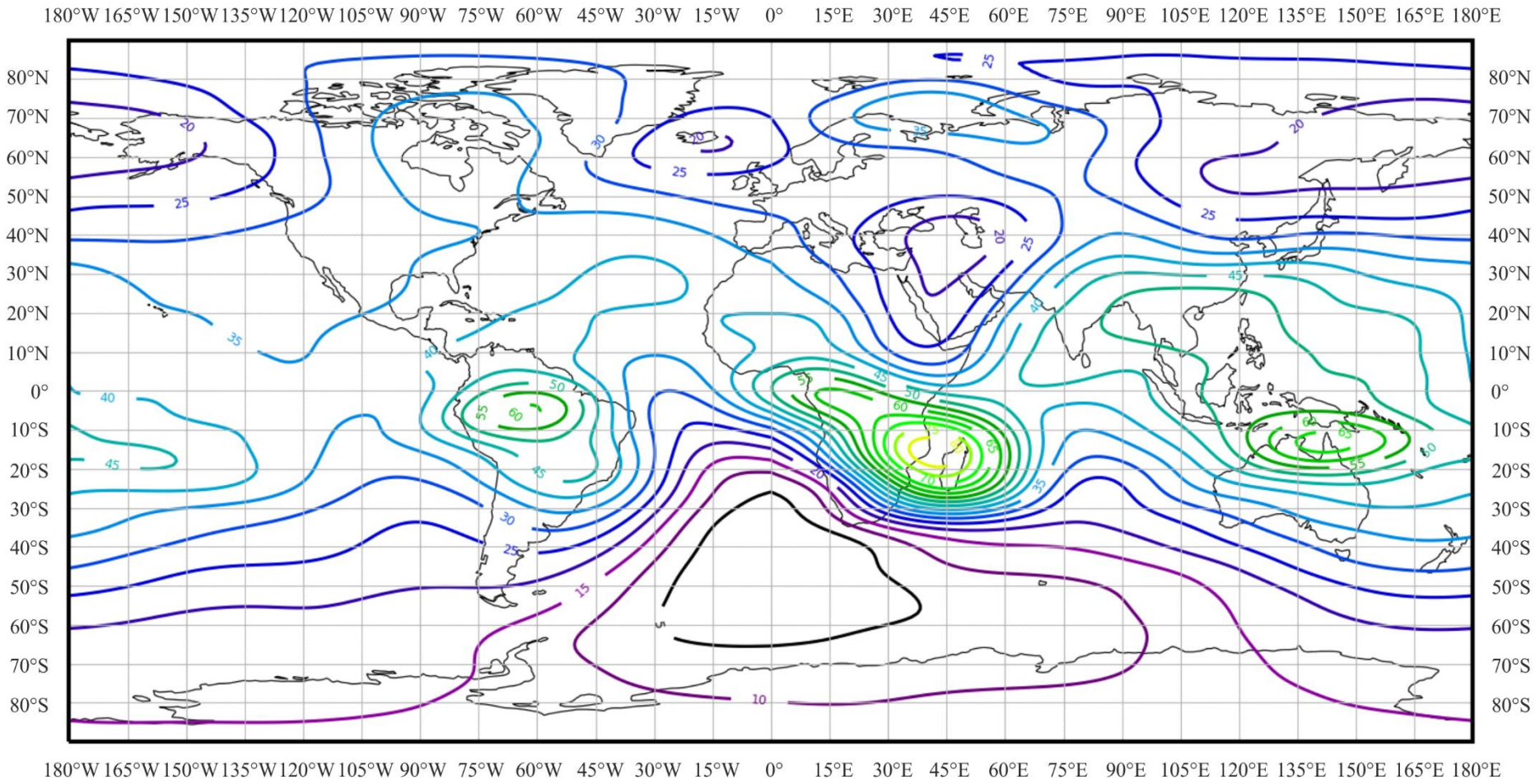

FIGURE 15b

Variation of radio noise with frequency (Northern hemisphere: Dec-Jan-Feb; Southern hemisphere: Jun-Jul-Aug; 0800-1200 LT)

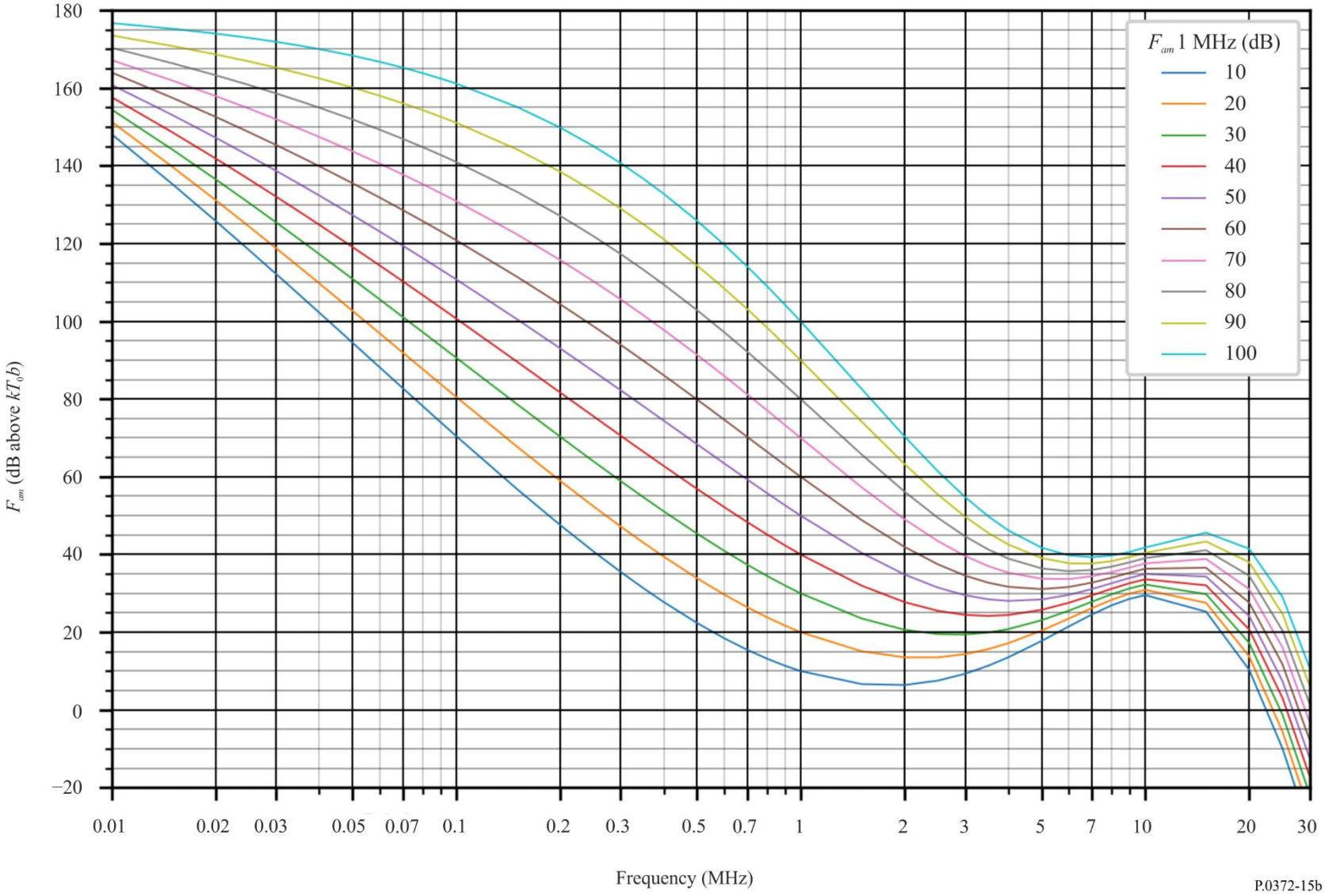

FIGURE 15c

Data on noise variability and character (Northern hemisphere: Dec-Jan-Feb; Southern hemisphere: Jun-Jul-Aug; 0800-1200 LT)

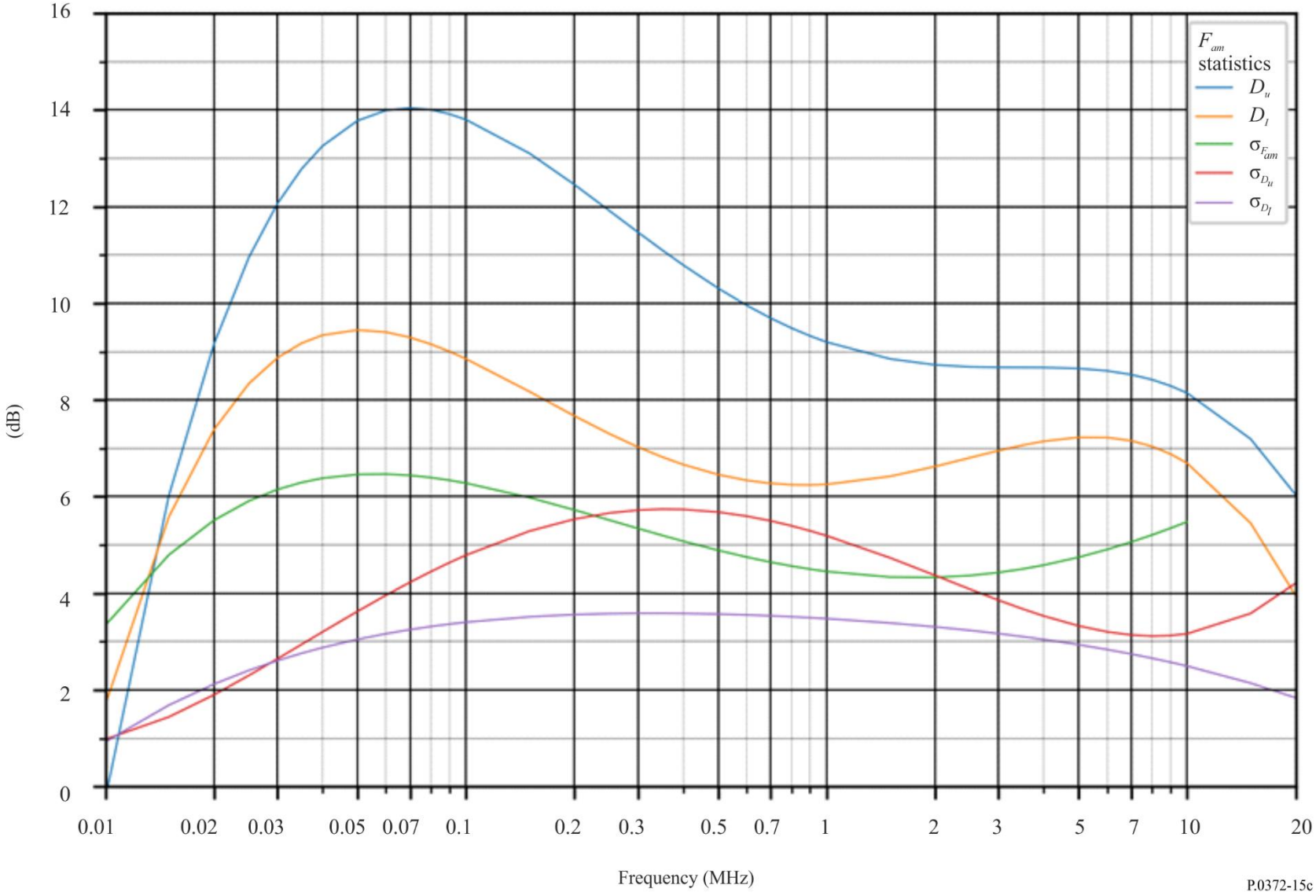

FIGURE 16a

Expected values of atmospheric radio noise, F_{am} (dB above kT_0b at 1 MHz) (Dec-Jan-Feb; 1200-1600 LT)

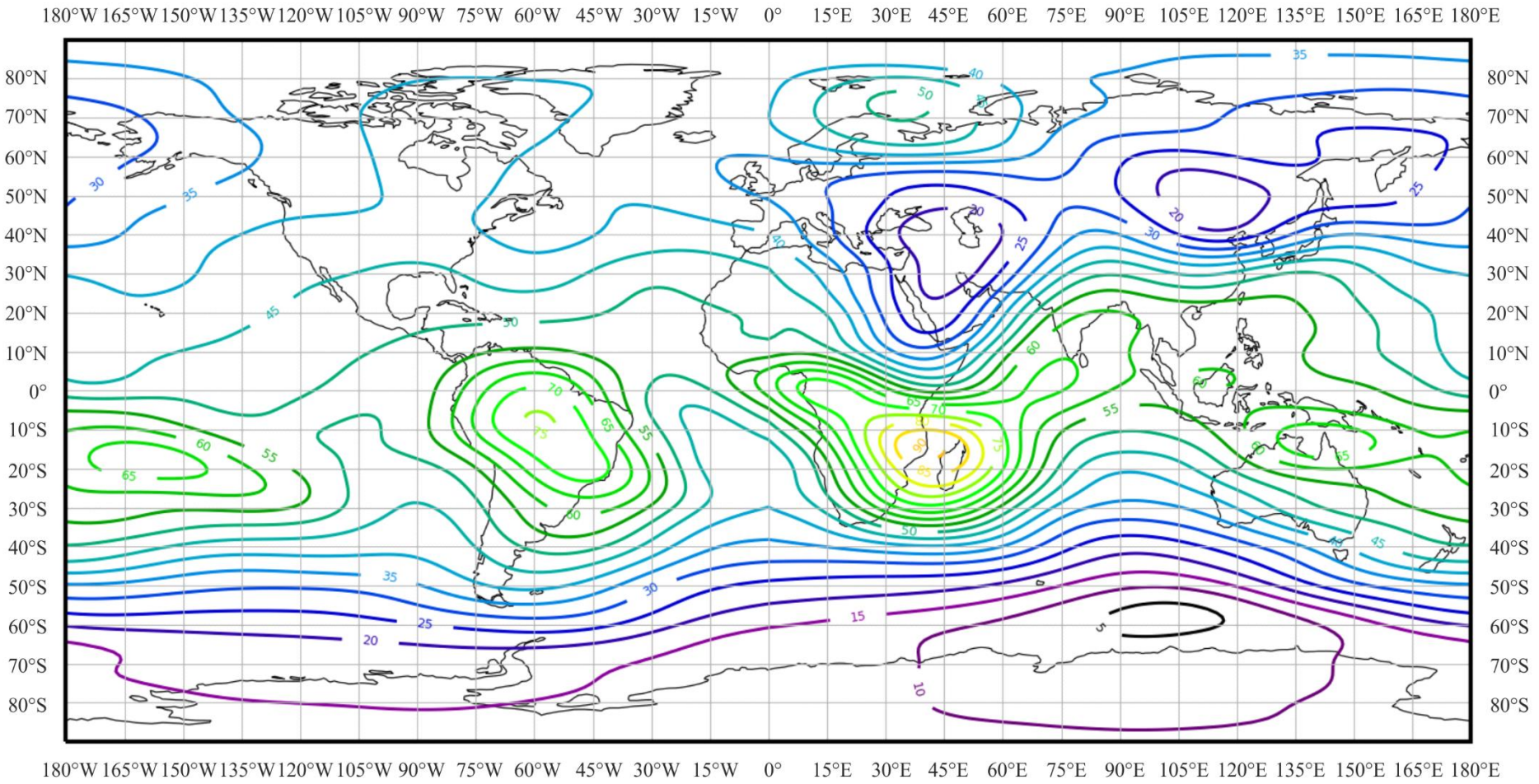

P.0372-16a

FIGURE 16b

Variation of radio noise with frequency (Northern hemisphere: Dec-Jan-Feb; Southern hemisphere: Jun-Jul-Aug; 1200-1600 LT)

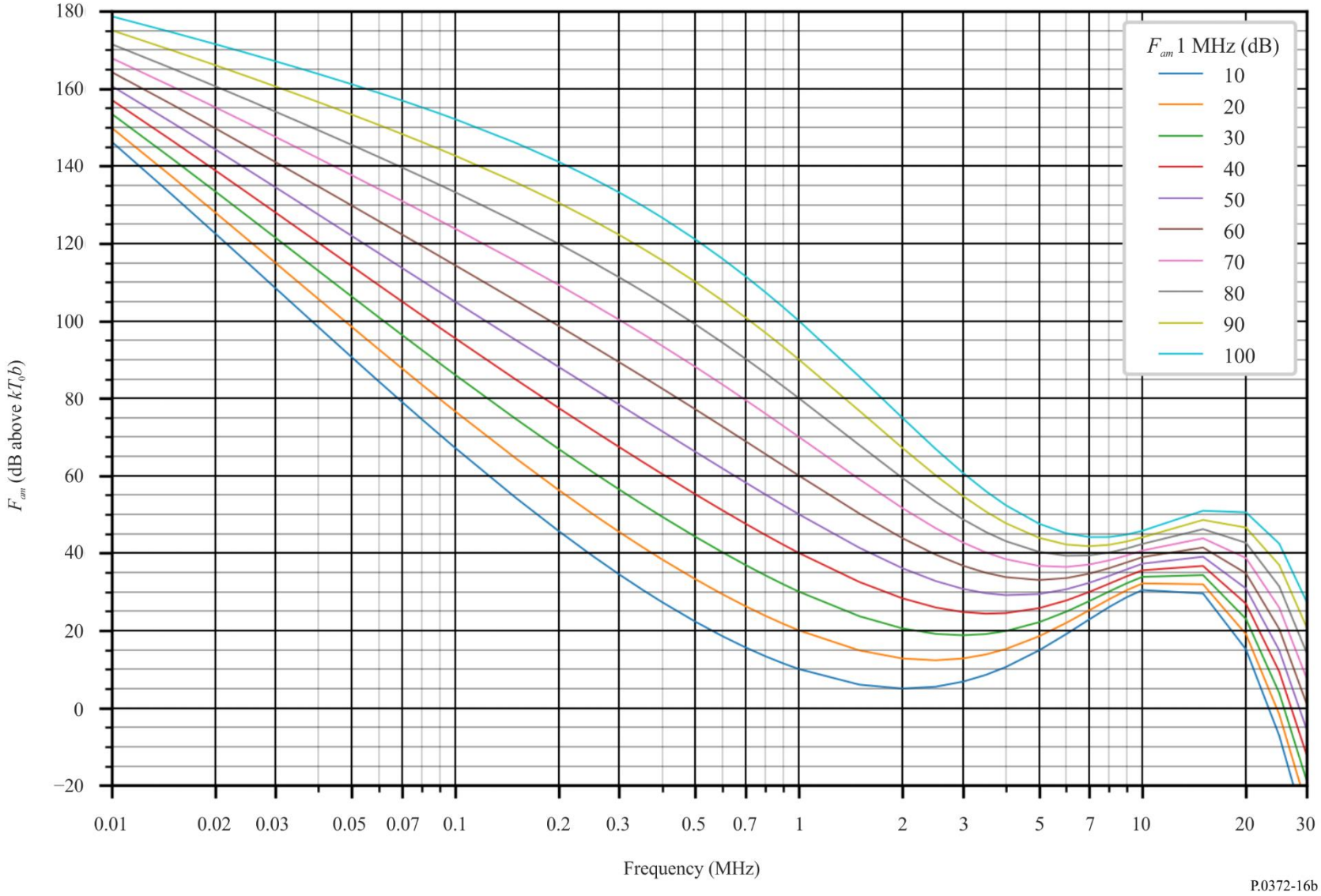

FIGURE 16c

Data on noise variability and character (Northern hemisphere: Dec-Jan-Feb; Southern hemisphere: Jun-Jul-Aug; 1200-1600 LT)

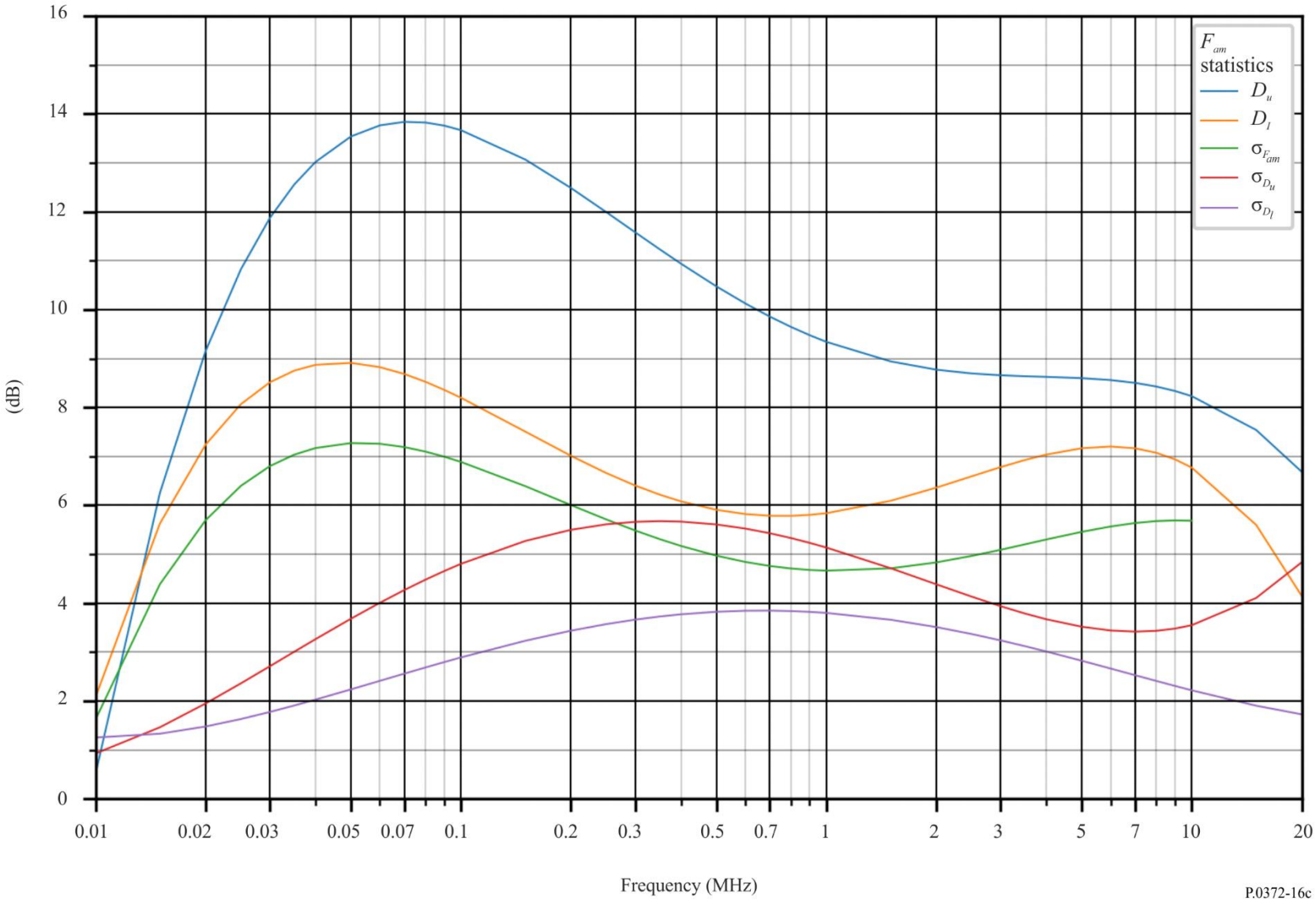

FIGURE 17a

Expected values of atmospheric radio noise, F_{am} (dB above kT_0b at 1 MHz) (Dec-Jan-Feb; 1600-2000 LT)

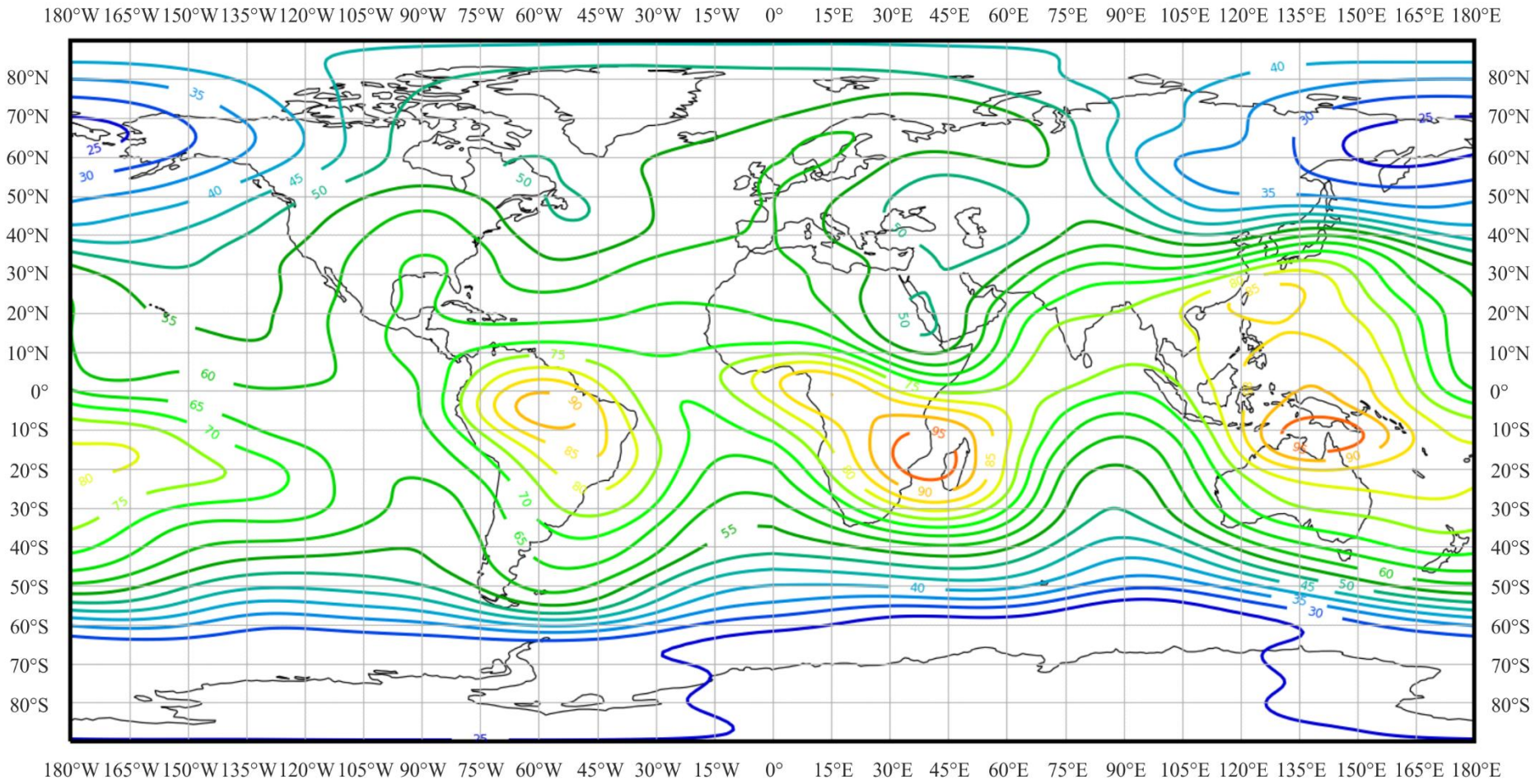

P.0372-17a

FIGURE 17b

Variation of radio noise with frequency (Northern hemisphere: Dec-Jan-Feb; Southern hemisphere: Jun-Jul-Aug; 1600-2000 LT)

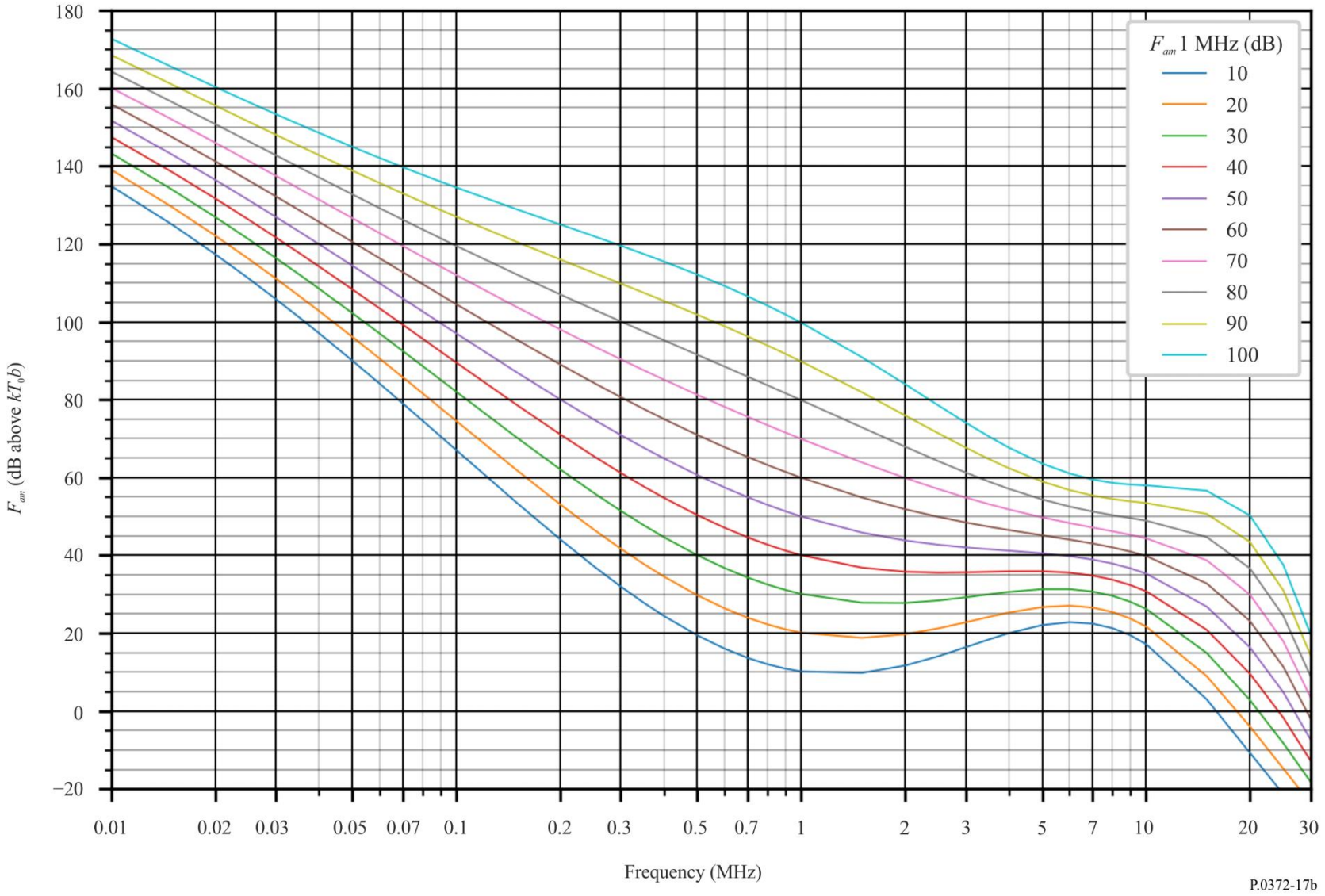

FIGURE 17c

Data on noise variability and character (Northern hemisphere: Dec-Jan-Feb; Southern hemisphere: Jun-Jul-Aug; 1600-2000 LT)

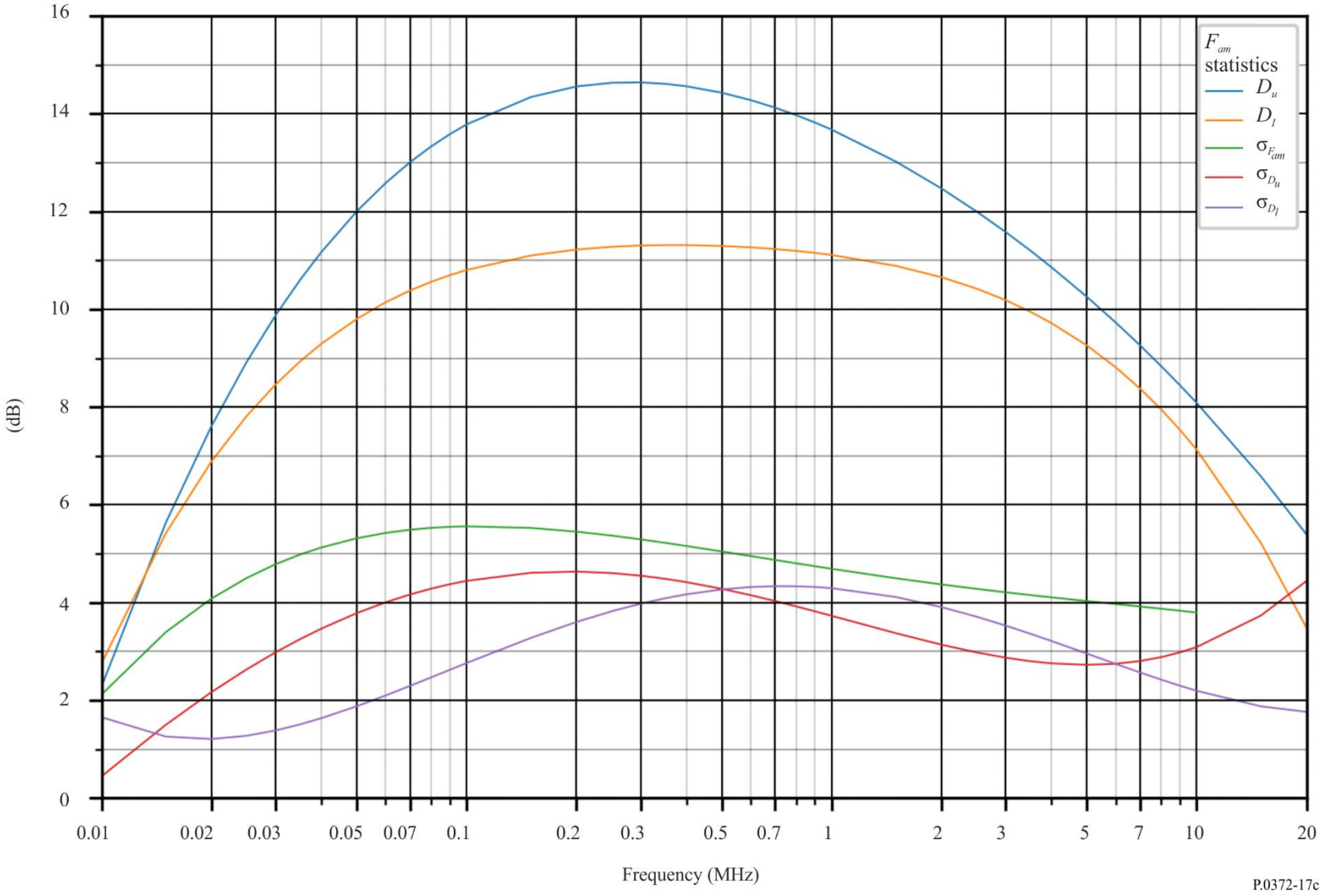

FIGURE 18a

Expected values of atmospheric radio noise, F_{am} (dB above kT_0b at 1 MHz) (Dec-Jan-Feb; 2000-2400 LT)

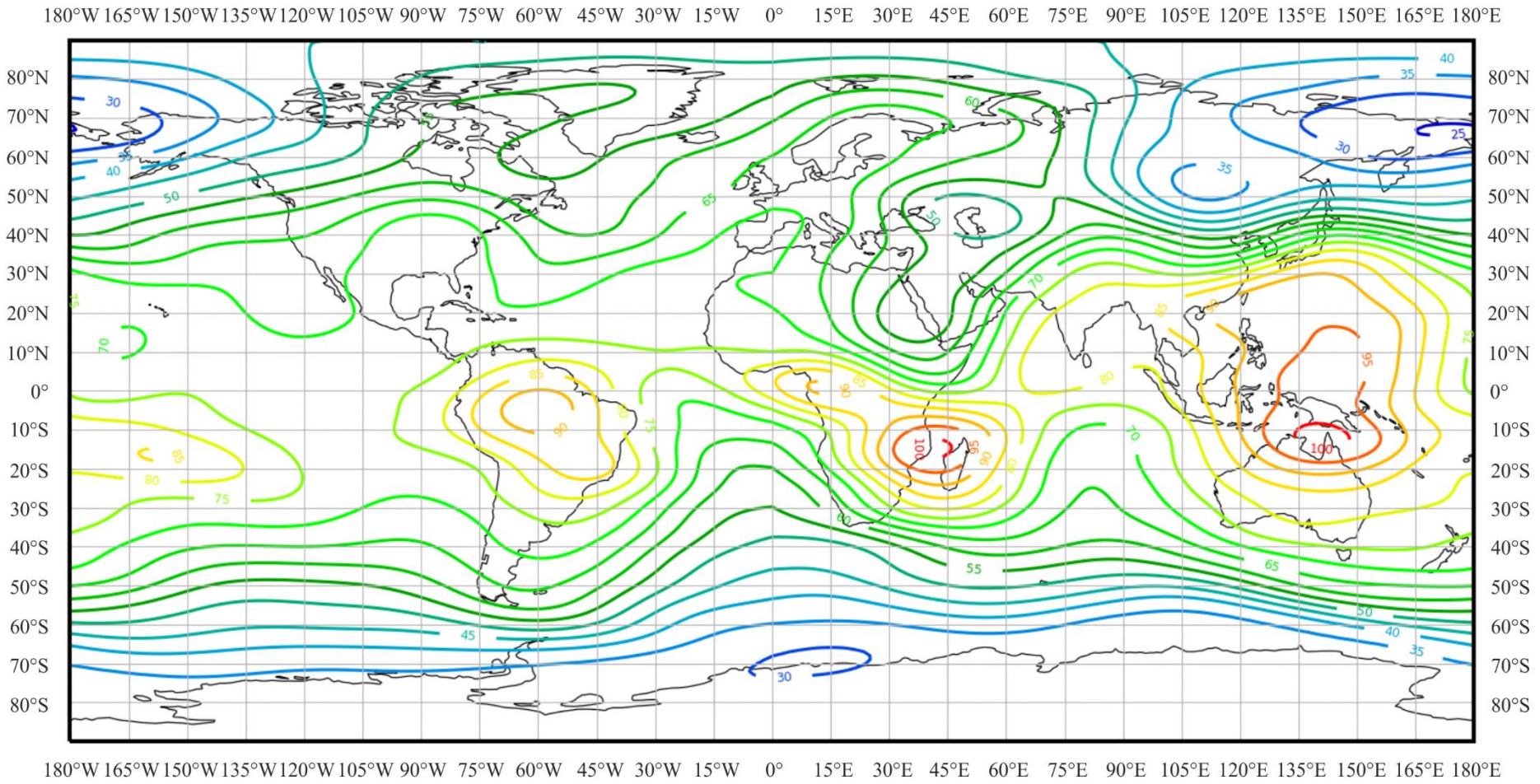

FIGURE 18b

Variation of radio noise with frequency (Northern hemisphere: Dec-Jan-Feb; Southern hemisphere: Jun-Jul-Aug; 2000-2400 LT)

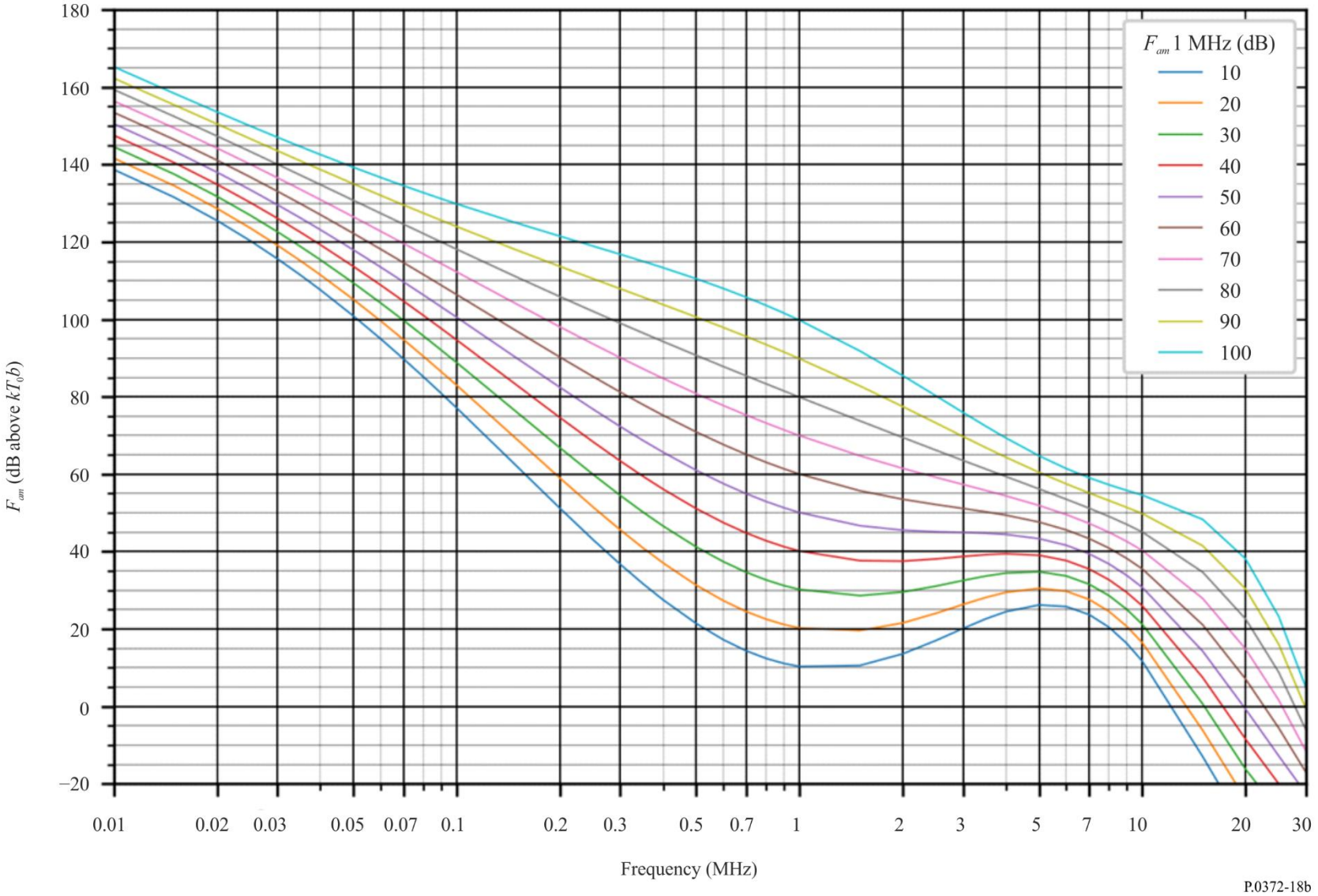

FIGURE 18c

Data on noise variability and character (Northern hemisphere: Dec-Jan-Feb; Southern hemisphere: Jun-Jul-Aug; 2000-2400 LT)

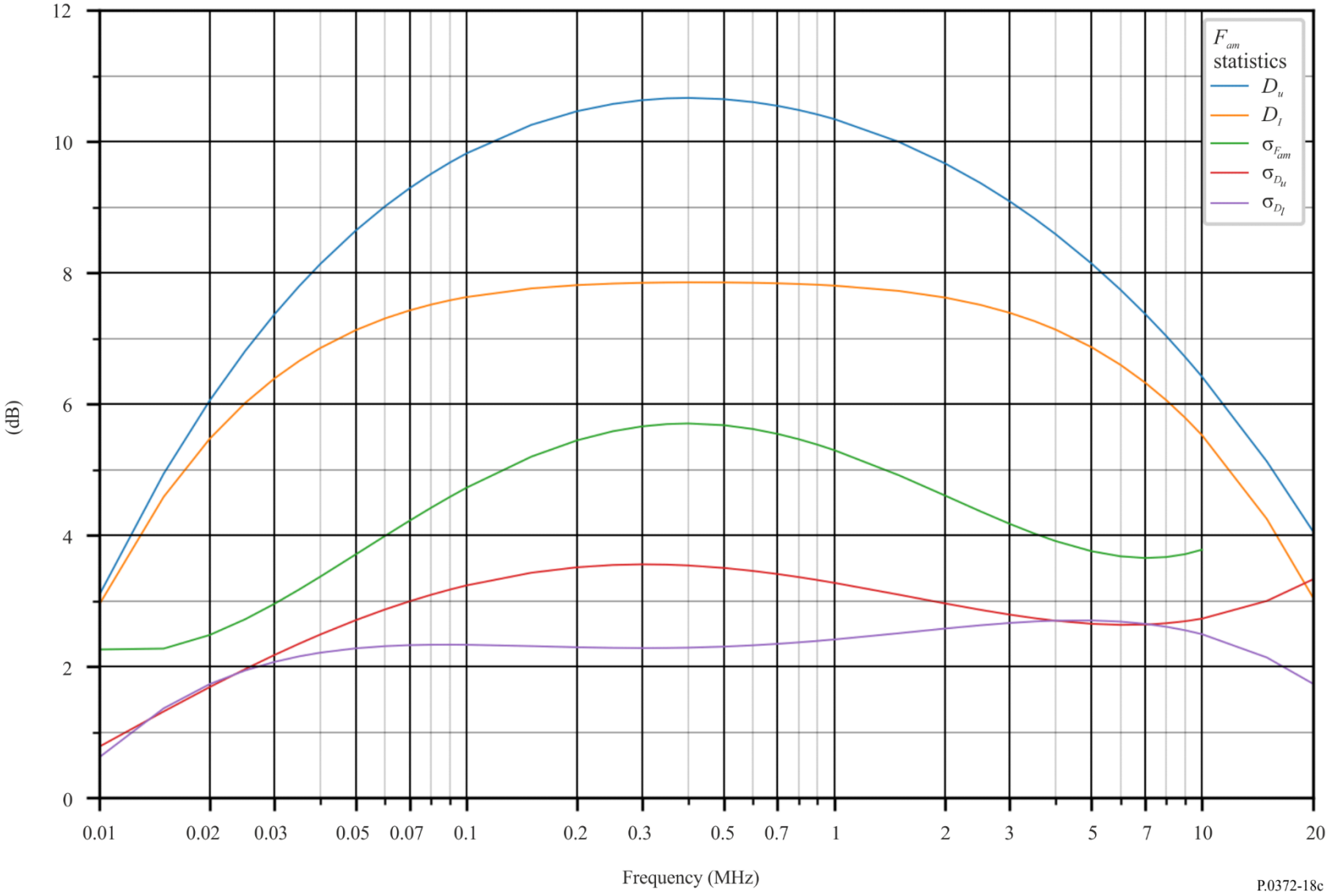

FIGURE 19a

Expected values of atmospheric radio noise, F_{am} (dB above kT_0b at 1 MHz) (Mar-Apr-May; 0000-0400 LT)

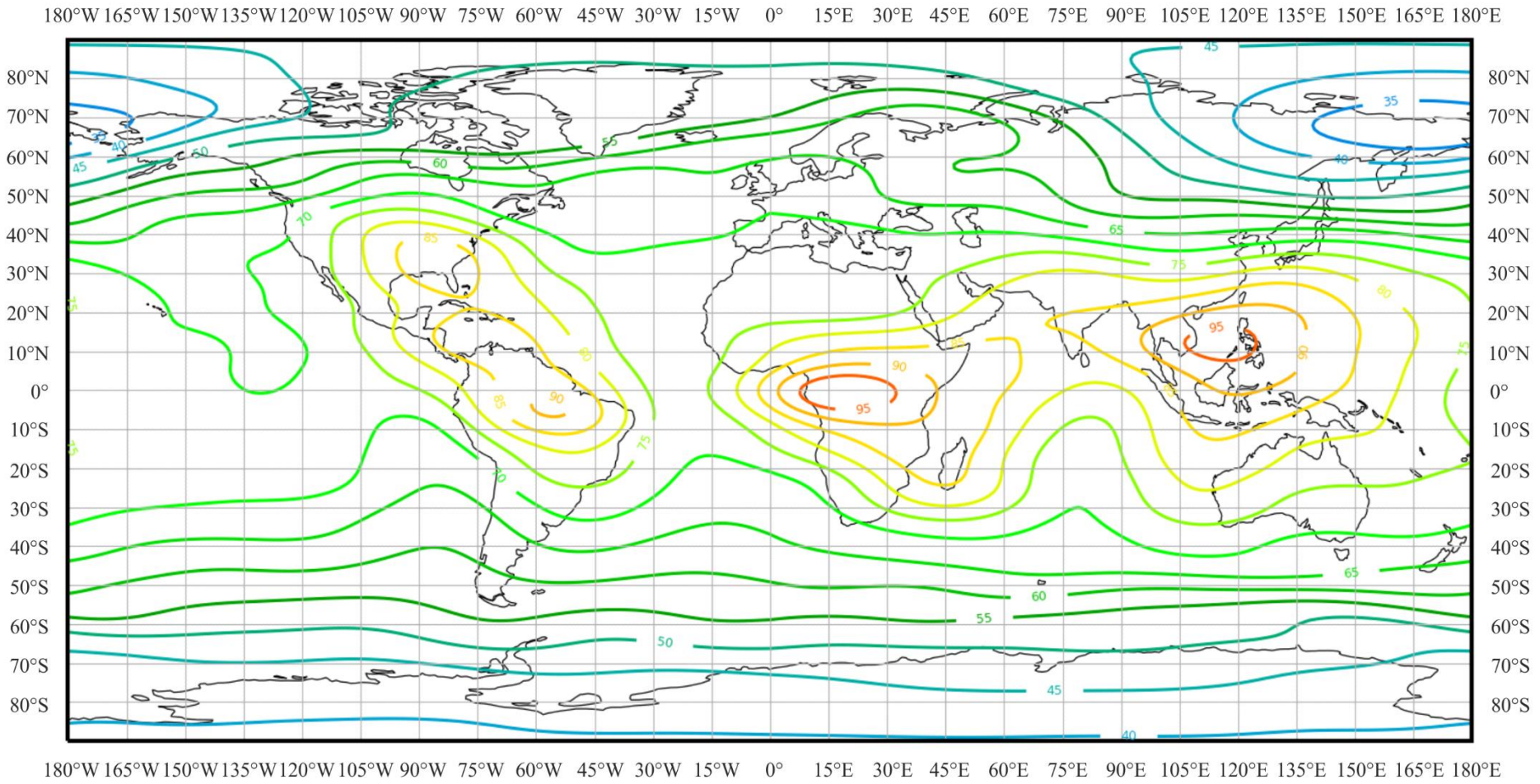

P.0372-19a

FIGURE 19b

Variation of radio noise with frequency (Northern hemisphere: Mar-Apr-May; Southern hemisphere: Sep-Oct-Nov; 0000-0400 LT)

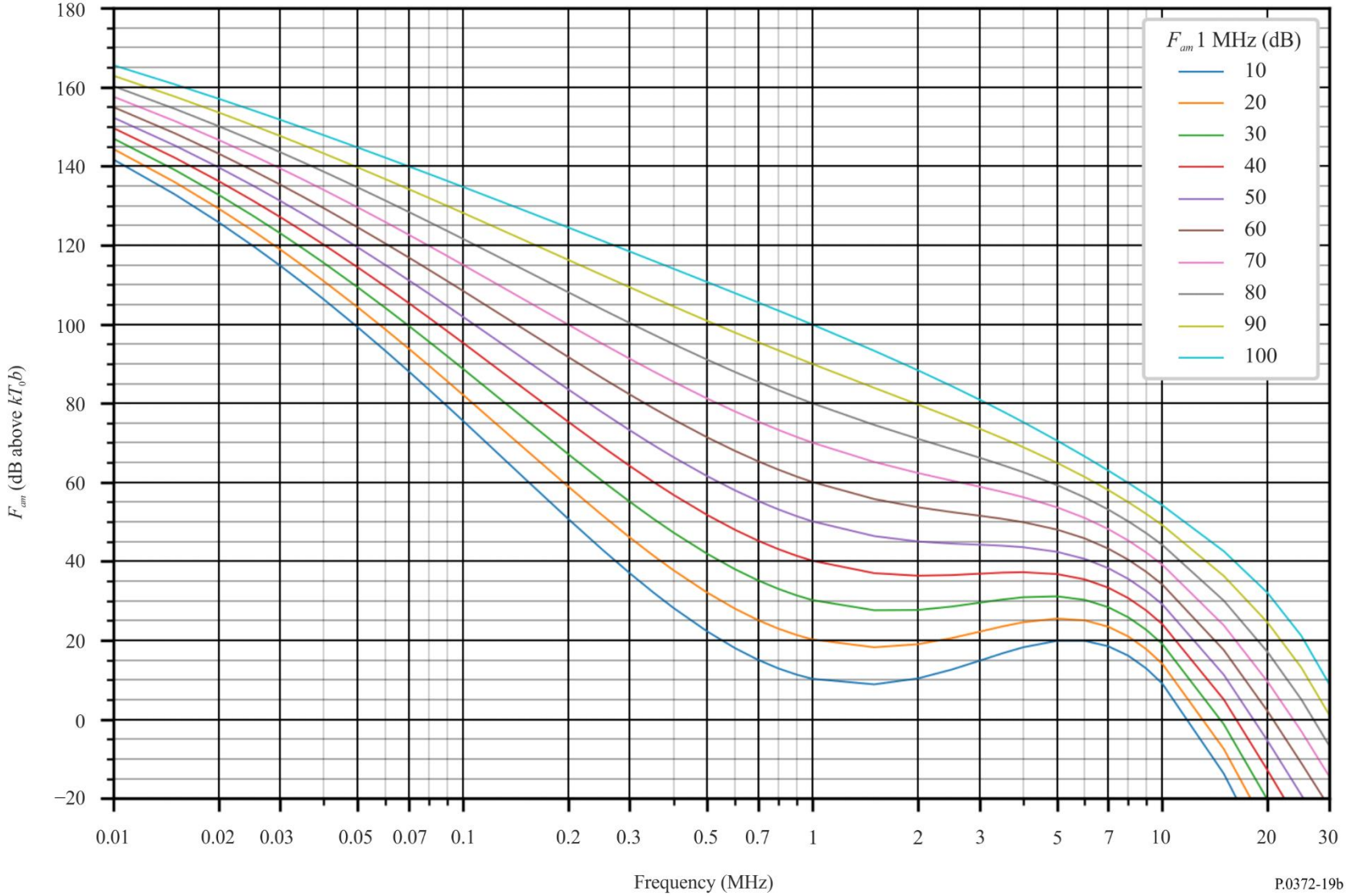

FIGURE 19c

Data on noise variability and character (Northern hemisphere: Mar-Apr-May; Southern hemisphere: Sep-Oct-Nov; 0000-0400 LT)

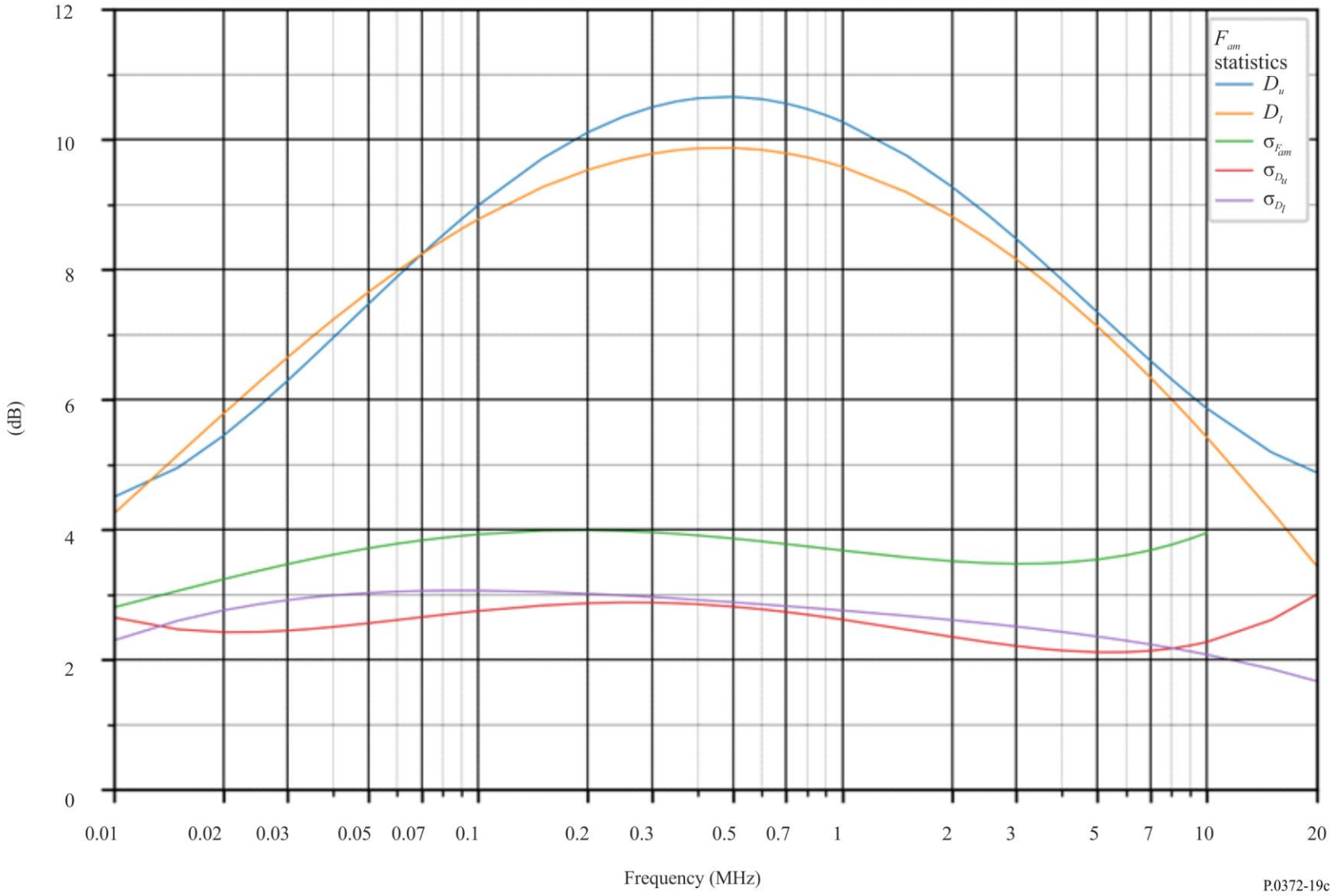

FIGURE 20a

Expected values of atmospheric radio noise, F_{am} (dB above kT_0b at 1 MHz) (Mar-Apr-May; 0400-0800 LT)

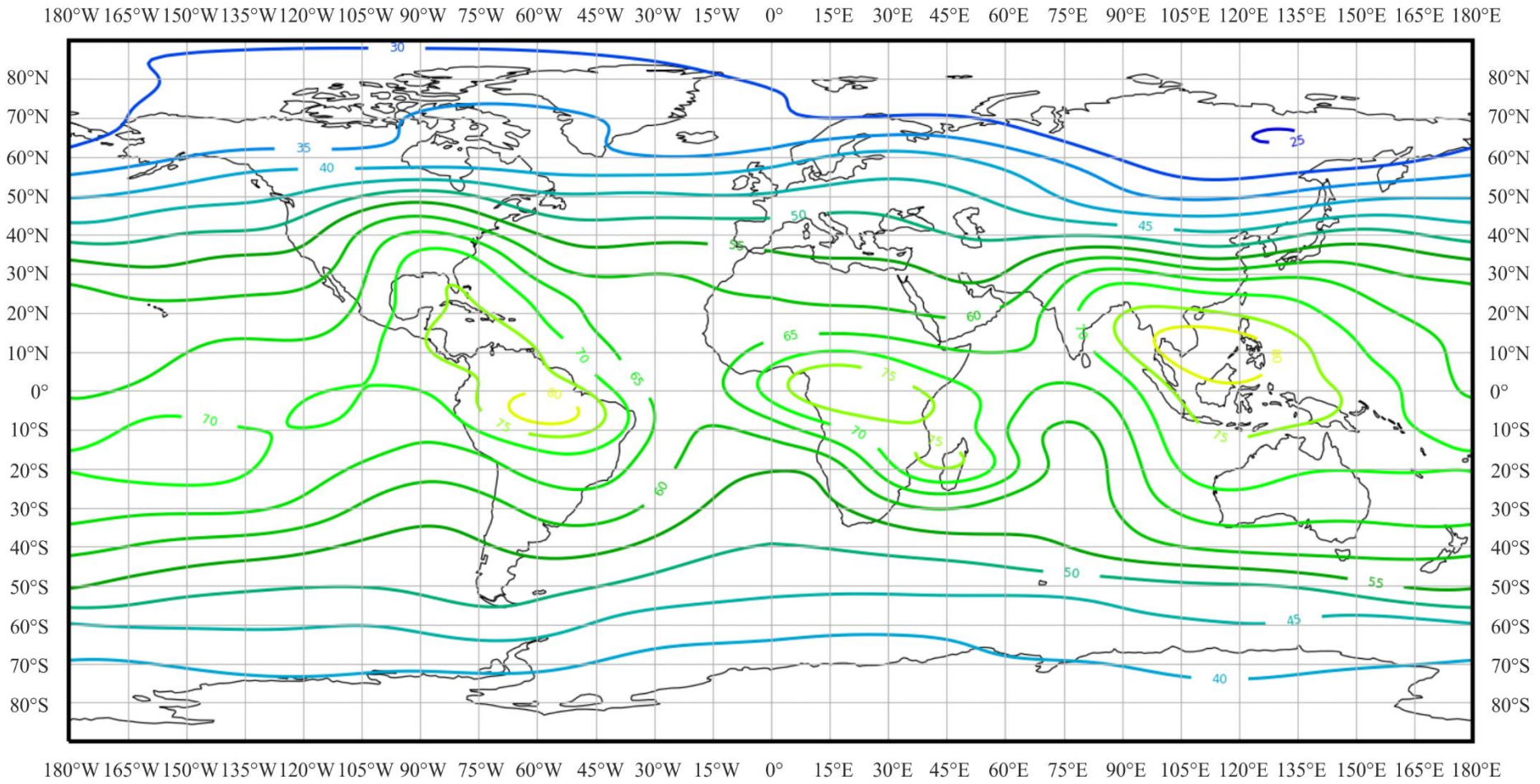

FIGURE 20b

Variation of radio noise with frequency (Northern hemisphere: Mar-Apr-May; Southern hemisphere: Sep-Oct-Nov; 0400-0800 LT)

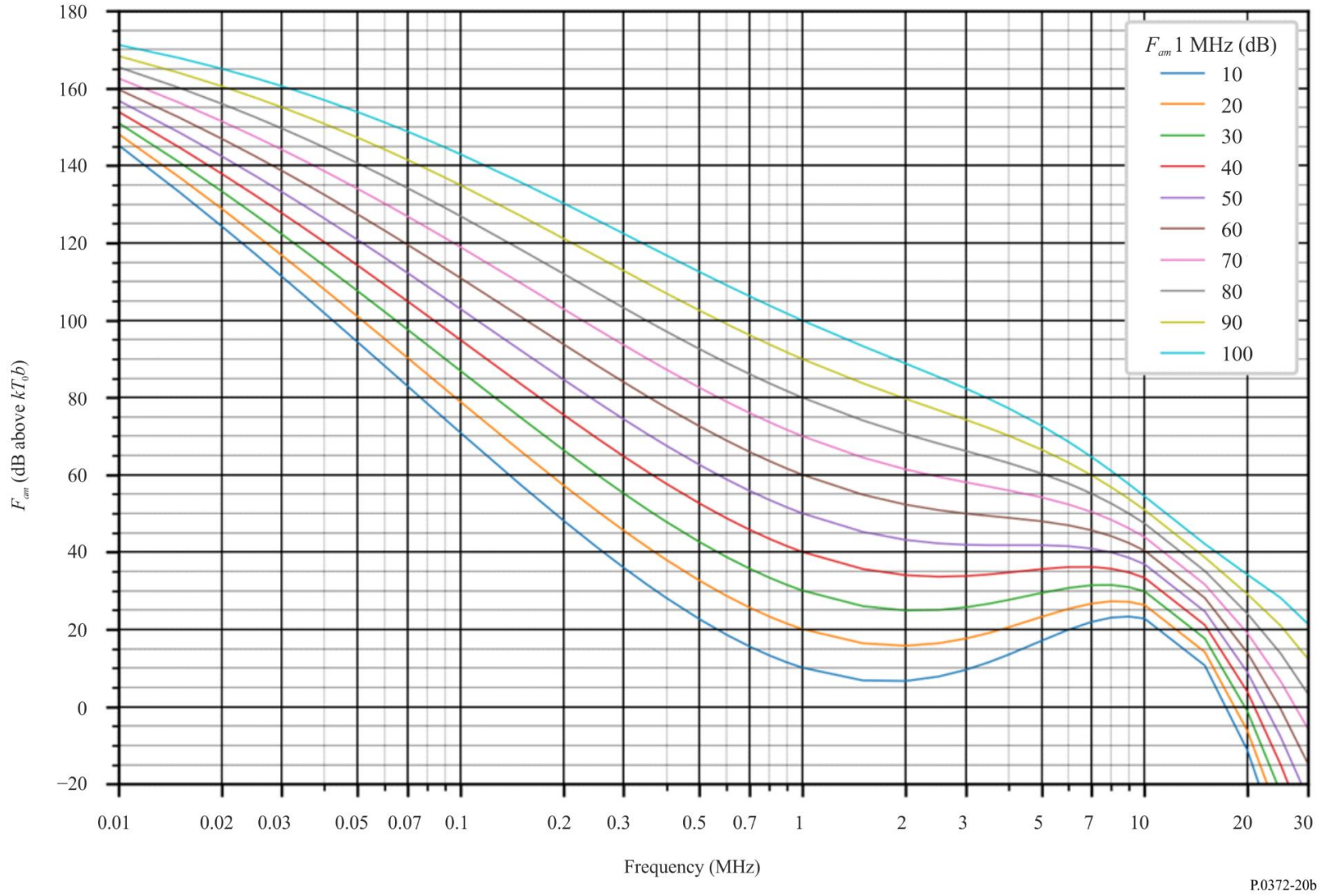

FIGURE 20c

Data on noise variability and character (Northern hemisphere: Mar-Apr-May; Southern hemisphere: Sep-Oct-Nov; 0400-0800 LT)

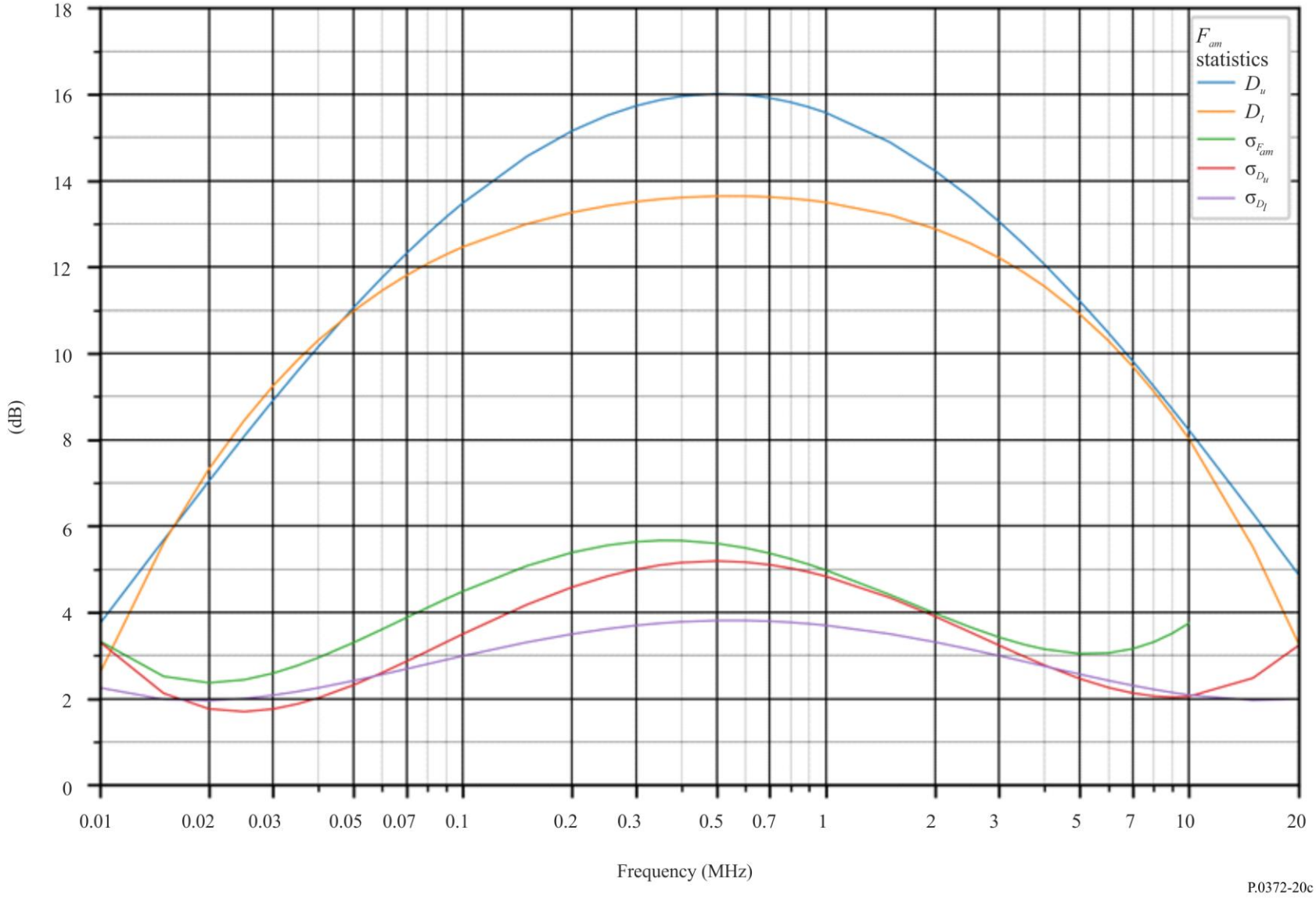

FIGURE 21a

Expected values of atmospheric radio noise, F_{am} (dB above kT_0b at 1 MHz) (Mar-Apr-May; 0800-1200 LT)

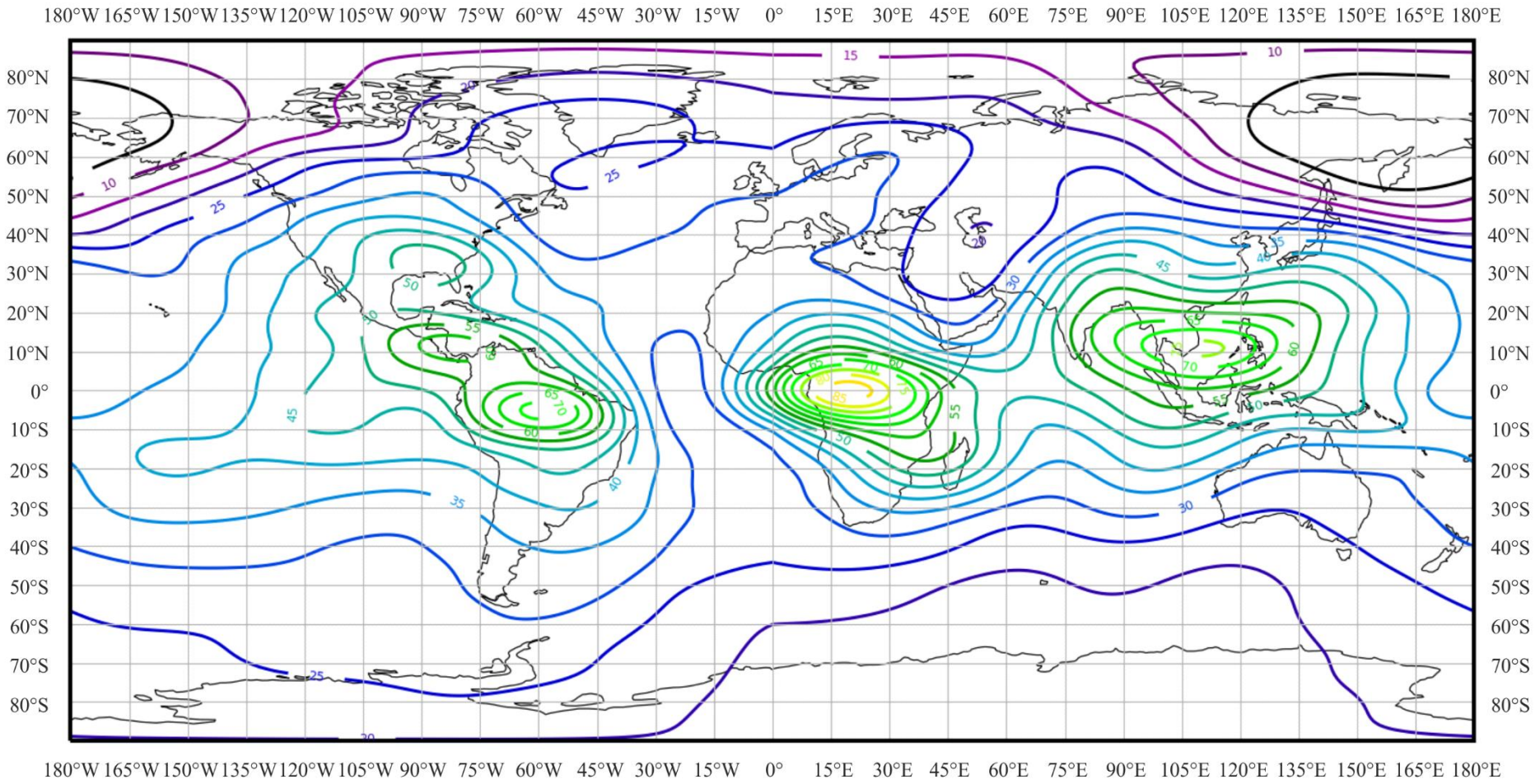

FIGURE 21b

Variation of radio noise with frequency (Northern hemisphere: Mar-Apr-May; Southern hemisphere: Sep-Oct-Nov; 0800-1200 LT)

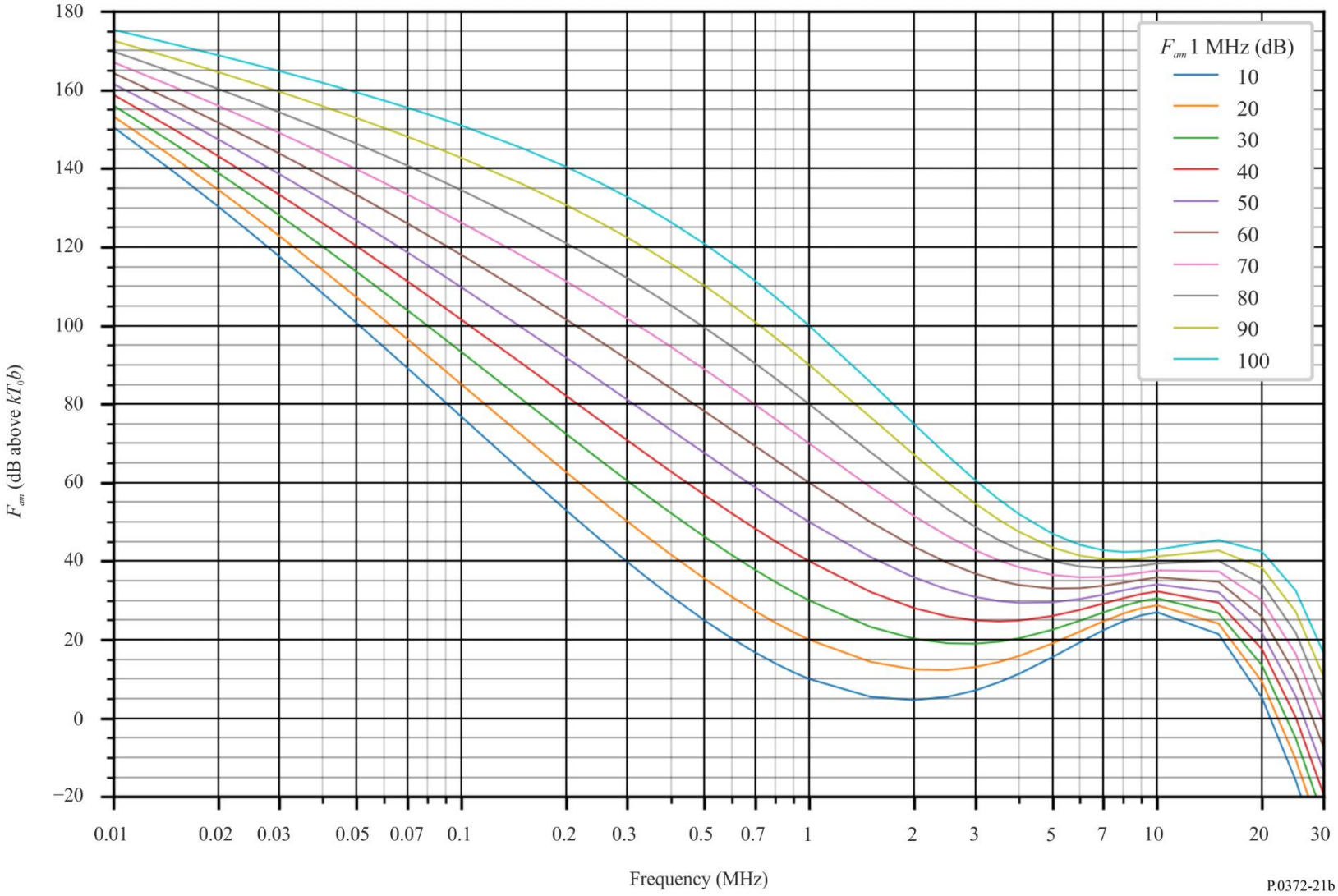

FIGURE 21c

Data on noise variability and character (Northern hemisphere: Mar-Apr-May; Southern hemisphere: Sep-Oct-Nov; 0800-1200 LT)

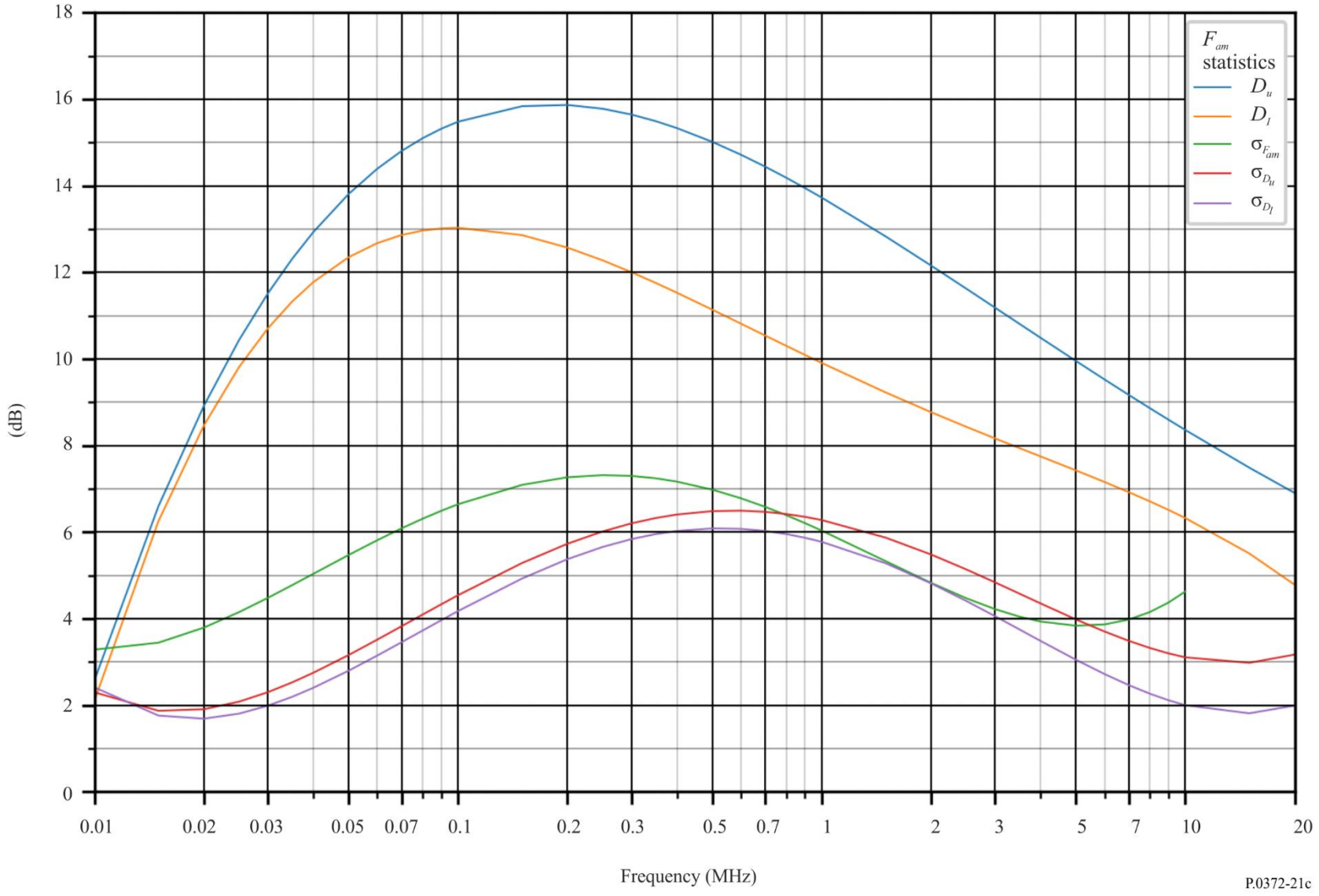

FIGURE 22a

Expected values of atmospheric radio noise, F_{am} (dB above kT_0b at 1 MHz) (Mar-Apr-May; 1200-1600 LT)

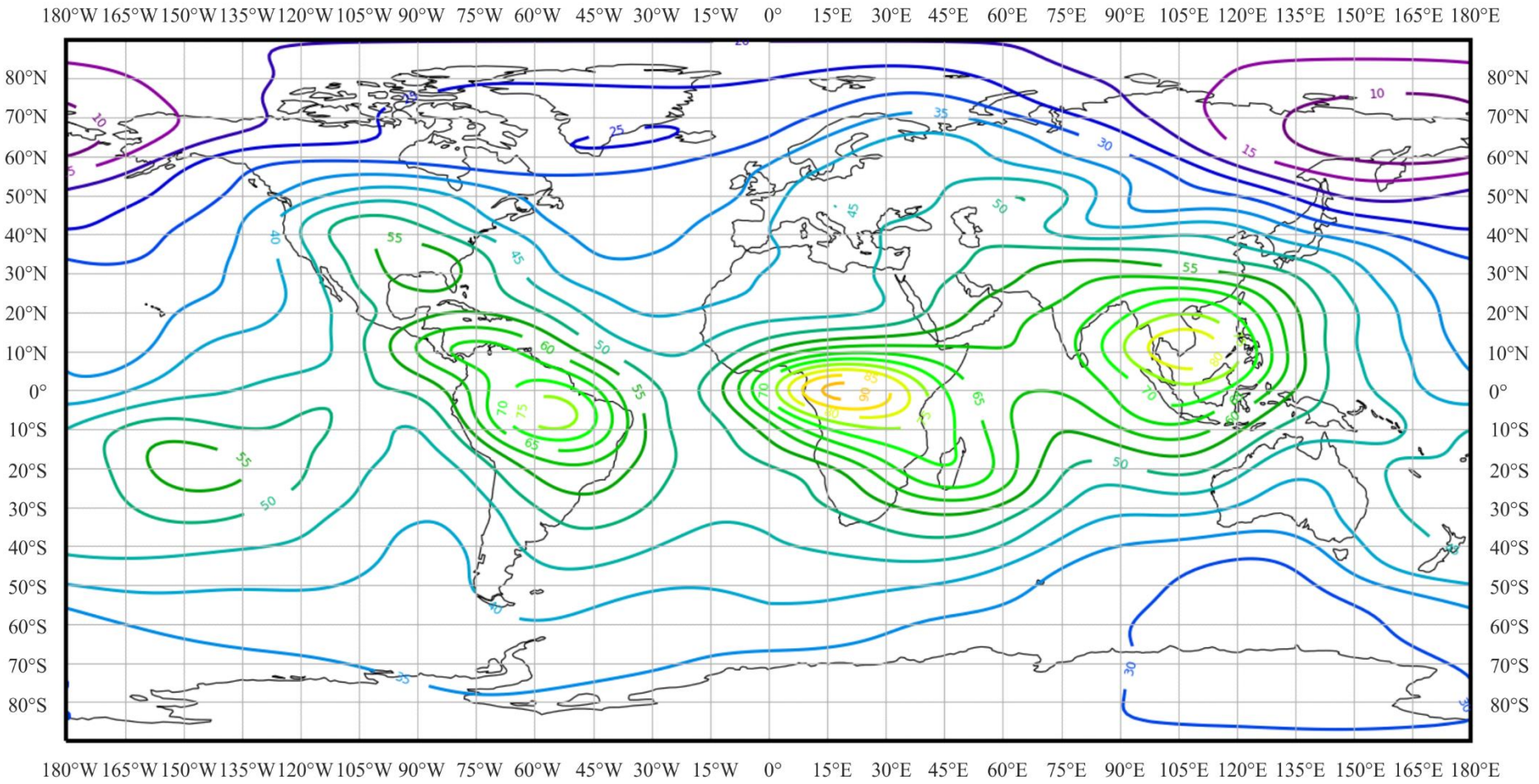

P.0372-22a

FIGURE 22b

Variation of radio noise with frequency (Northern hemisphere: Mar-Apr-May; Southern hemisphere: Sep-Oct-Nov; 1200-1600 LT)

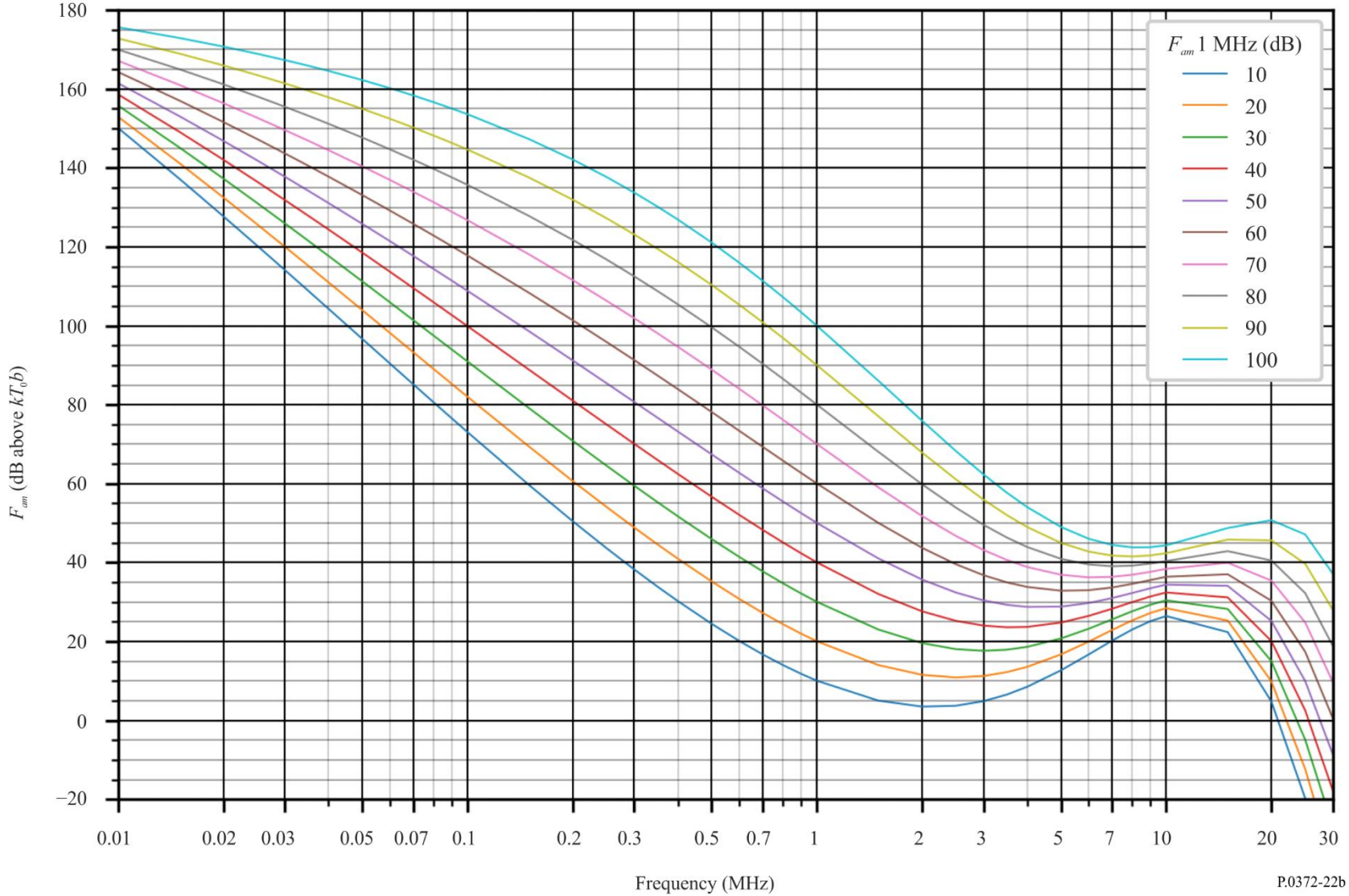

FIGURE 22c

Data on noise variability and character (Northern hemisphere: Mar-Apr-May; Southern hemisphere: Sep-Oct-Nov; 1200-1600 LT)

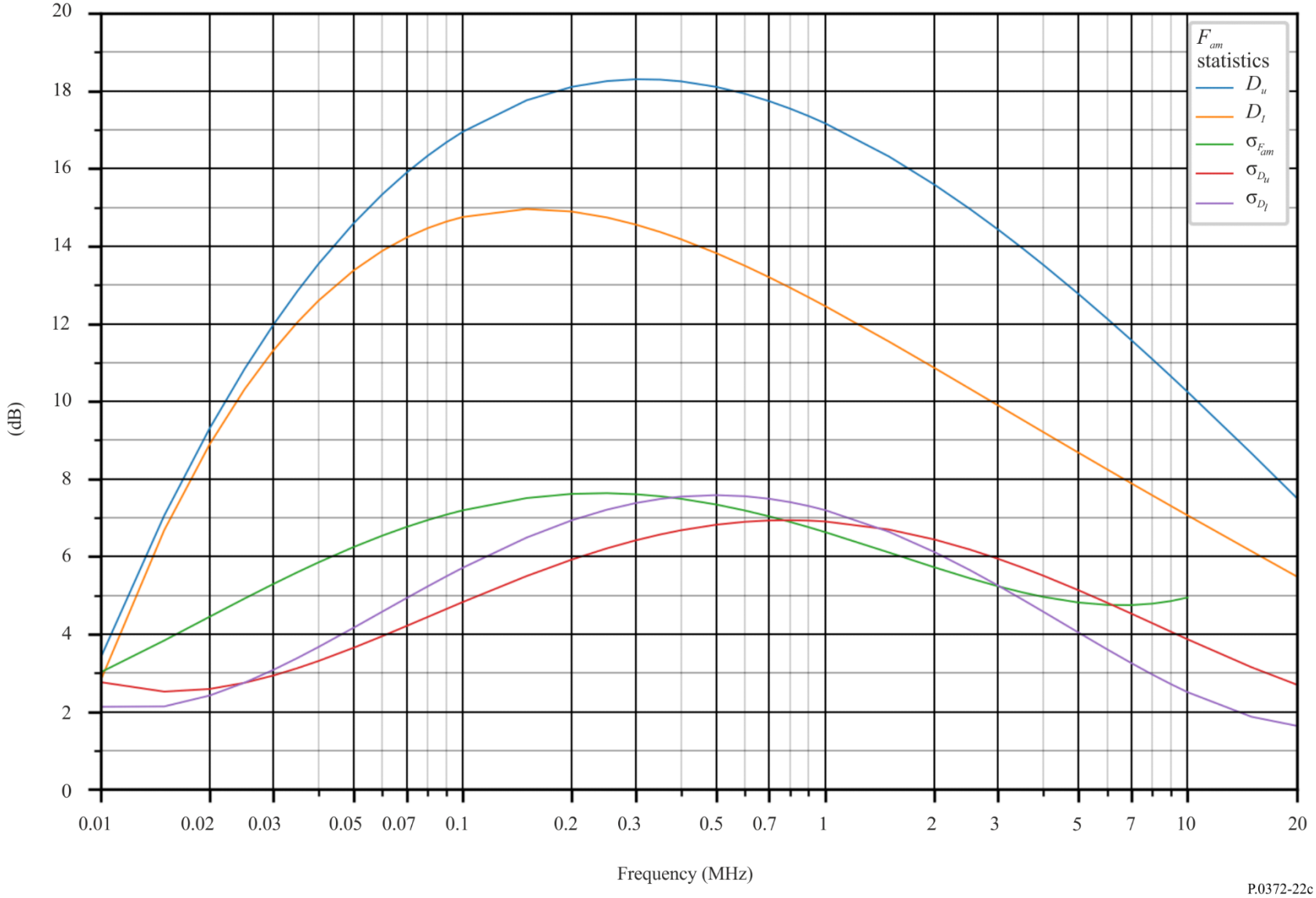

FIGURE 23a

Expected values of atmospheric radio noise, F_{am} (dB above kT_0b at 1 MHz) (Mar-Apr-May; 1600-2000 LT)

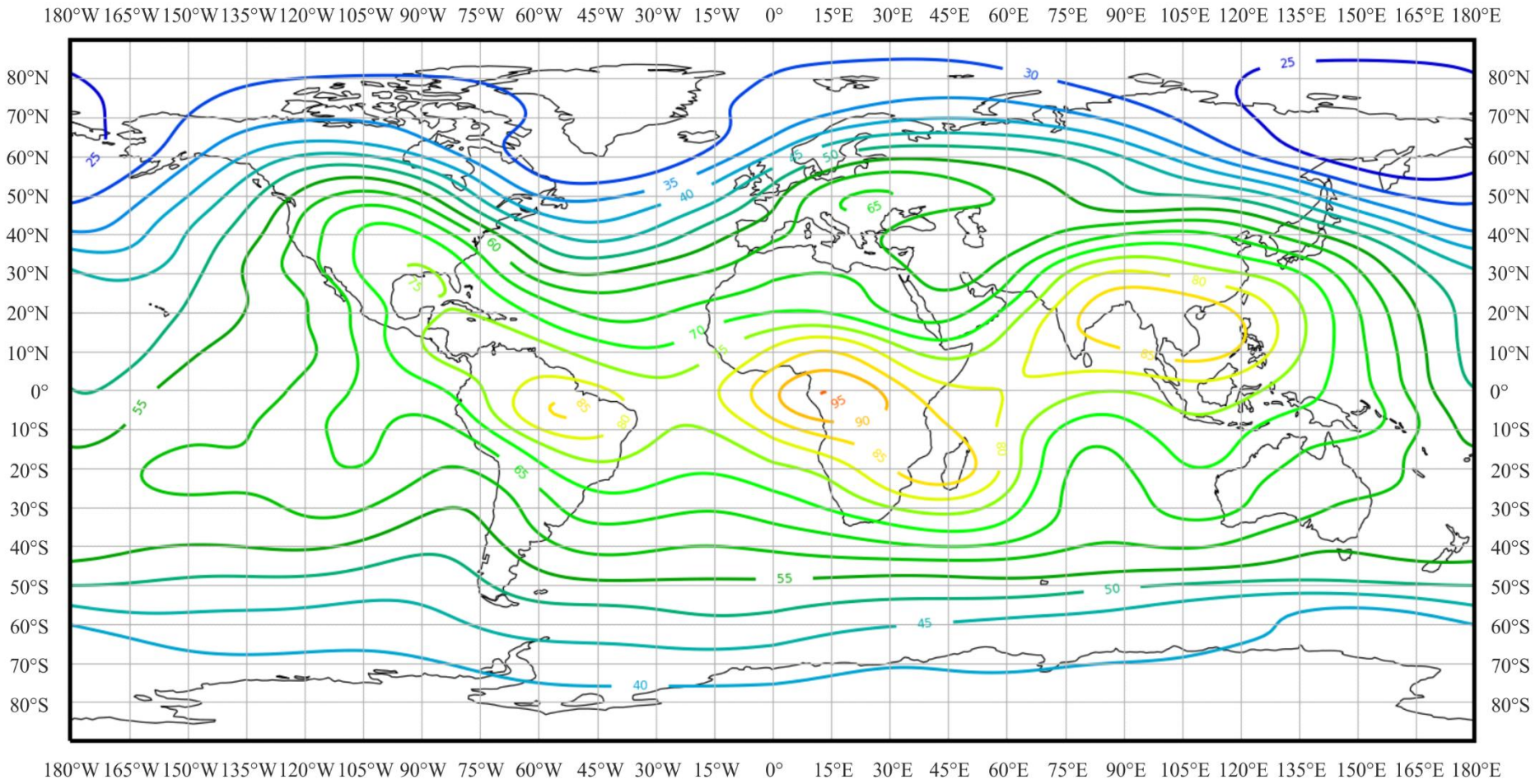

P.0372-23a

FIGURE 23b

Variation of radio noise with frequency (Northern hemisphere: Mar-Apr-May; Southern hemisphere: Sep-Oct-Nov; 1600-2000 LT)

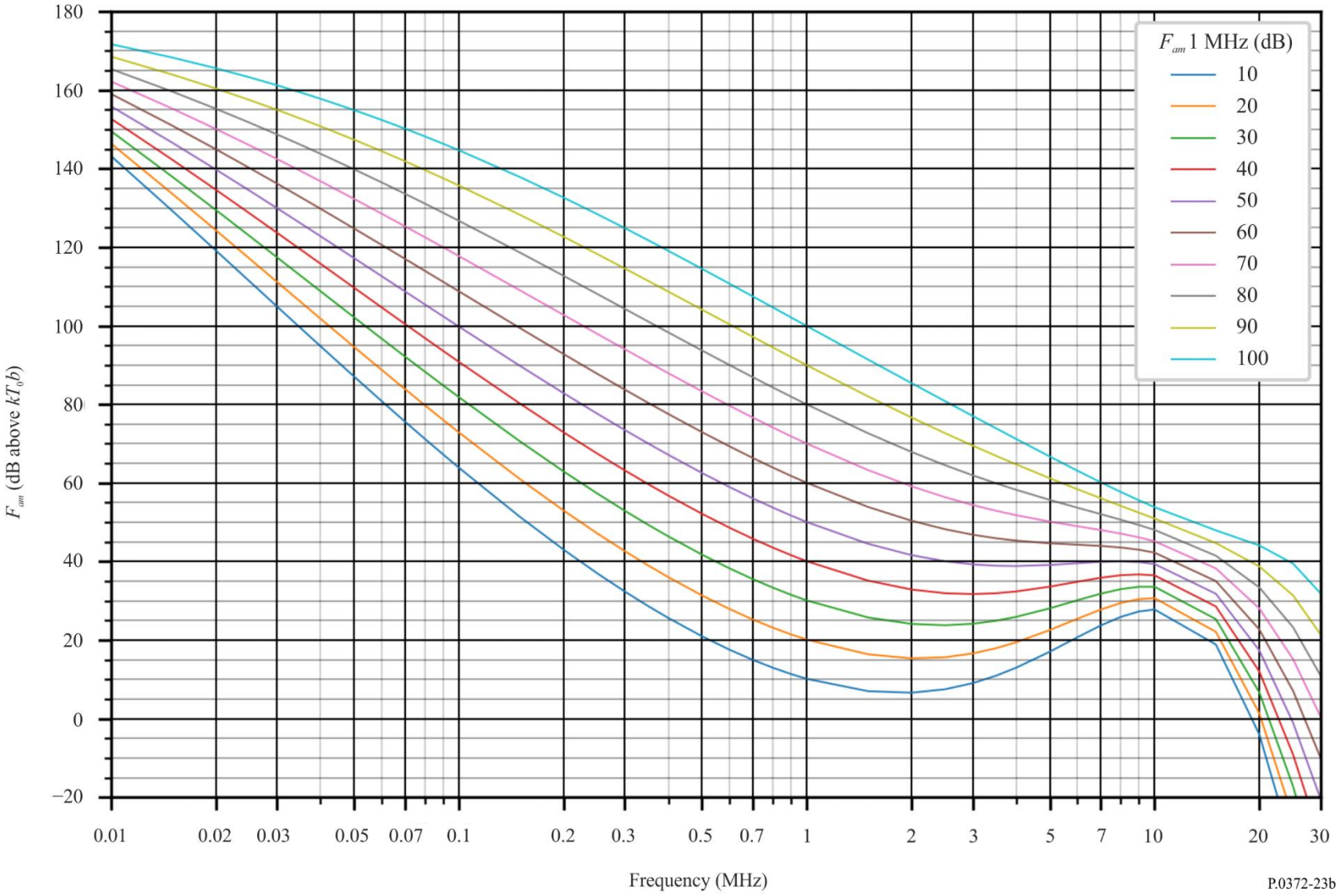

FIGURE 23c

Data on noise variability and character (Northern hemisphere: Mar-Apr-May; Southern hemisphere: Sep-Oct-Nov;1600-2000 LT)

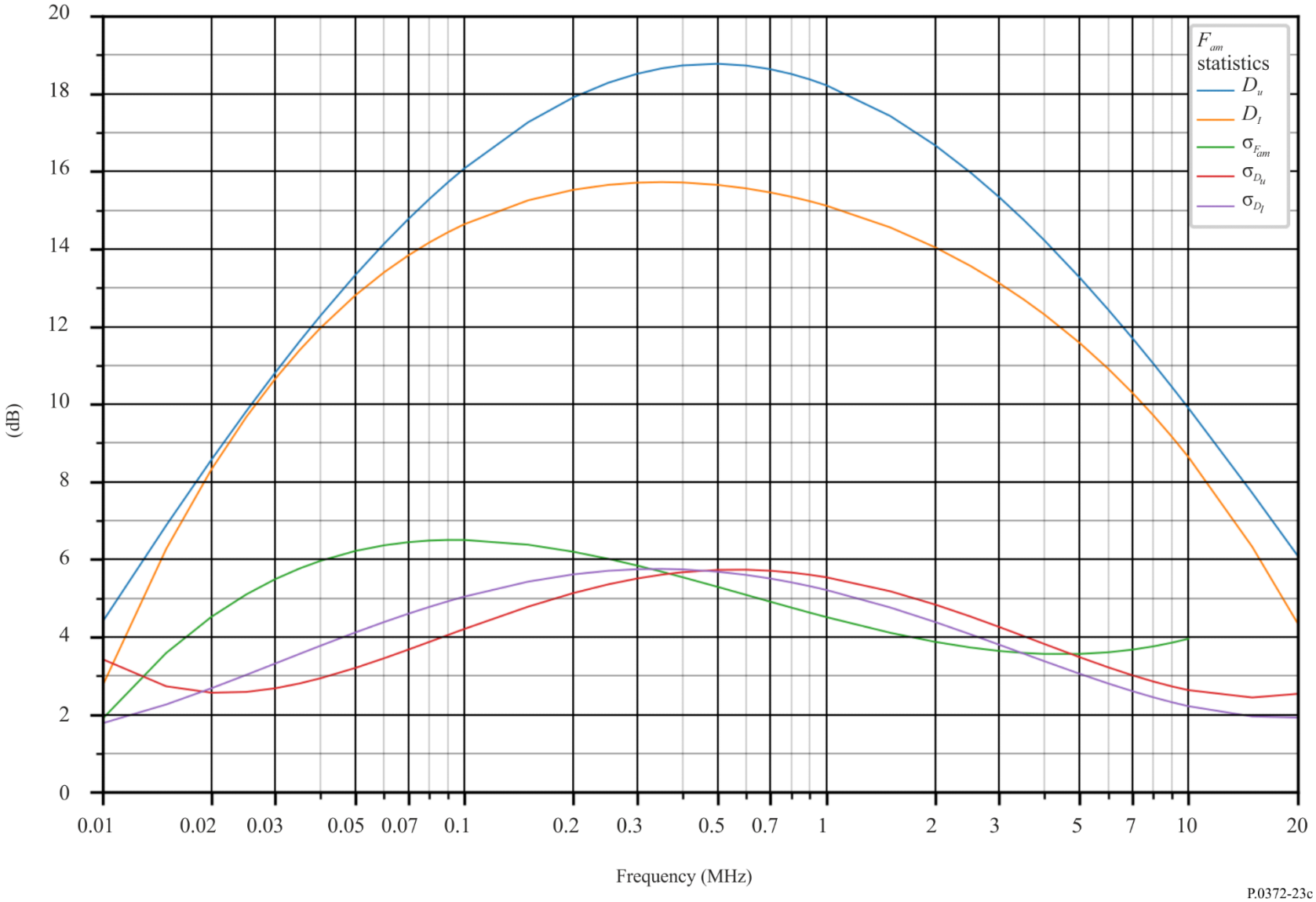

FIGURE 24a

Expected values of atmospheric radio noise, F_{am} (dB above kT_0b at 1 MHz) (Mar-Apr-May; 2000-2400 LT)

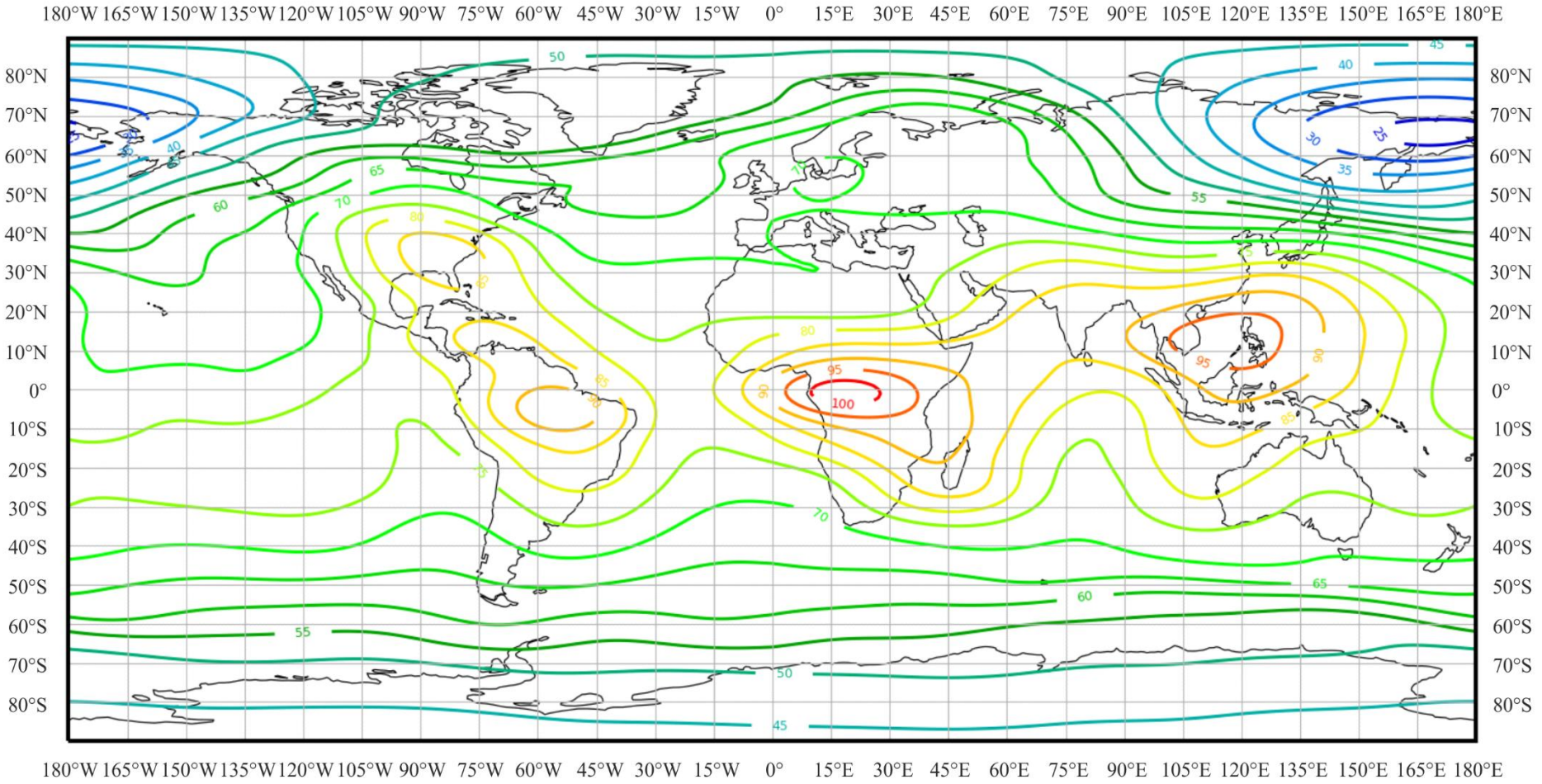

P.0372-24a

FIGURE 24b

Variation of radio noise with frequency (Northern hemisphere: Mar-Apr-May; Southern hemisphere: Sep-Oct-Nov; 2000-2400 LT)

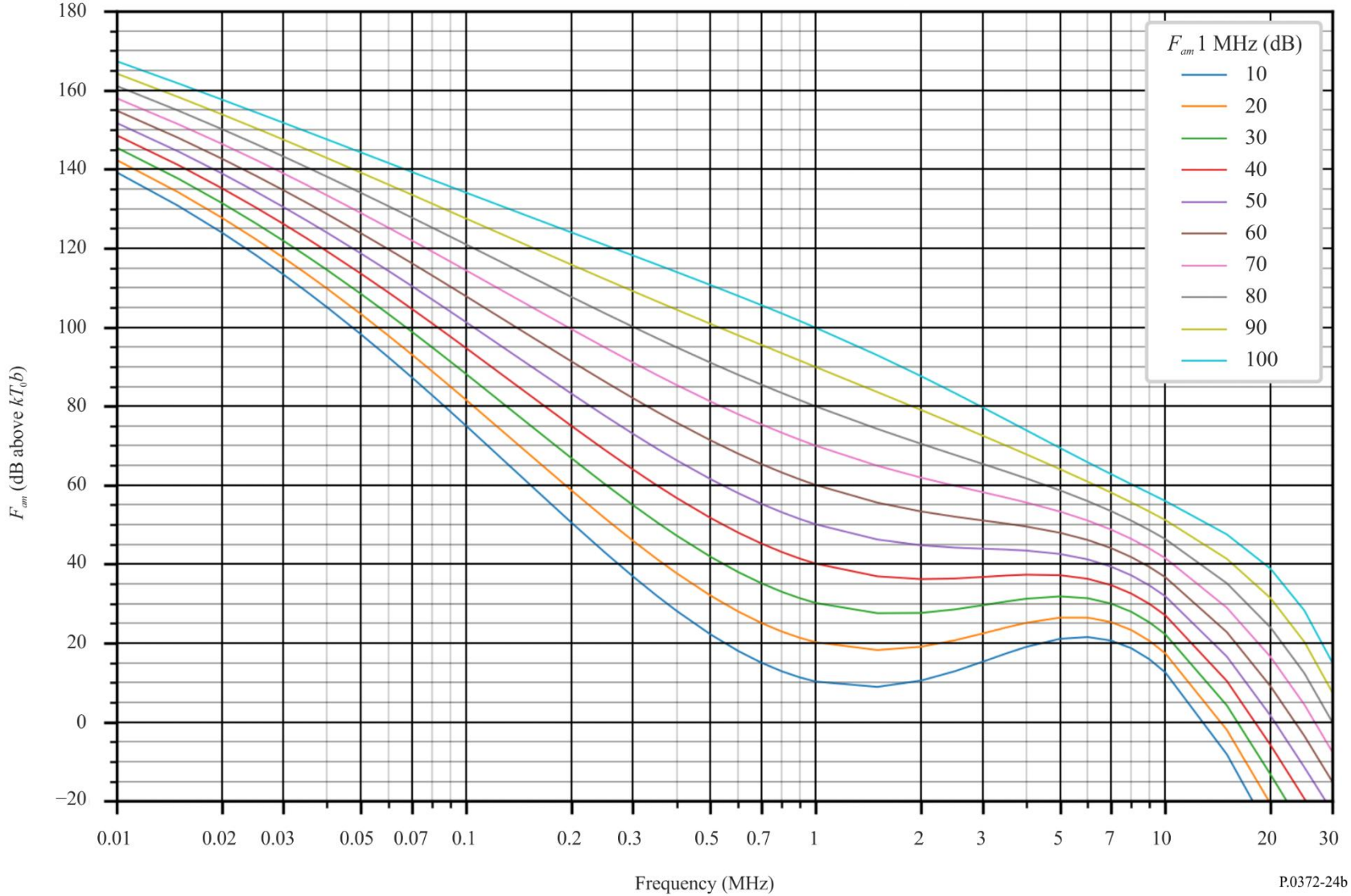

FIGURE 24c

Data on noise variability and character (Northern hemisphere: Mar-Apr-May; Southern hemisphere: Sep-Oct-Nov; 2000-2400 LT)

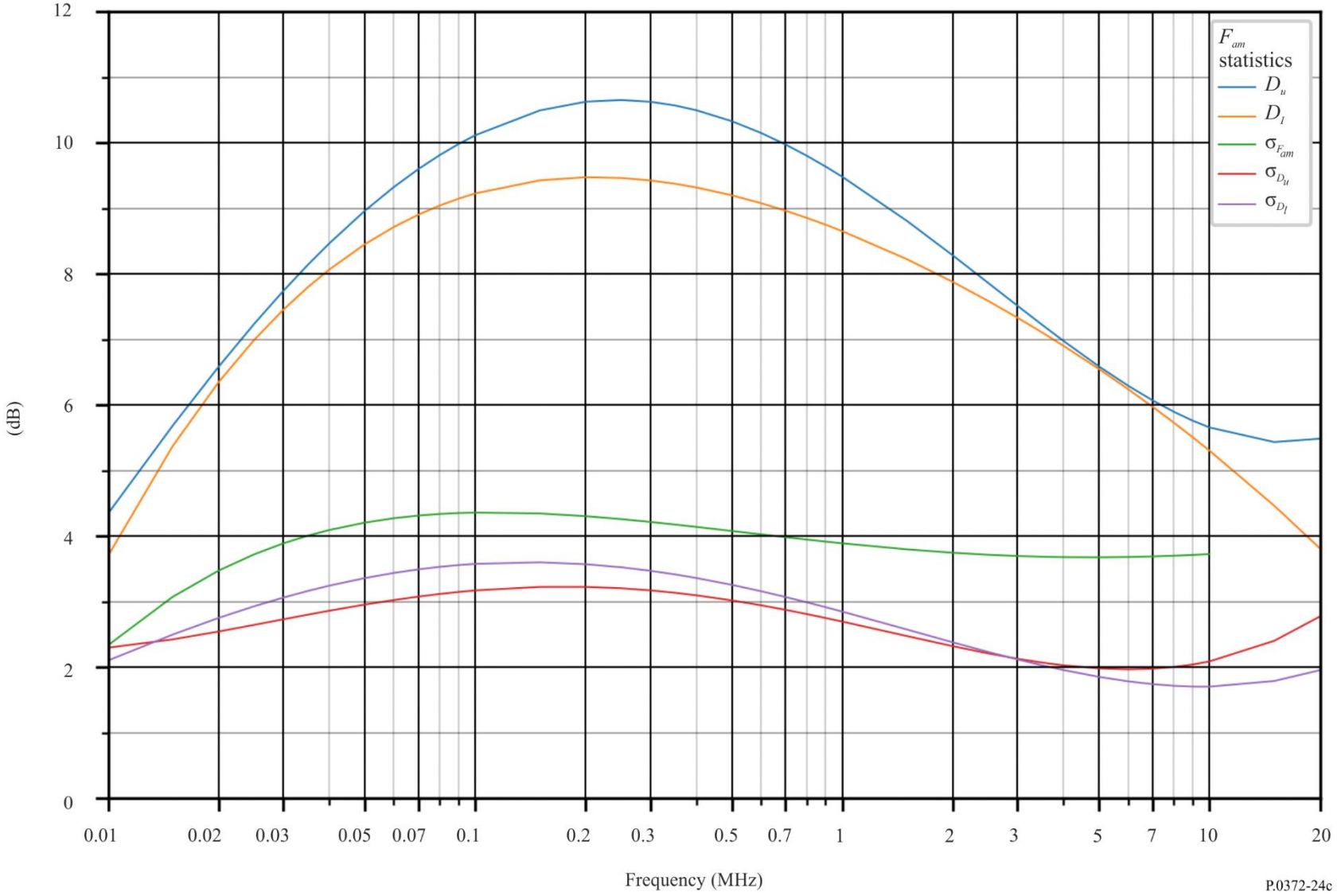

FIGURE 25a

Expected values of atmospheric radio noise, F_{am} (dB above kT_0b at 1 MHz) (Jun-Jul-Aug; 0000-0400 LT)

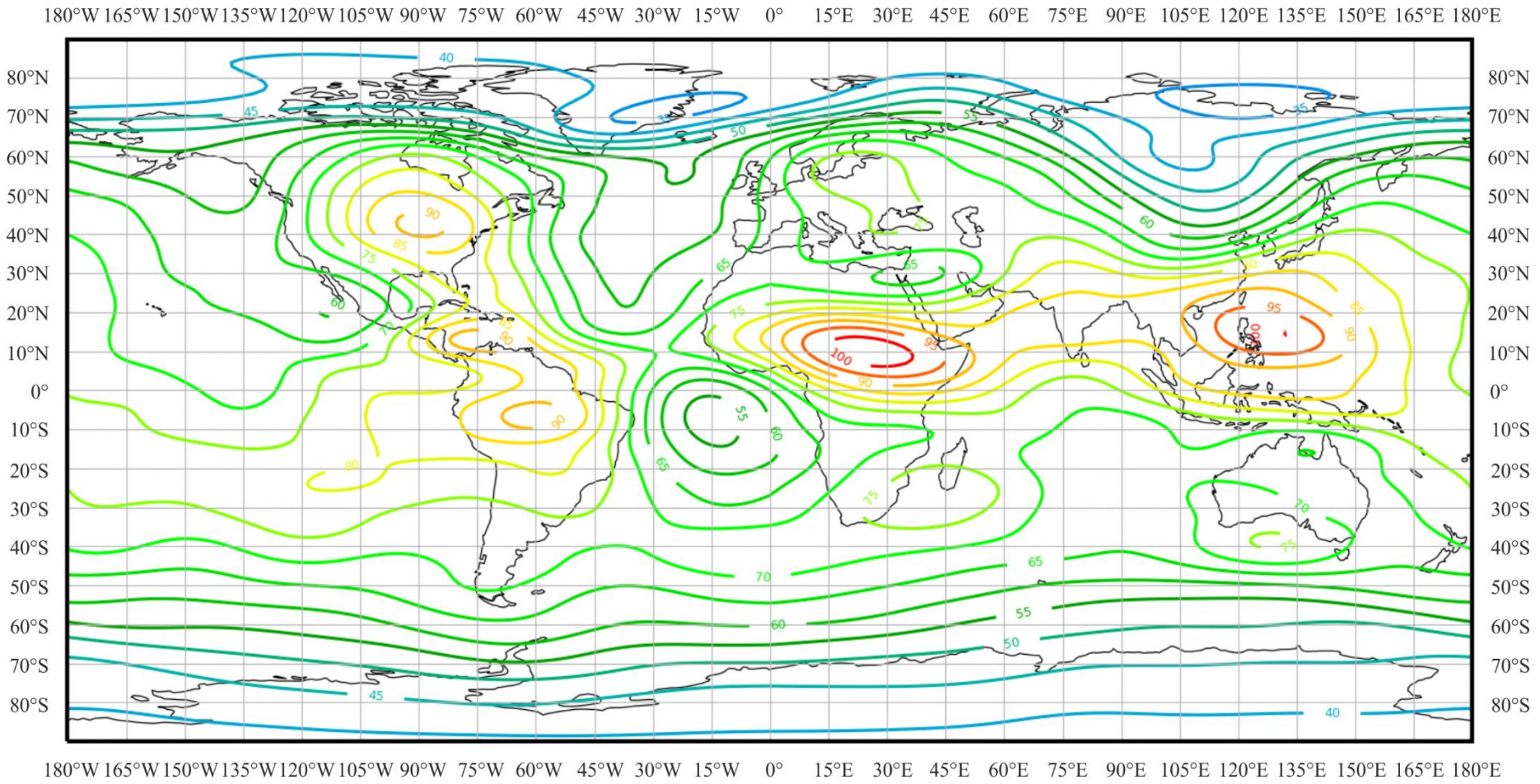

FIGURE 25b

Variation of radio noise with frequency (Northern hemisphere: Jun-Jul-Aug; Southern hemisphere: Dec-Jan-Feb; 0000-0400 LT)

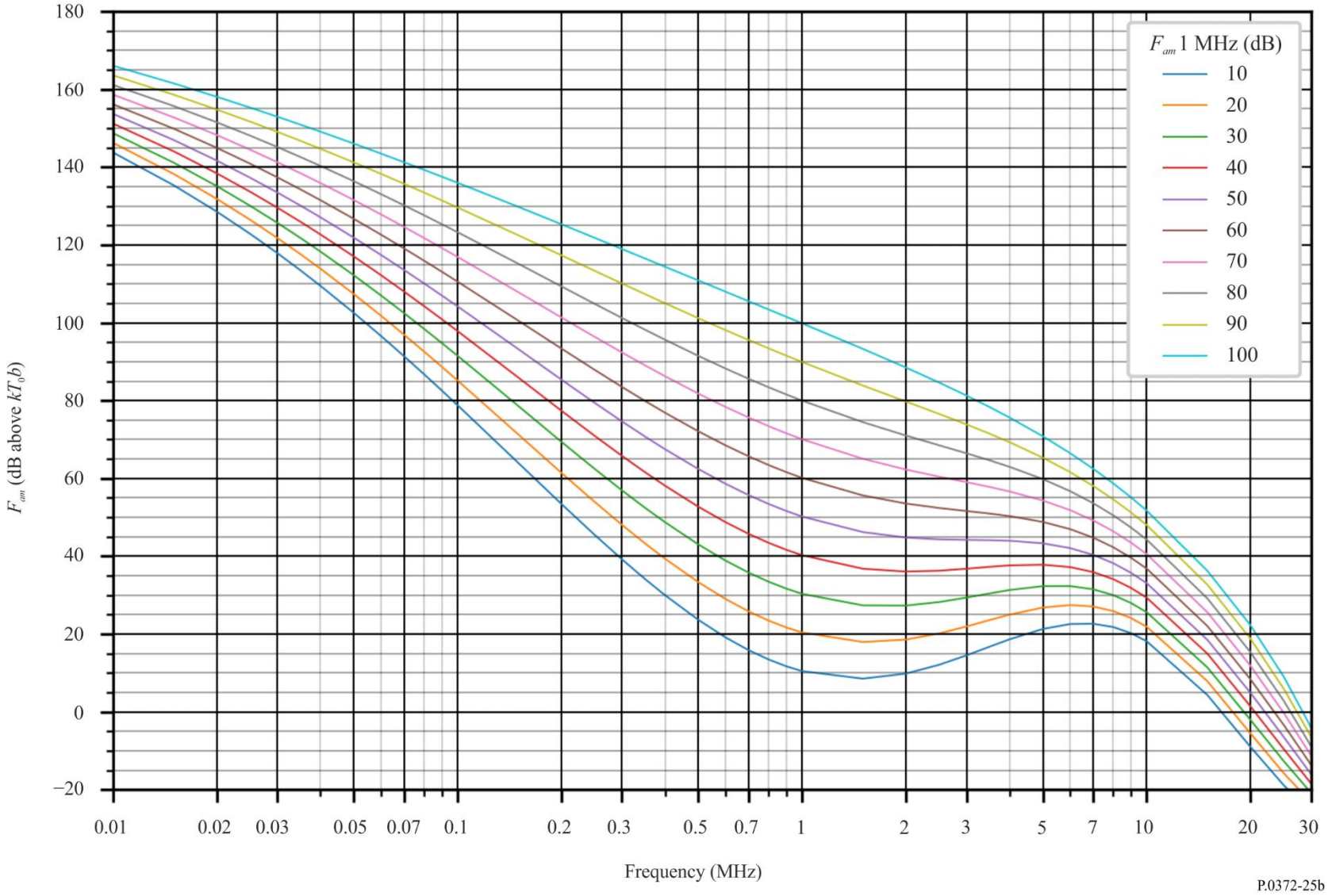

FIGURE 25c

Data on noise variability and character (Northern hemisphere: Jun-Jul-Aug; Southern hemisphere: Dec-Jan-Feb; 0000-0400 LT)

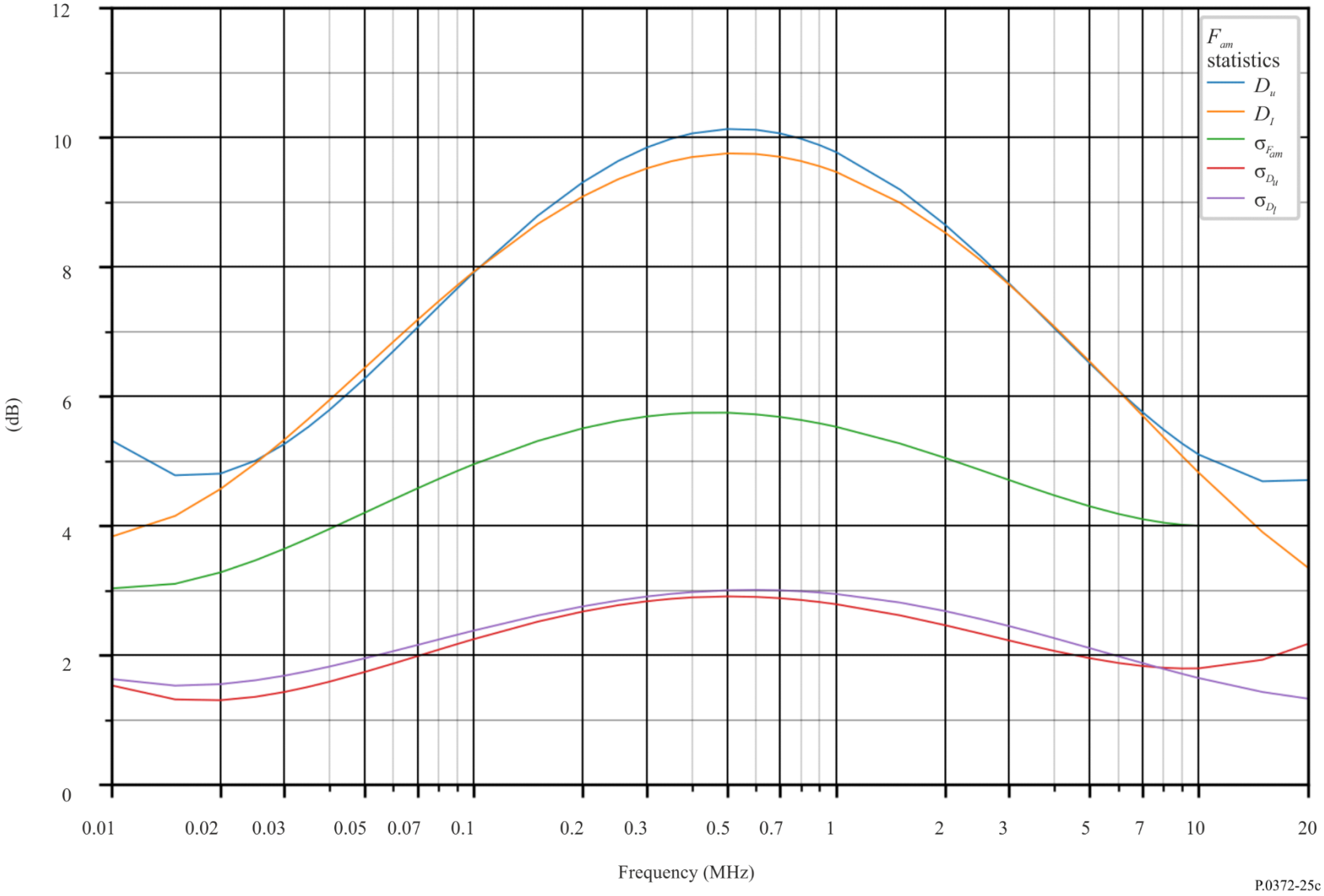

FIGURE 26a

Expected values of atmospheric radio noise, F_{am} (dB above kT_0b at 1 MHz) (Jun-Jul-Aug; 0400-0800 LT)

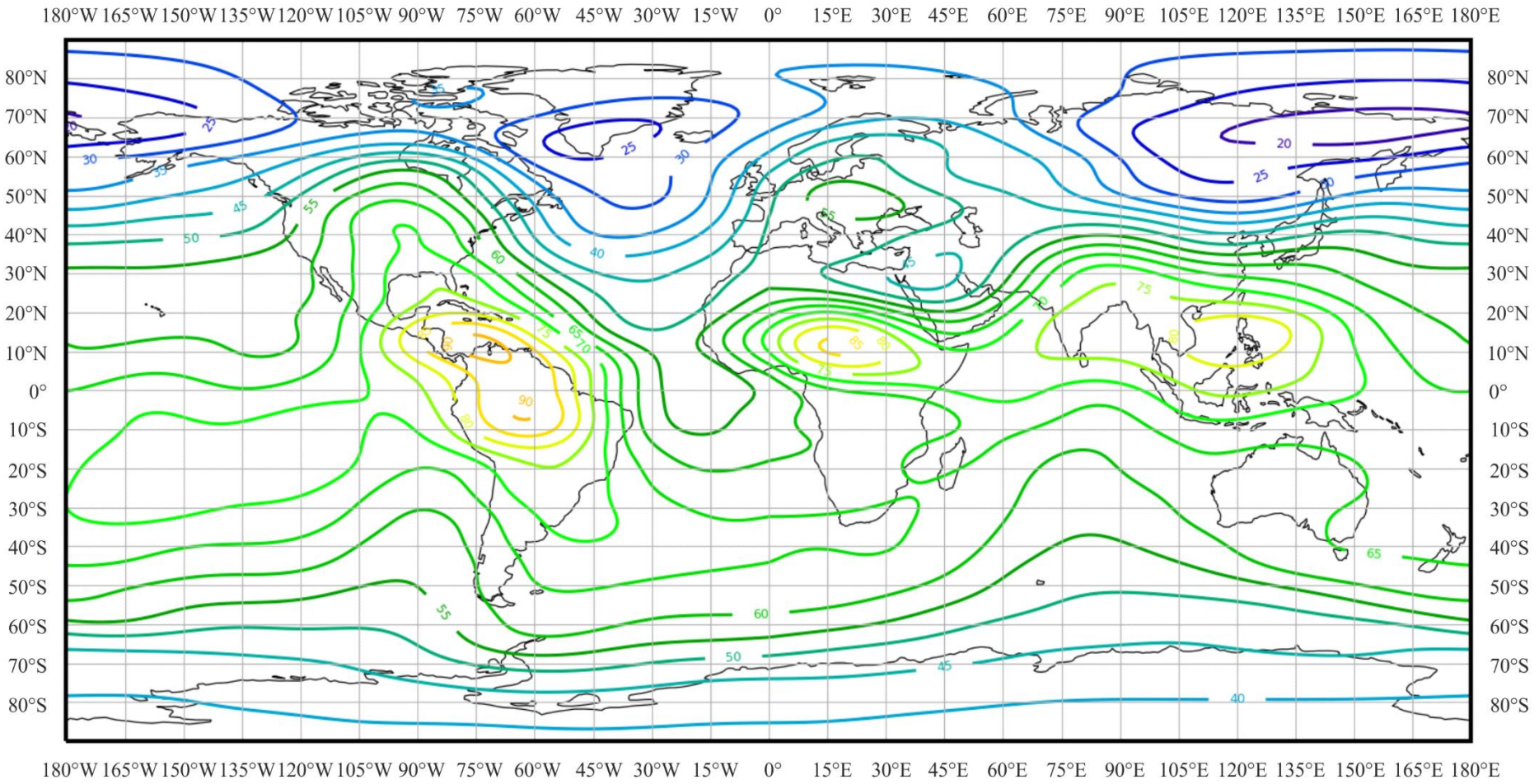

P.0372-26a

FIGURE 26b

Variation of radio noise with frequency (Northern hemisphere: Jun-Jul-Aug; Southern hemisphere: Dec-Jan-Feb; 0400-0800 LT)

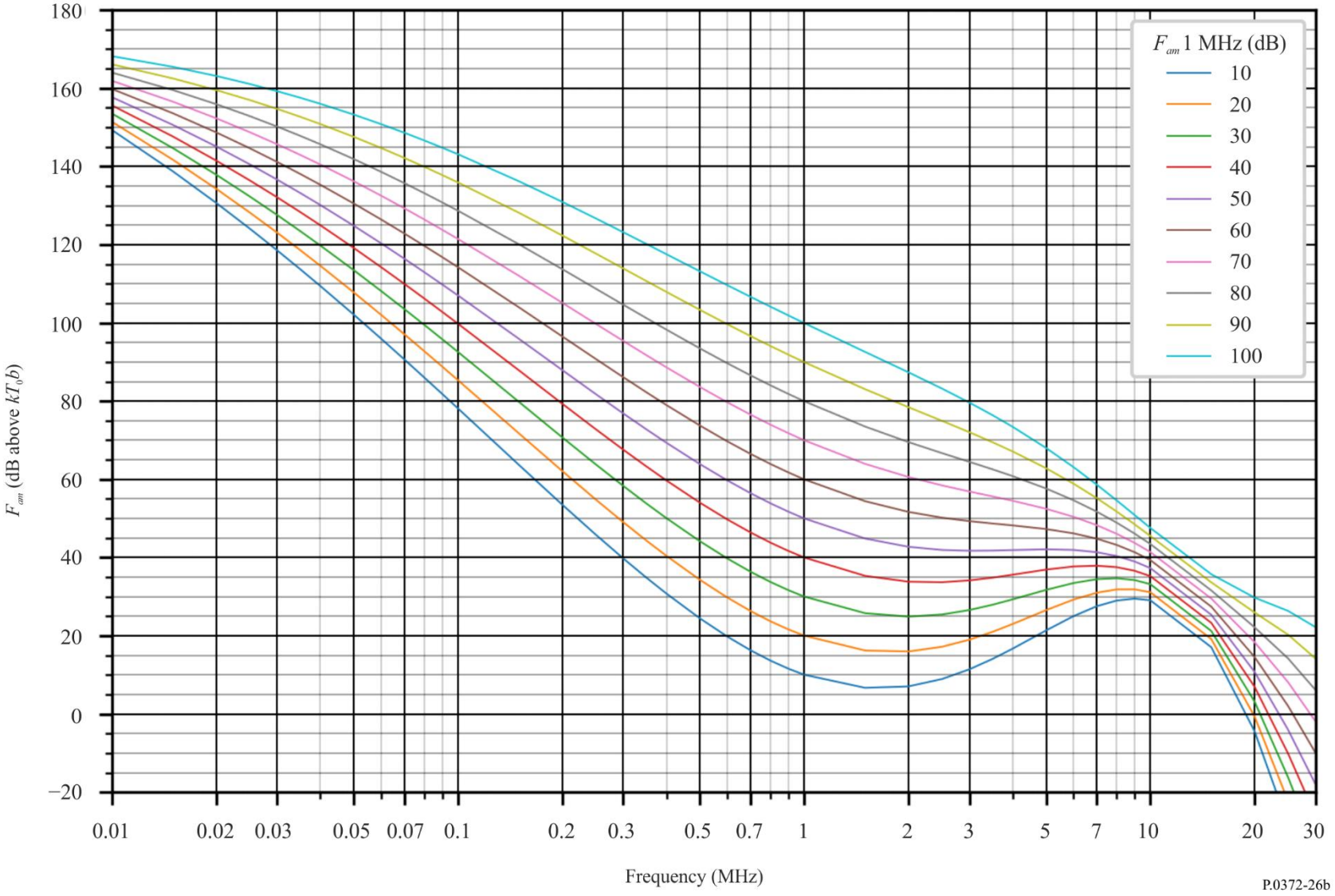

FIGURE 26c

Data on noise variability and character (Northern hemisphere: Jun-Jul-Aug; Southern hemisphere: Dec-Jan-Feb; 0400-0800 LT)

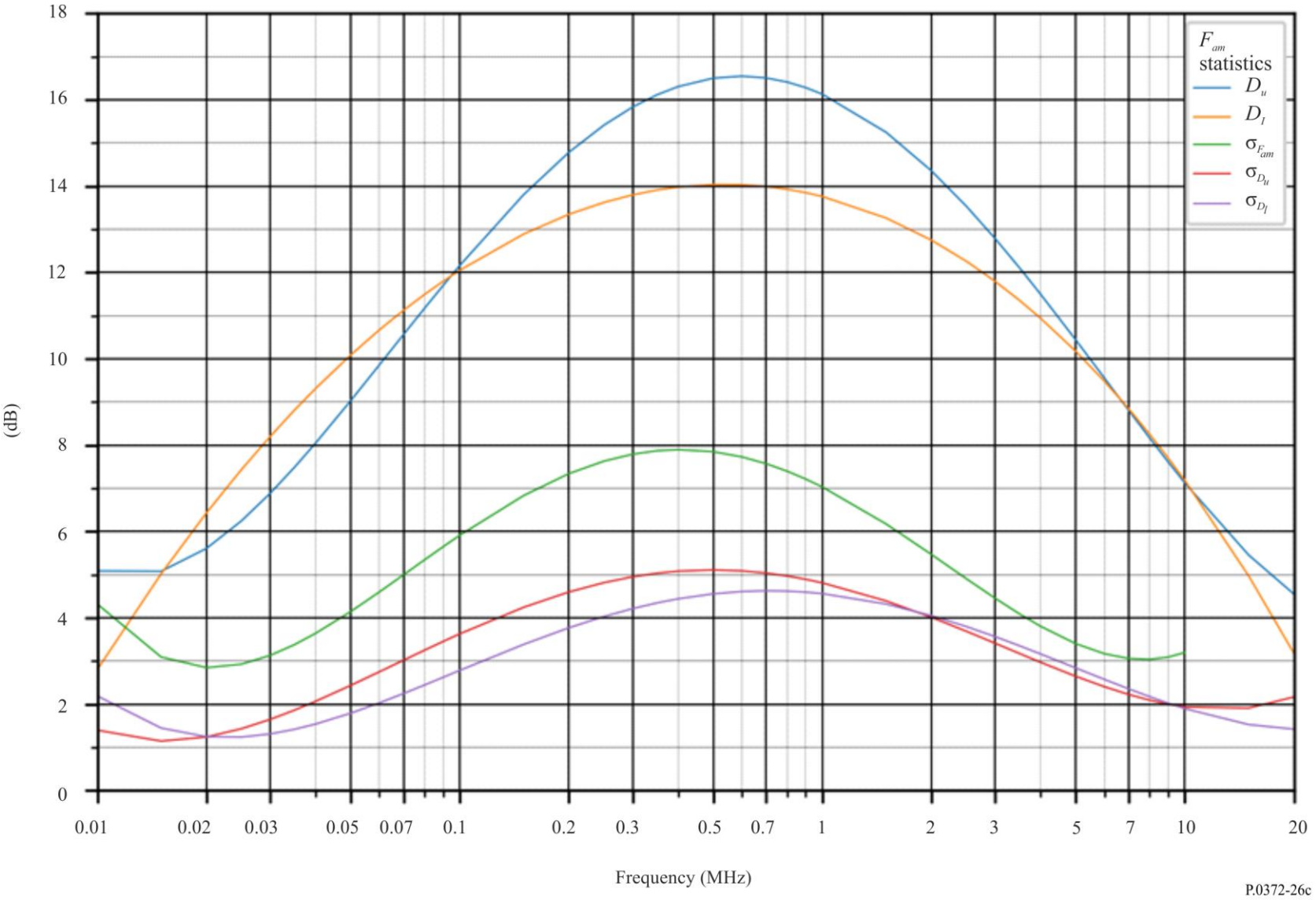

FIGURE 27a

Expected values of atmospheric radio noise, F_{am} (dB above kT_0b at 1 MHz) (Jun-Jul-Aug; 0800-1200 LT)

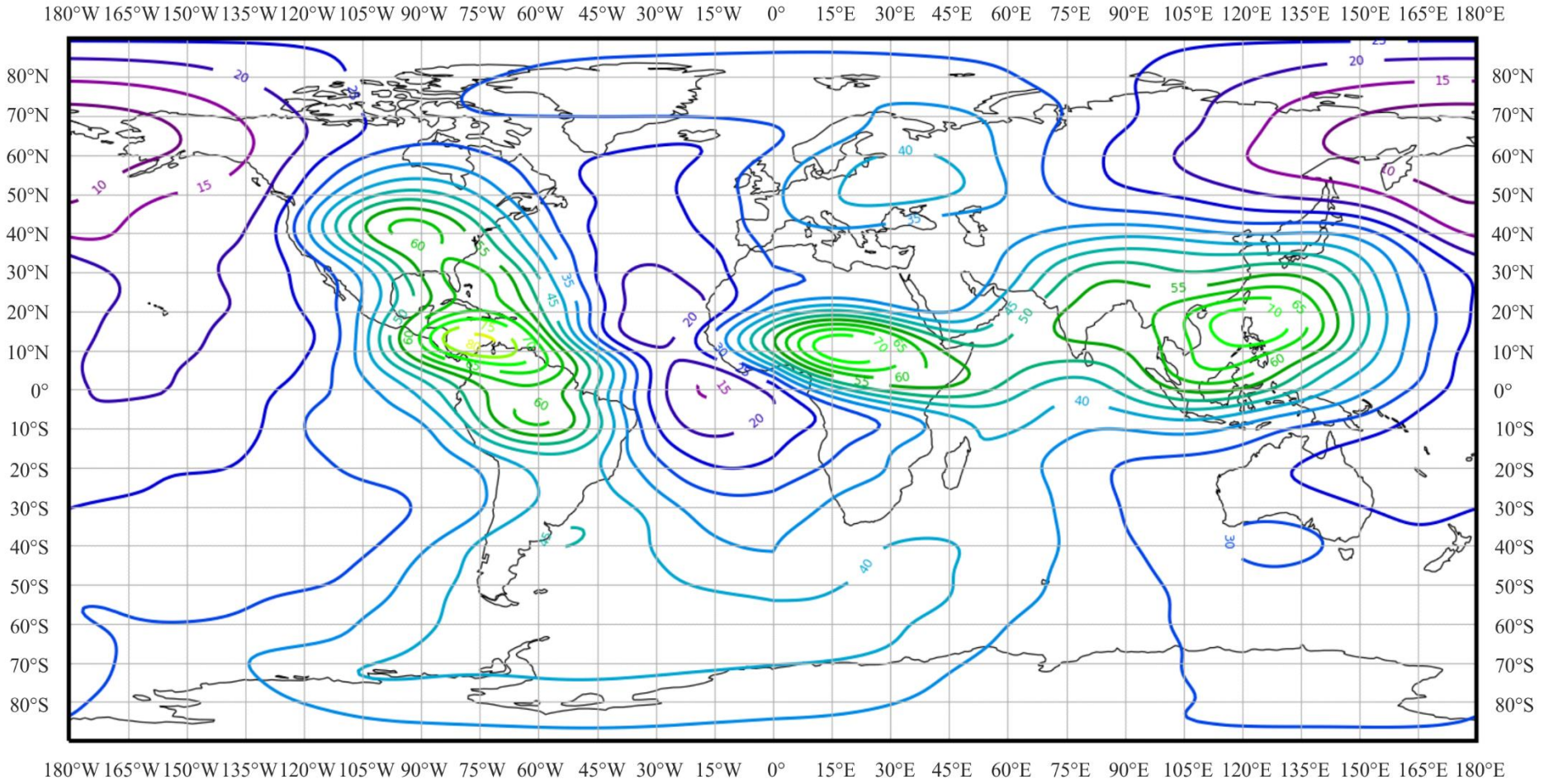

P.0372-27a

FIGURE 27b

Variation of radio noise with frequency (Northern hemisphere: Jun-Jul-Aug; Southern hemisphere: Dec-Jan-Feb; 0800-1200 LT)

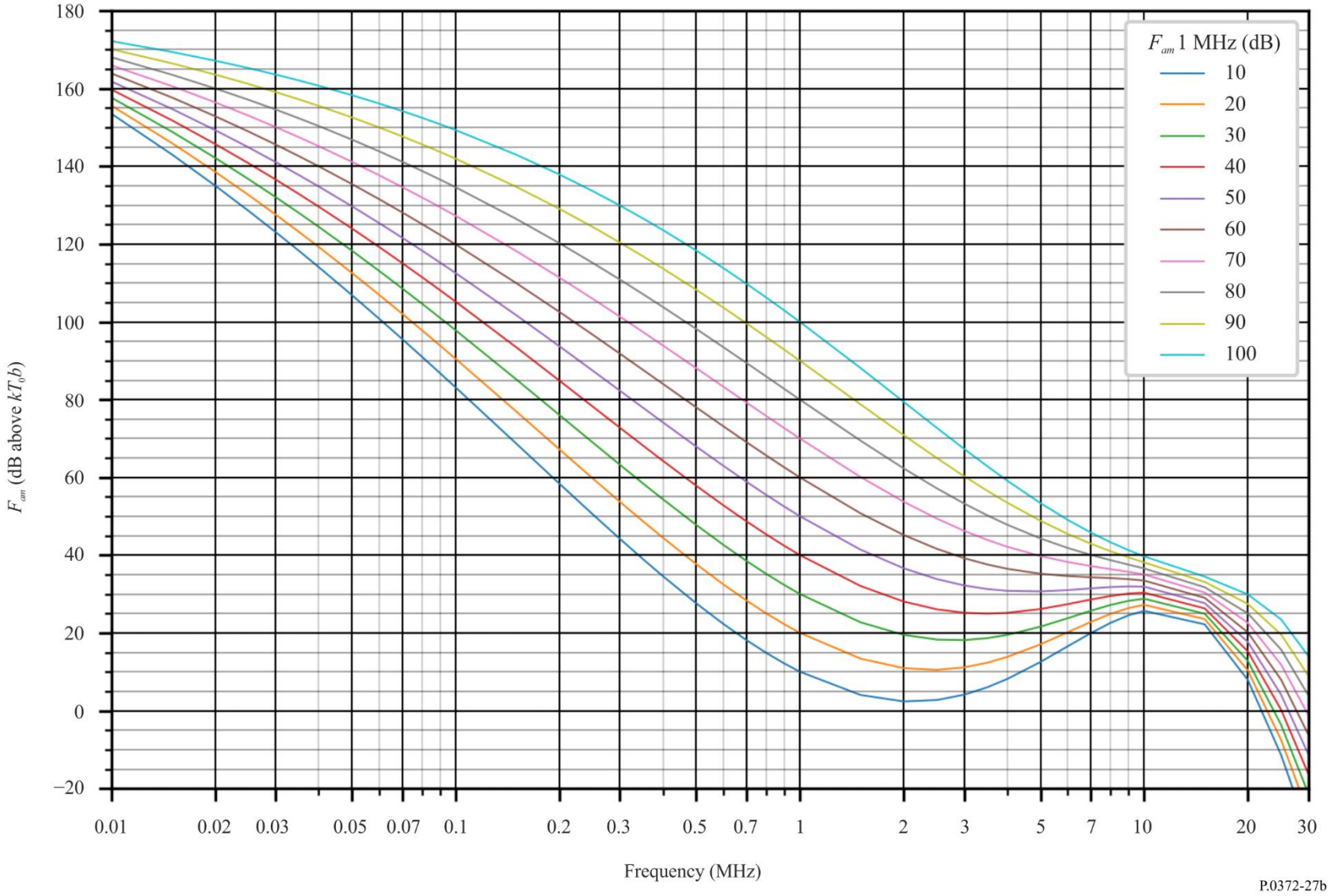

FIGURE 27c

Data on noise variability and character (Northern hemisphere: Jun-Jul-Aug; Southern hemisphere: Dec-Jan-Feb; 0800-1200 LT)

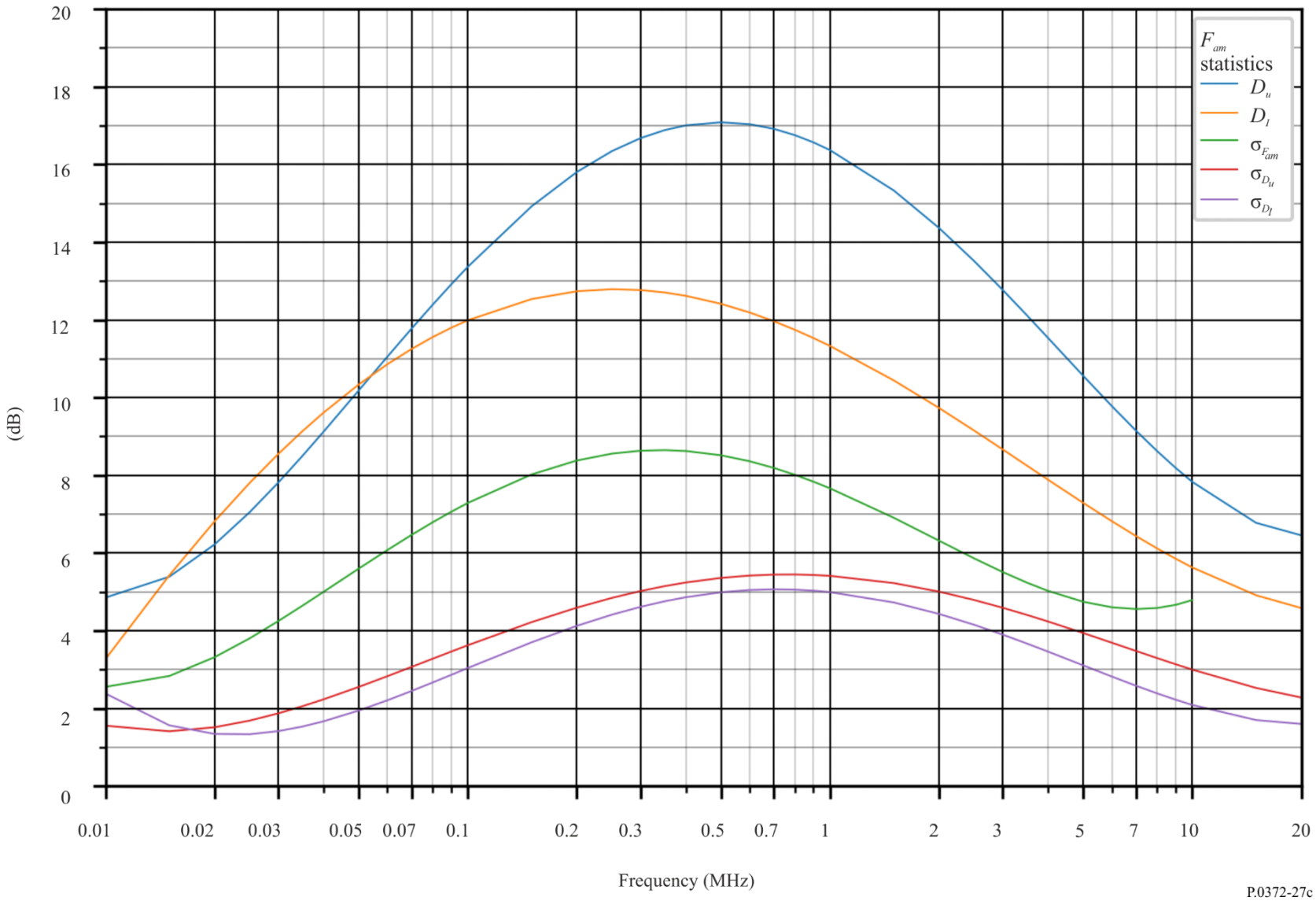

FIGURE 28a

Expected values of atmospheric radio noise, F_{am} (dB above kT_0b at 1 MHz) (Jun-Jul-Aug; 1200-1600 LT)

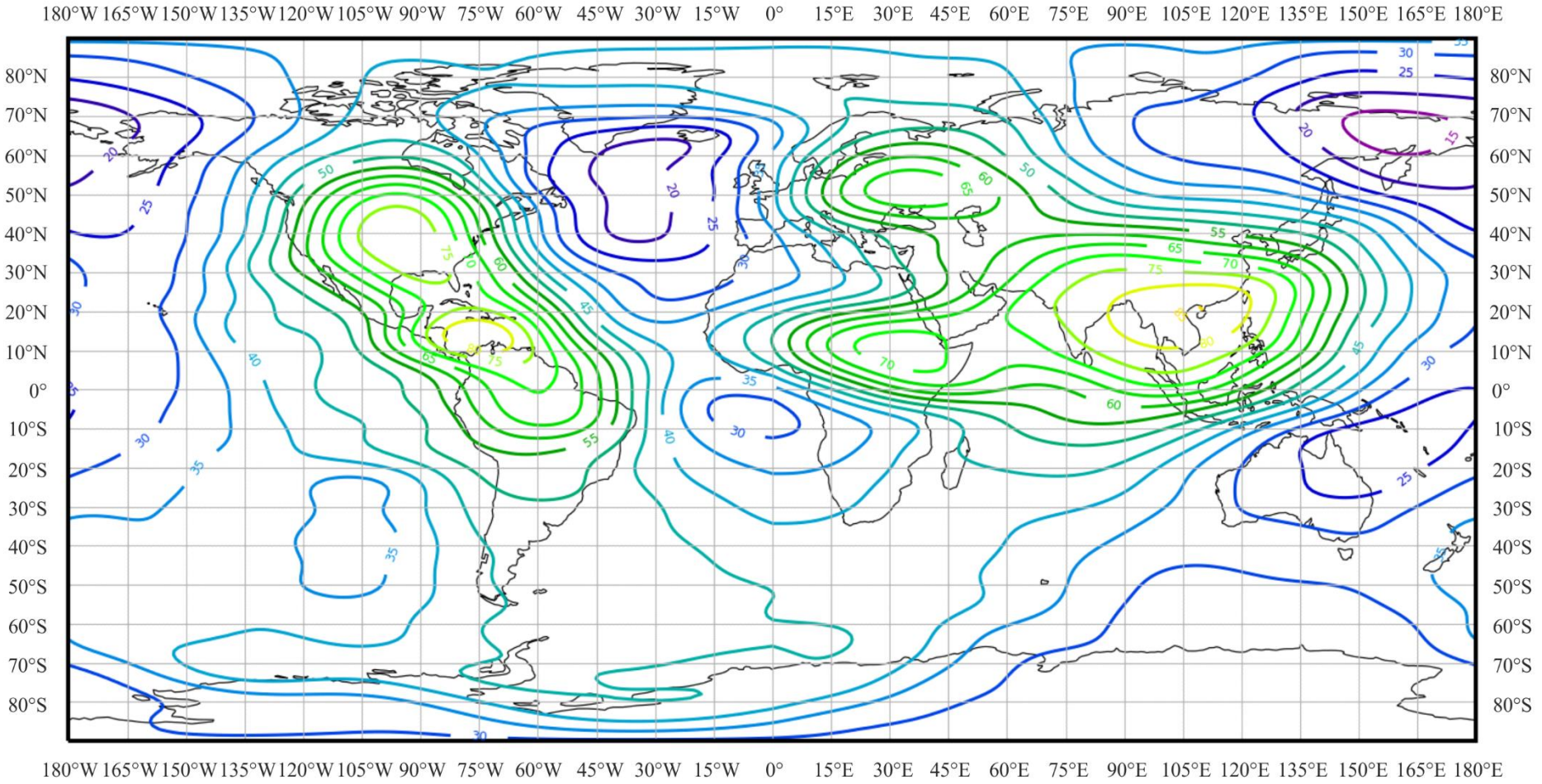

P.0372-28a

FIGURE 28b

Variation of radio noise with frequency (Northern hemisphere: Jun-Jul-Aug; Southern hemisphere: Dec-Jan-Feb; 1200-1600 LT)

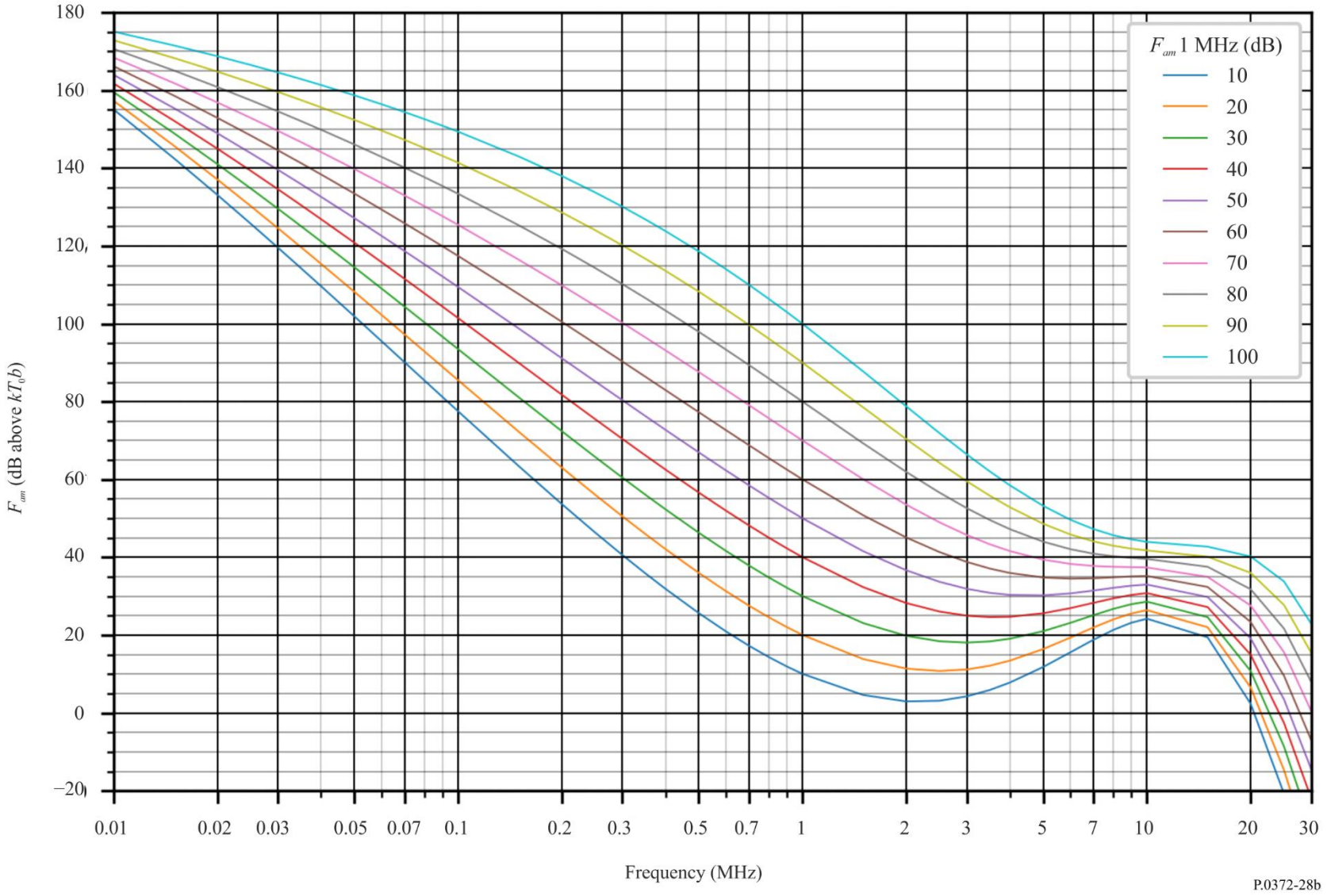

FIGURE 28c

Data on noise variability and character (Northern hemisphere: Jun-Jul-Aug; Southern hemisphere: Dec-Jan-Feb; 1200-1600 LT)

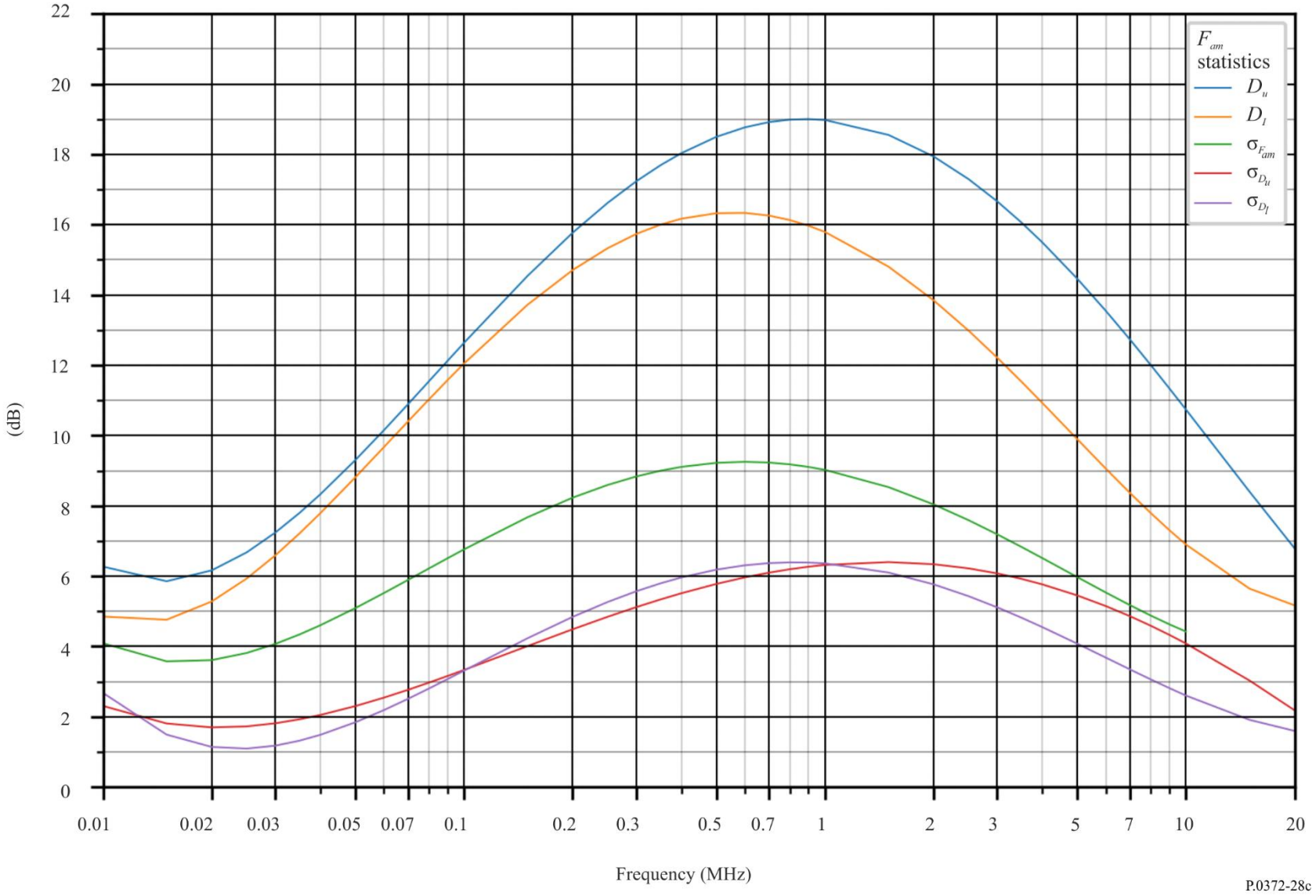

FIGURE 29a

Expected values of atmospheric radio noise, F_{am} (dB above kT_0b at 1 MHz) (Jun-Jul-Aug; 1600-2000 LT)

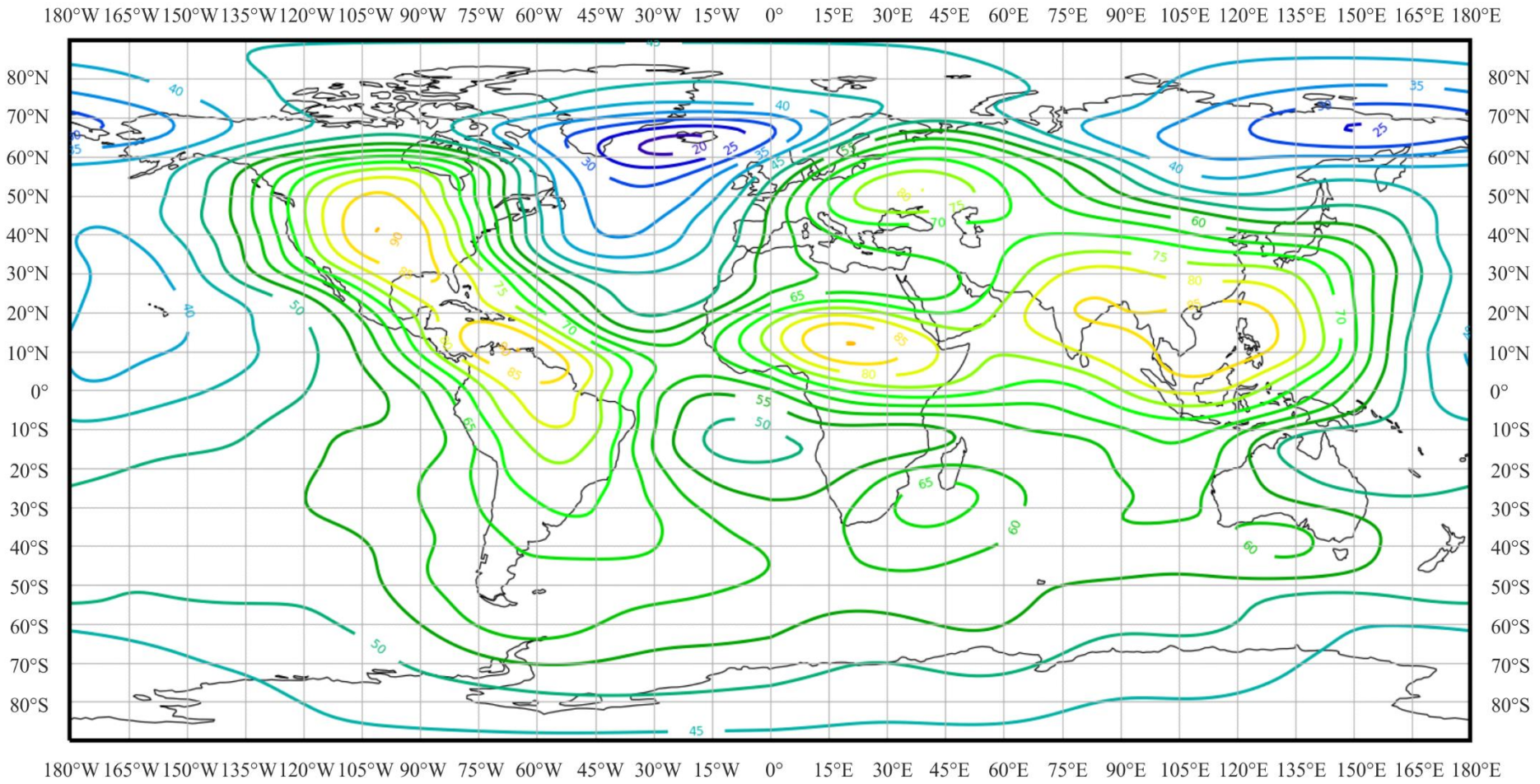

P.0372-29a

FIGURE 29b

Variation of radio noise with frequency (Northern hemisphere: Jun-Jul-Aug; Southern hemisphere: Dec-Jan-Feb; 1600-2000 LT)

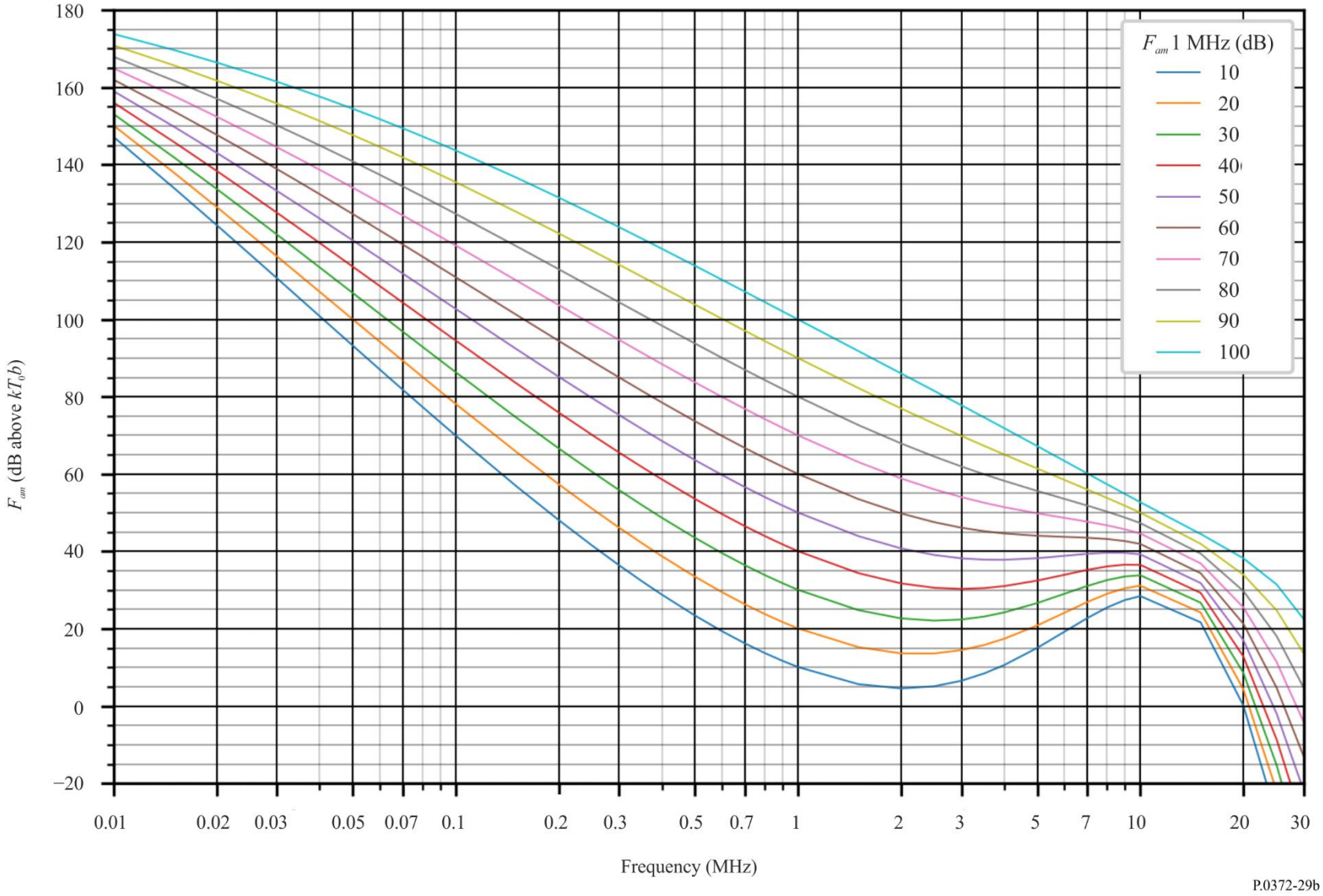

FIGURE 29c

Data on noise variability and character (Northern hemisphere: Jun-Jul-Aug; Southern hemisphere: Dec-Jan-Feb; 1600-2000 LT)

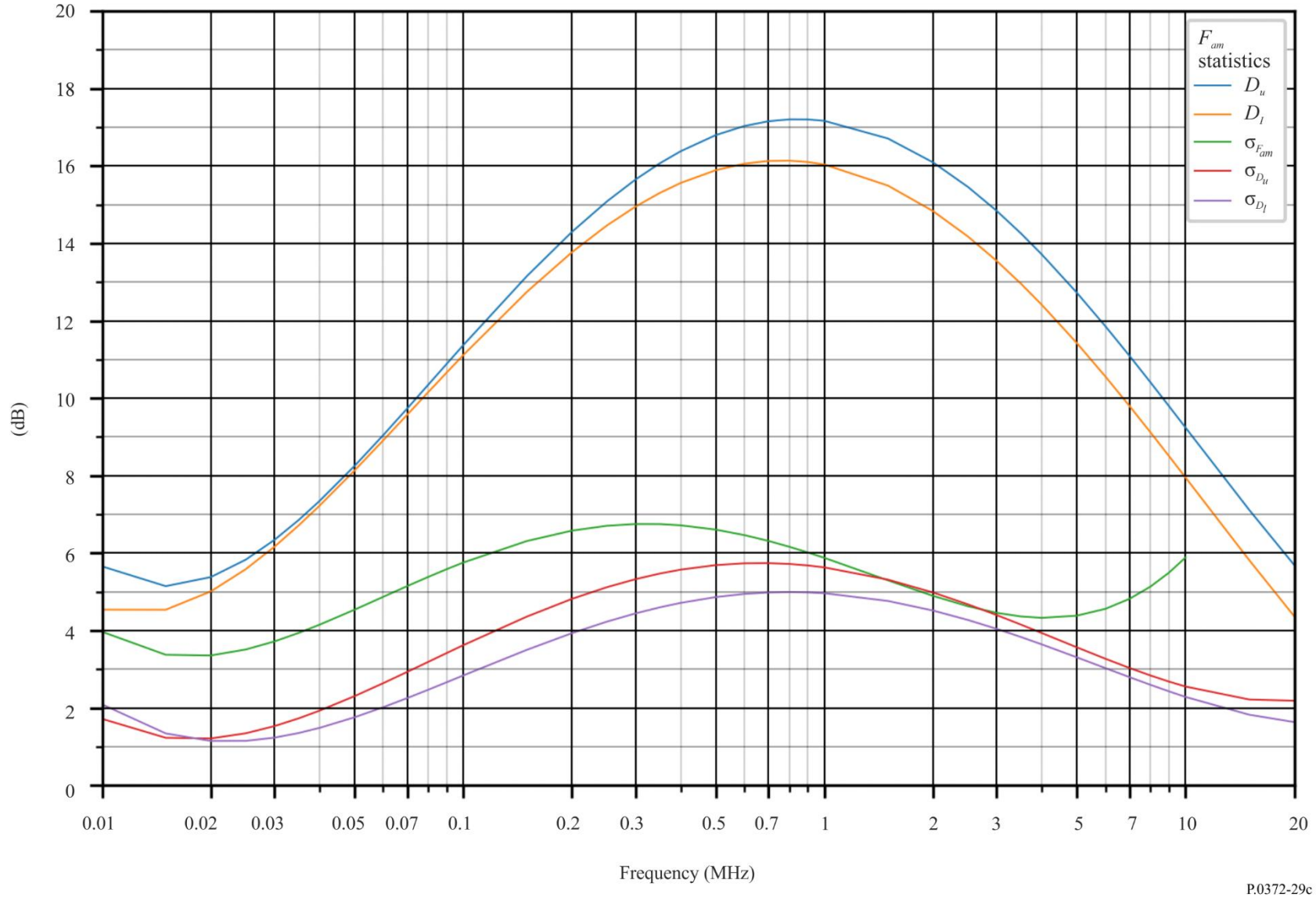

FIGURE 30a

Expected values of atmospheric radio noise, F_{am} (dB above kT_0b at 1 MHz) (Jun-Jul-Aug; 2000-2400 LT)

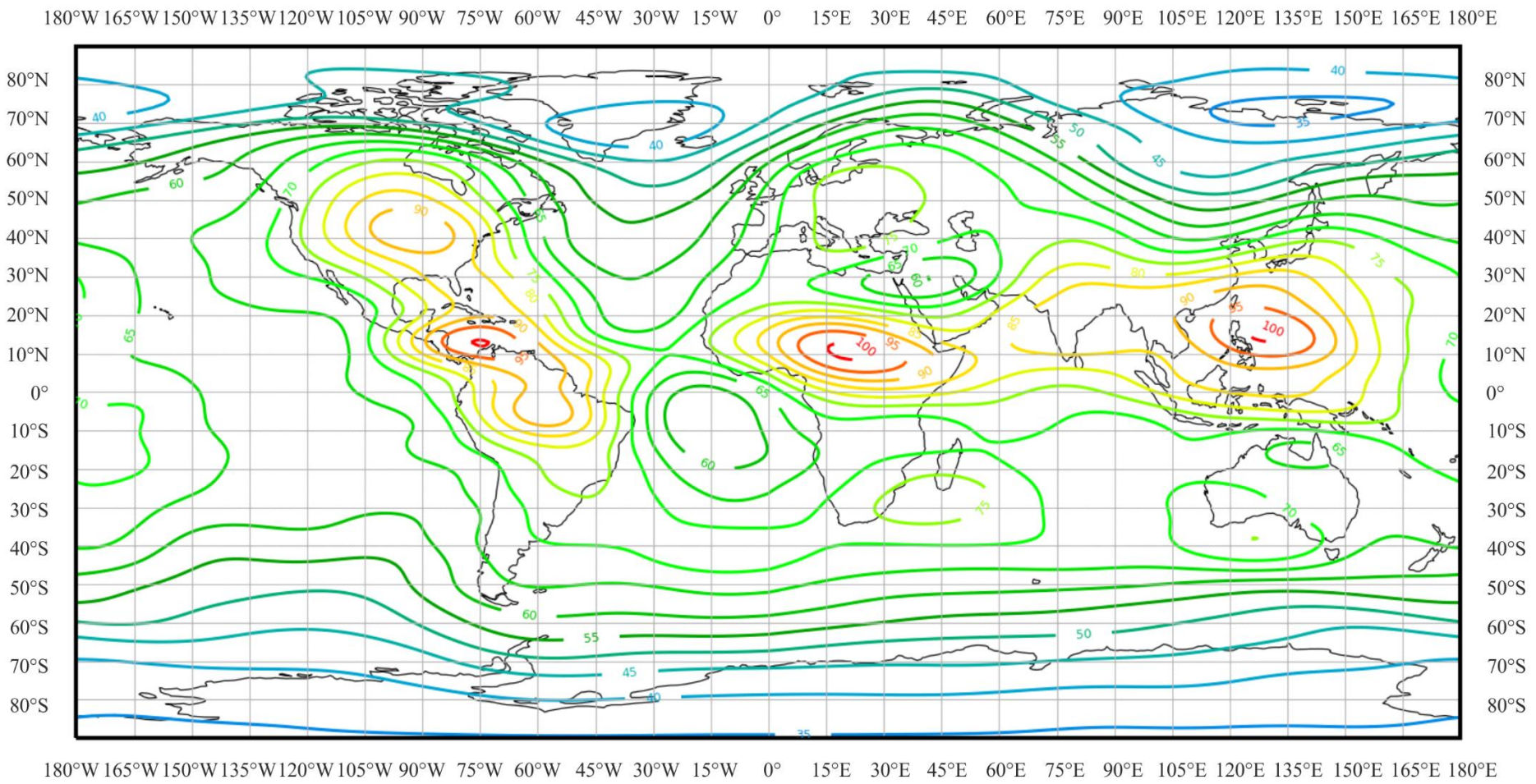

FIGURE 30b

Variation of radio noise with frequency (Northern hemisphere: Jun-Jul-Aug; Southern hemisphere: Dec-Jan-Feb; 2000-2400 LT)

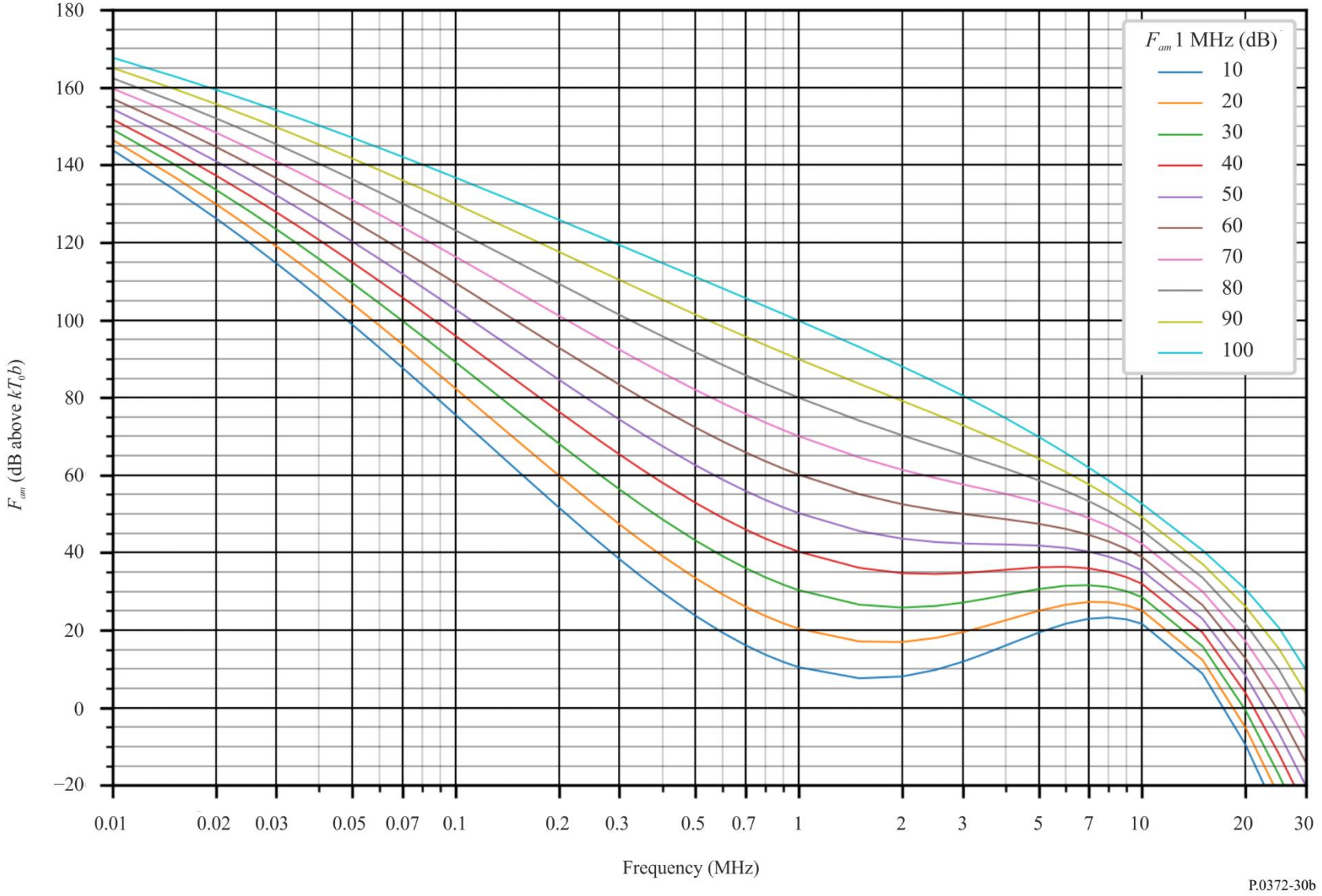

FIGURE 30c

Data on noise variability and character (Northern hemisphere: Jun-Jul-Aug; Southern hemisphere: Dec-Jan-Feb; 2000-2400 LT)

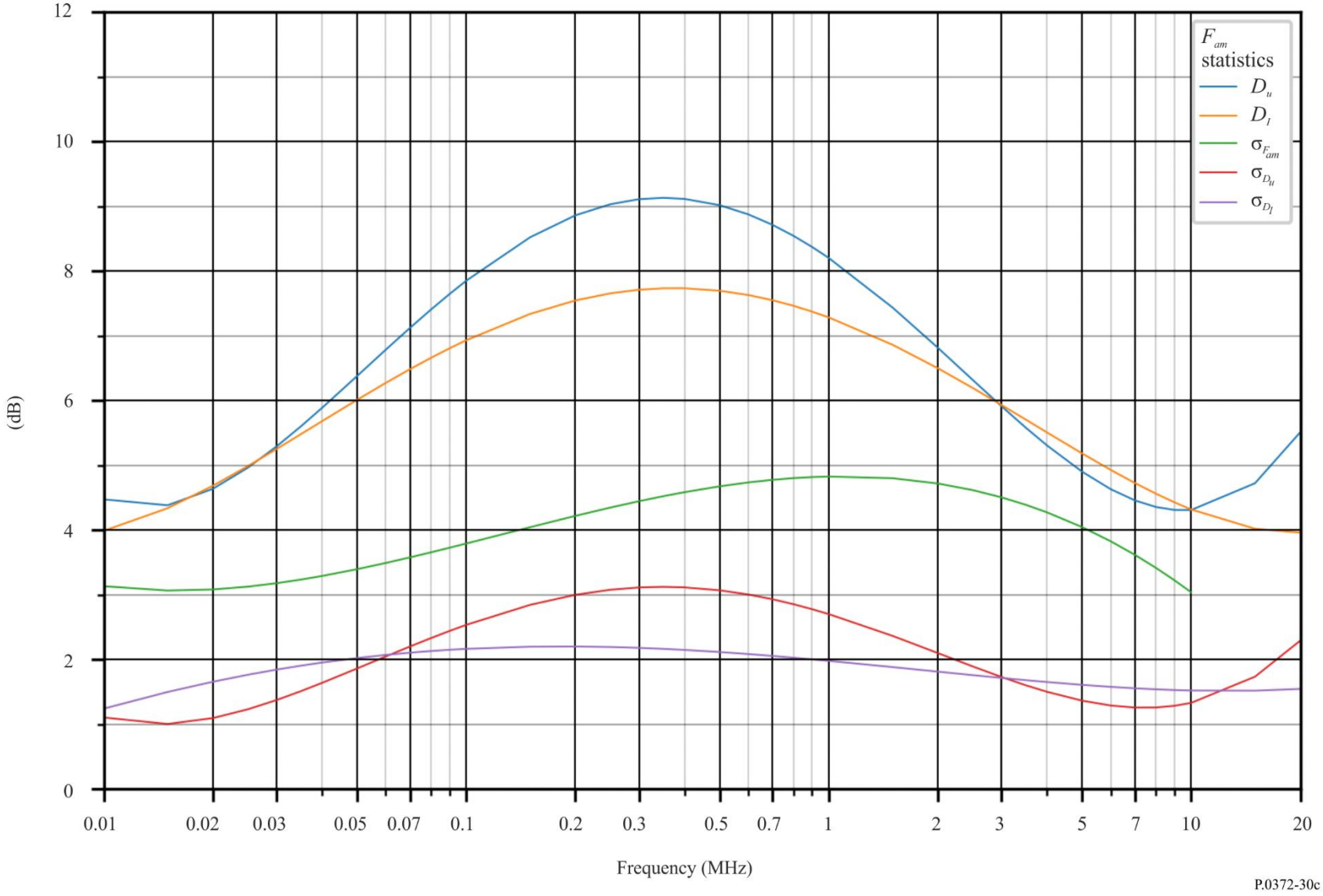

FIGURE 31a

Expected values of atmospheric radio noise, F_{am} (dB above kT_0b at 1 MHz) (Sep-Oct-Nov; 0000-0400 LT)

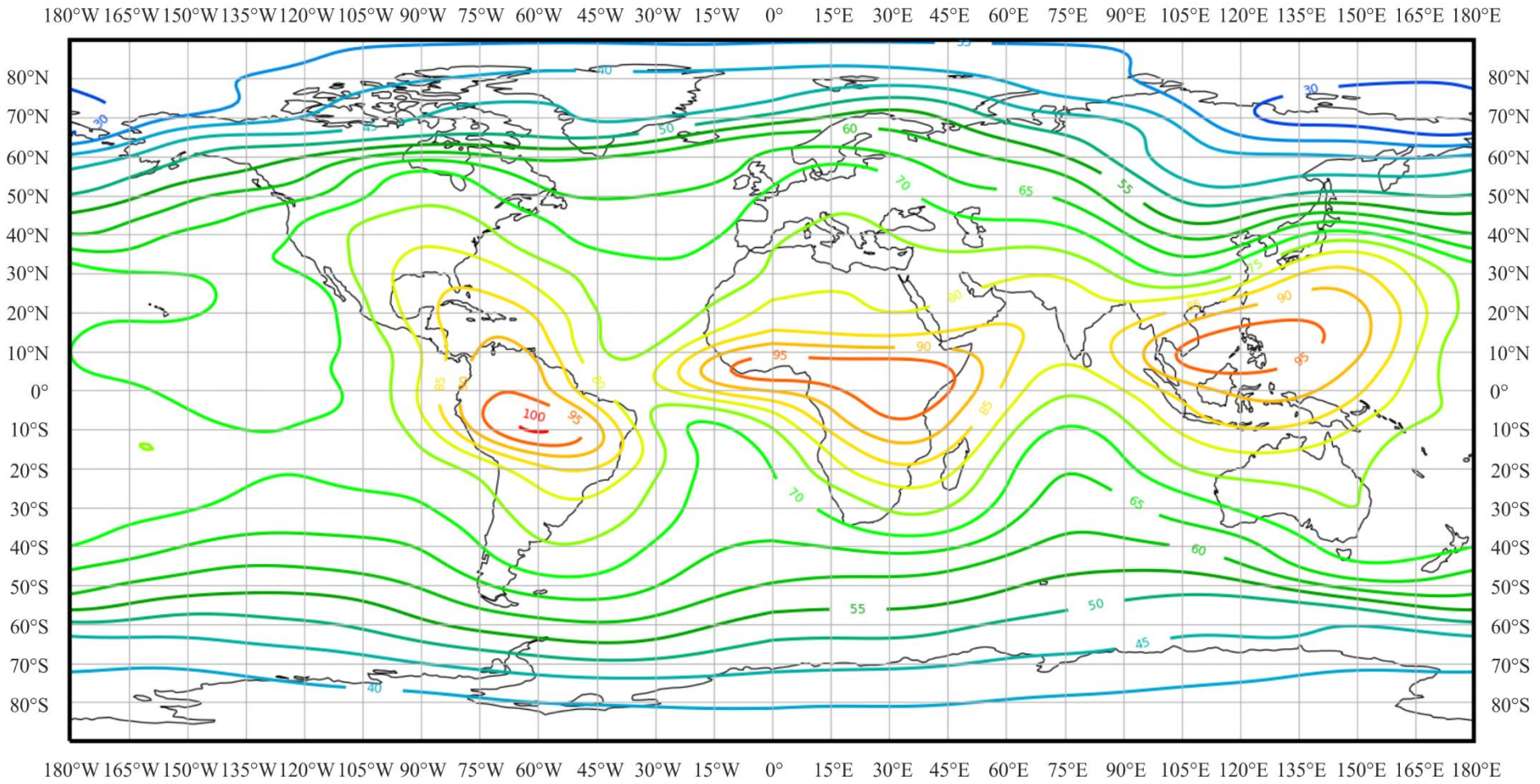

P.0372-31a

FIGURE 31b

Variation of radio noise with frequency (Northern hemisphere: Sep-Oct-Nov; Southern hemisphere: Mar-Apr-May; 0000-0400 LT)

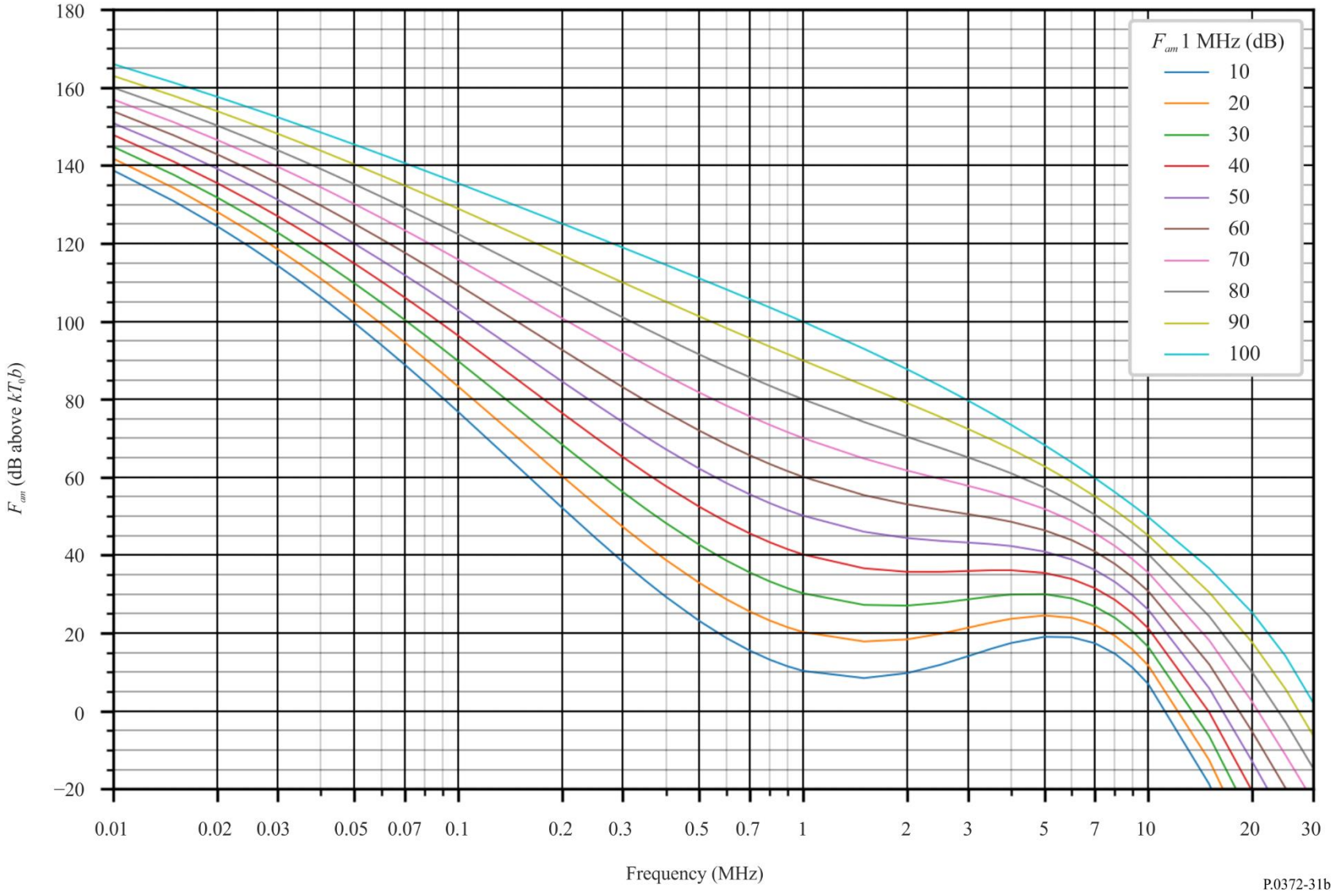

FIGURE 31c

Data on noise variability and character (Northern hemisphere: Sep-Oct-Nov; Southern hemisphere: Mar-Apr-May; 0000-0400 LT)

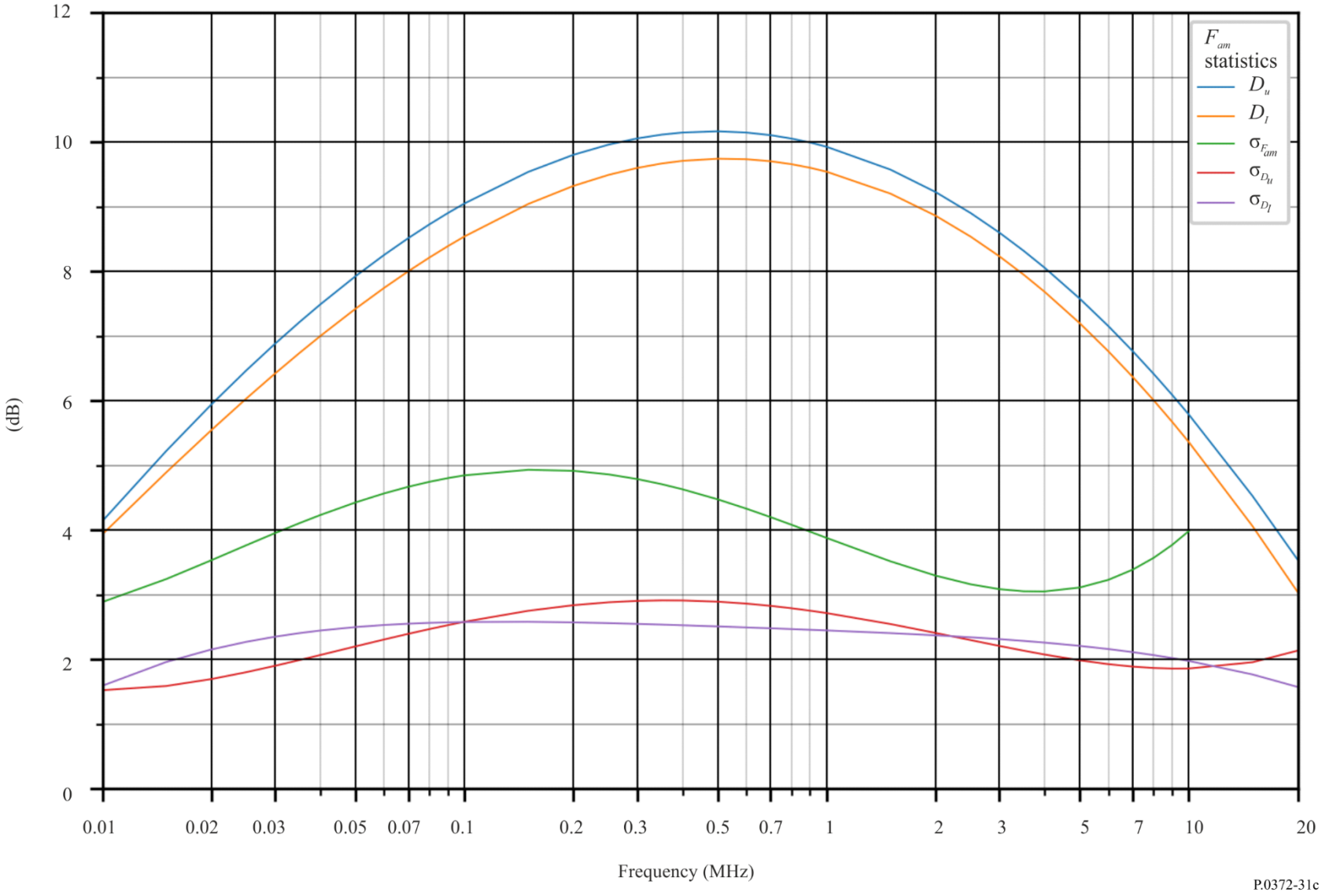

FIGURE 32a

Expected values of atmospheric radio noise, F_{am} (dB above kT_0b at 1 MHz) (Sep-Oct-Nov; 0400-0800 LT)

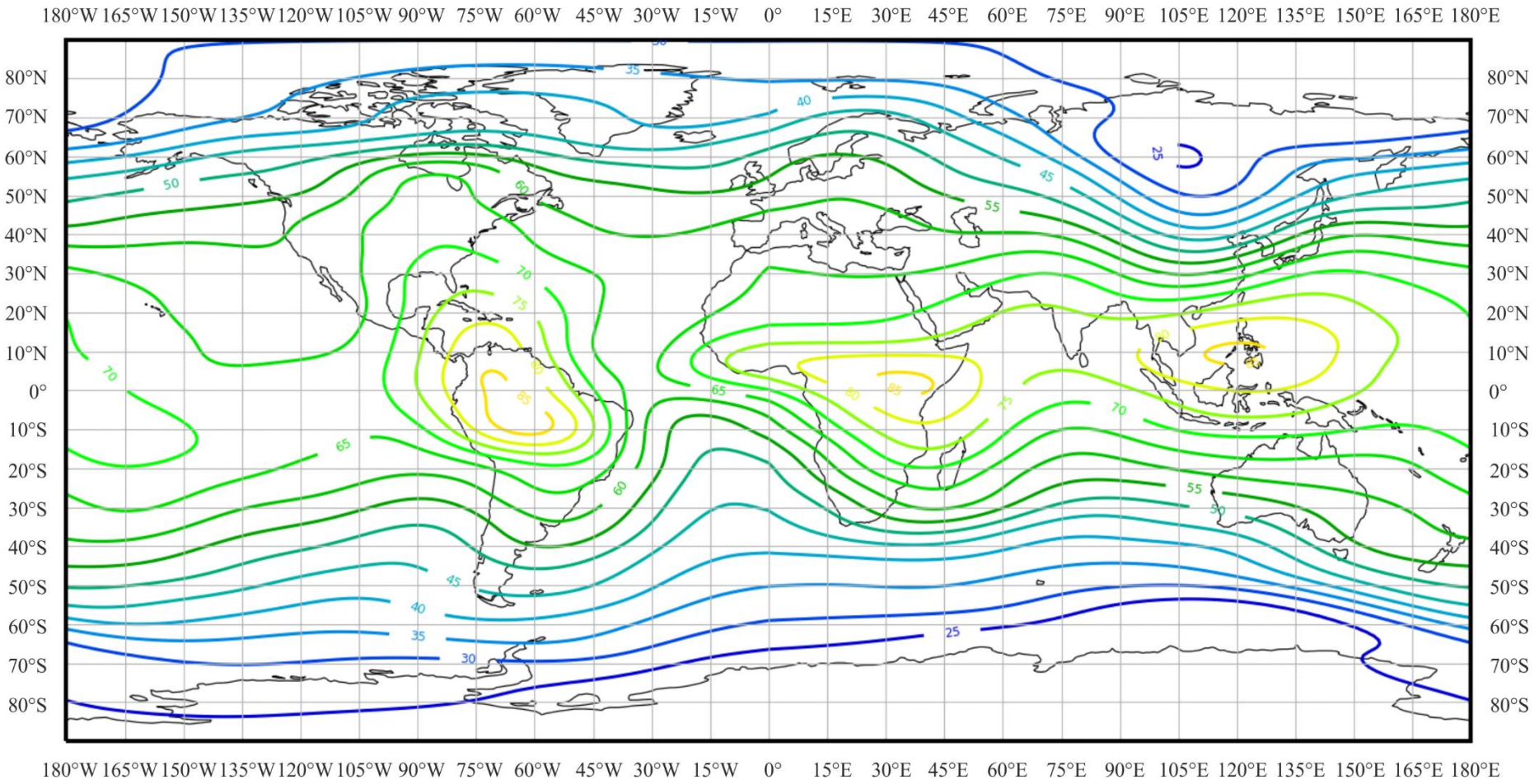

P.0372-32a

FIGURE 32b

Variation of radio noise with frequency (Northern hemisphere: Sep-Oct-Nov; Southern hemisphere: Mar-Apr-May; 0400-0800 LT)

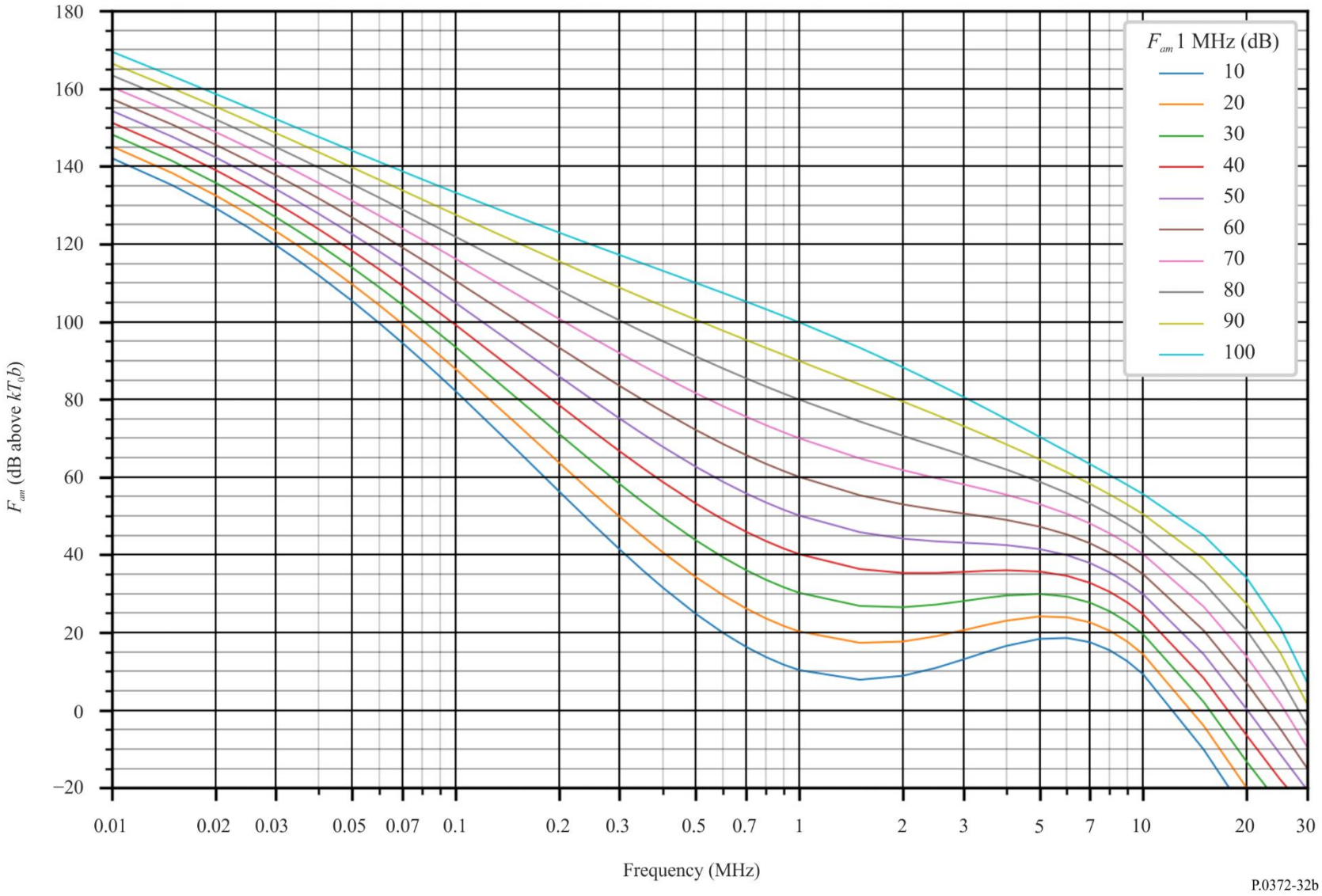

FIGURE 32c

Data on noise variability and character (Northern hemisphere: Sep-Oct-Nov; Southern hemisphere: Mar-Apr-May; 0400-0800 LT)

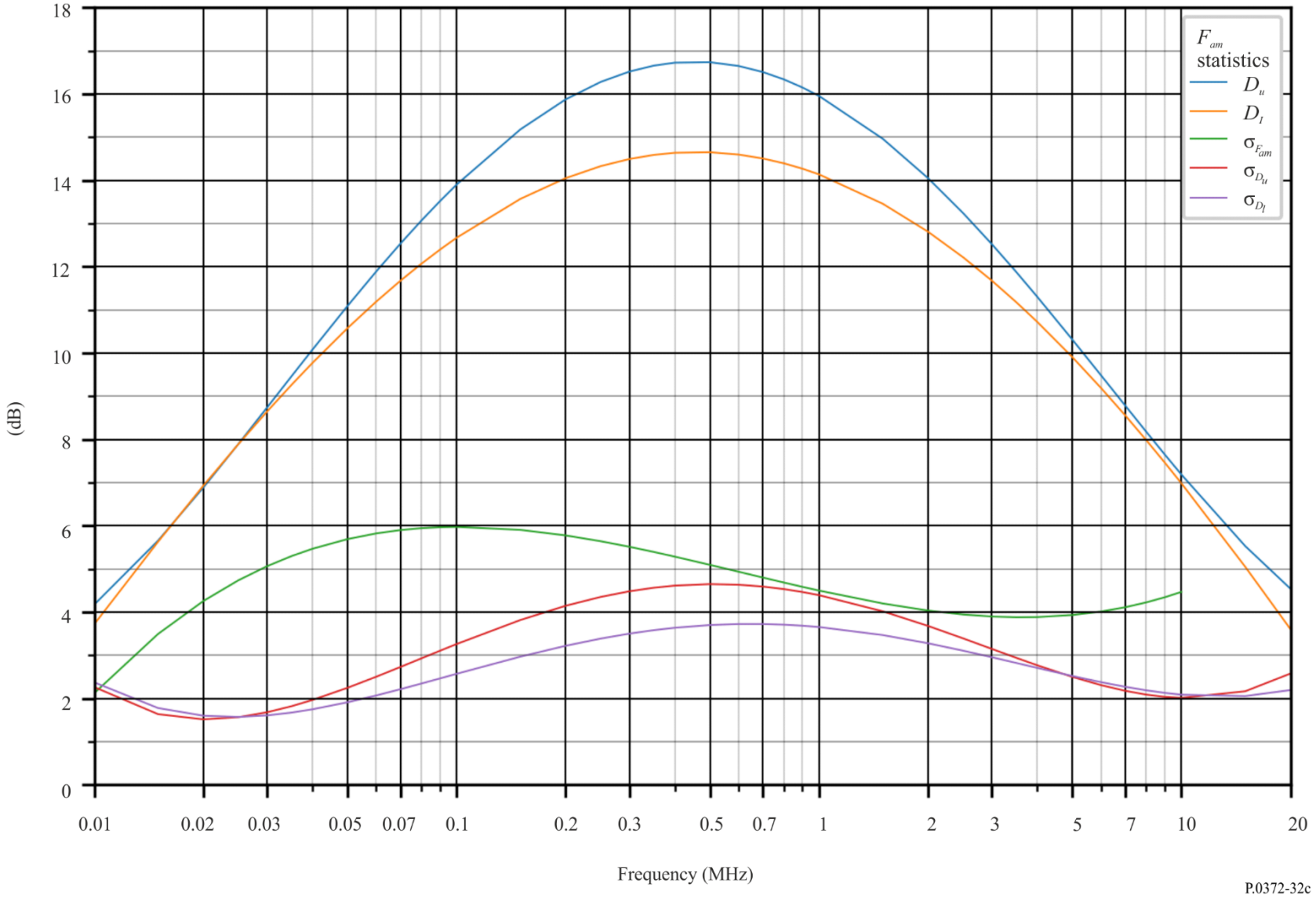

FIGURE 33a

Expected values of atmospheric radio noise, F_{am} (dB above kT_0b at 1 MHz) (Sep-Oct-Nov; 0800-1200 LT)

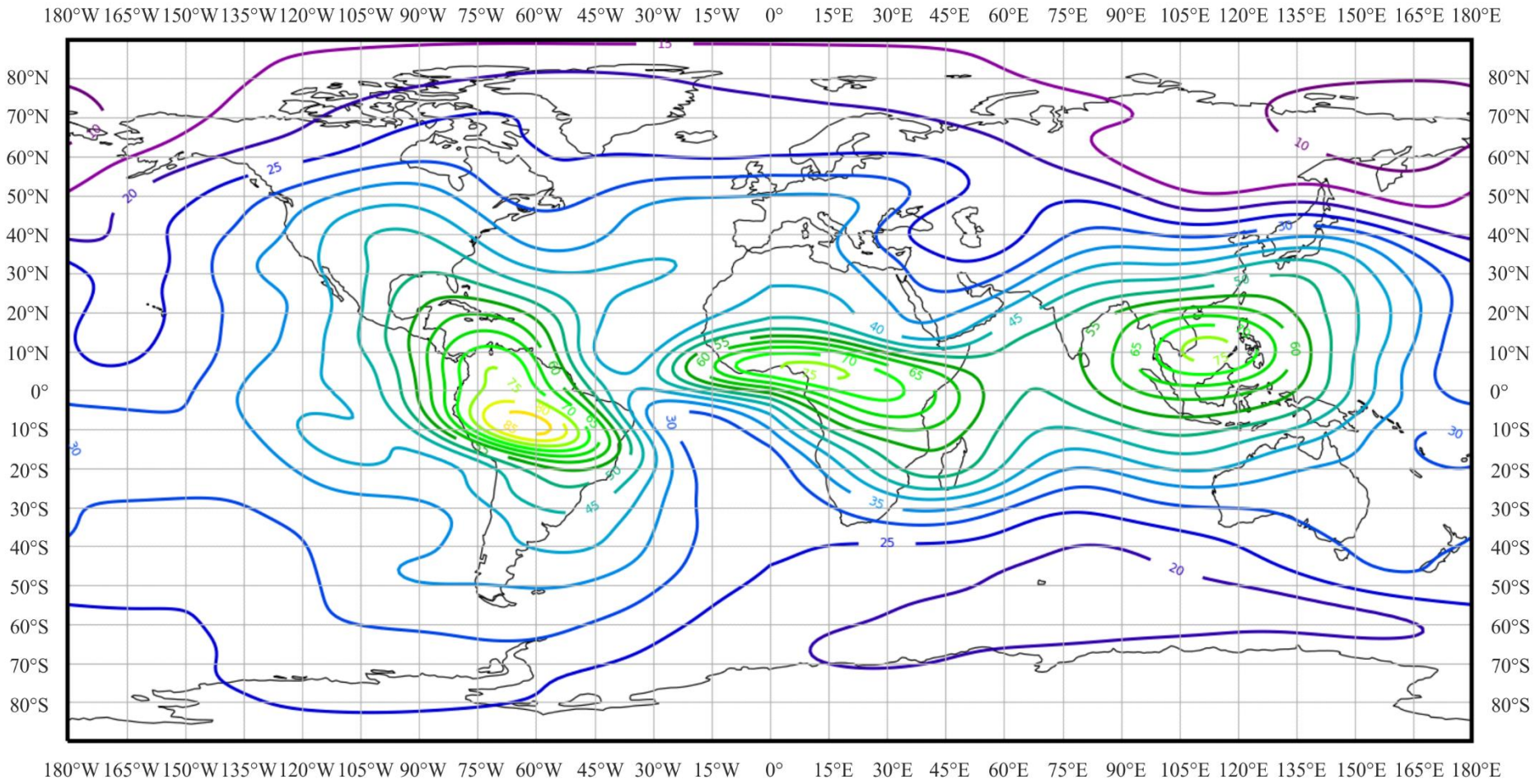

P.0372-33a

FIGURE 33b

Variation of radio noise with frequency (Northern hemisphere: Sep-Oct-Nov; Southern hemisphere: Mar-Apr-May; 0800-1200 LT)

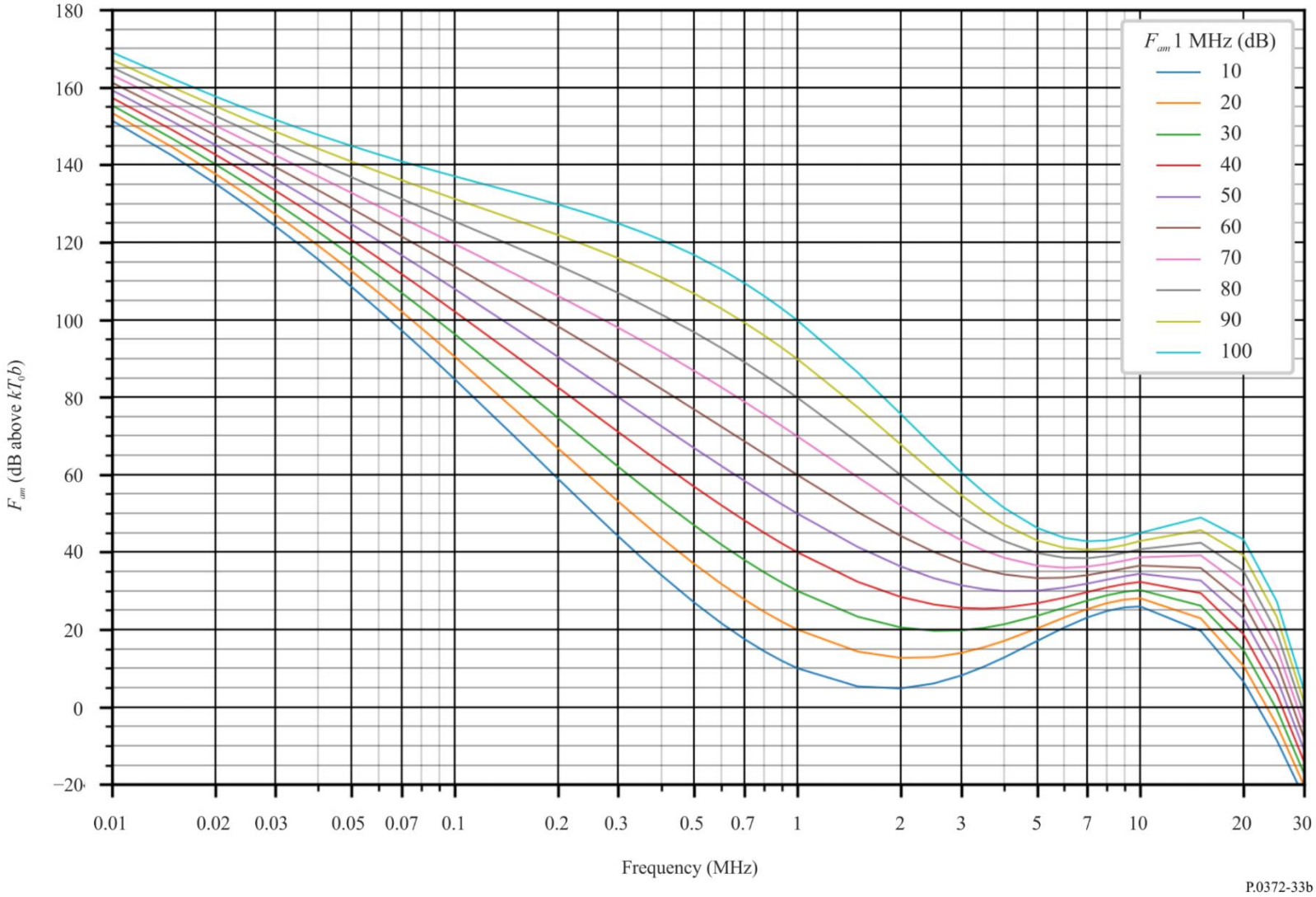

FIGURE 33c

Data on noise variability and character (Northern hemisphere: Sep-Oct-Nov; Southern hemisphere: Mar-Apr-May; 0800-1200 LT)

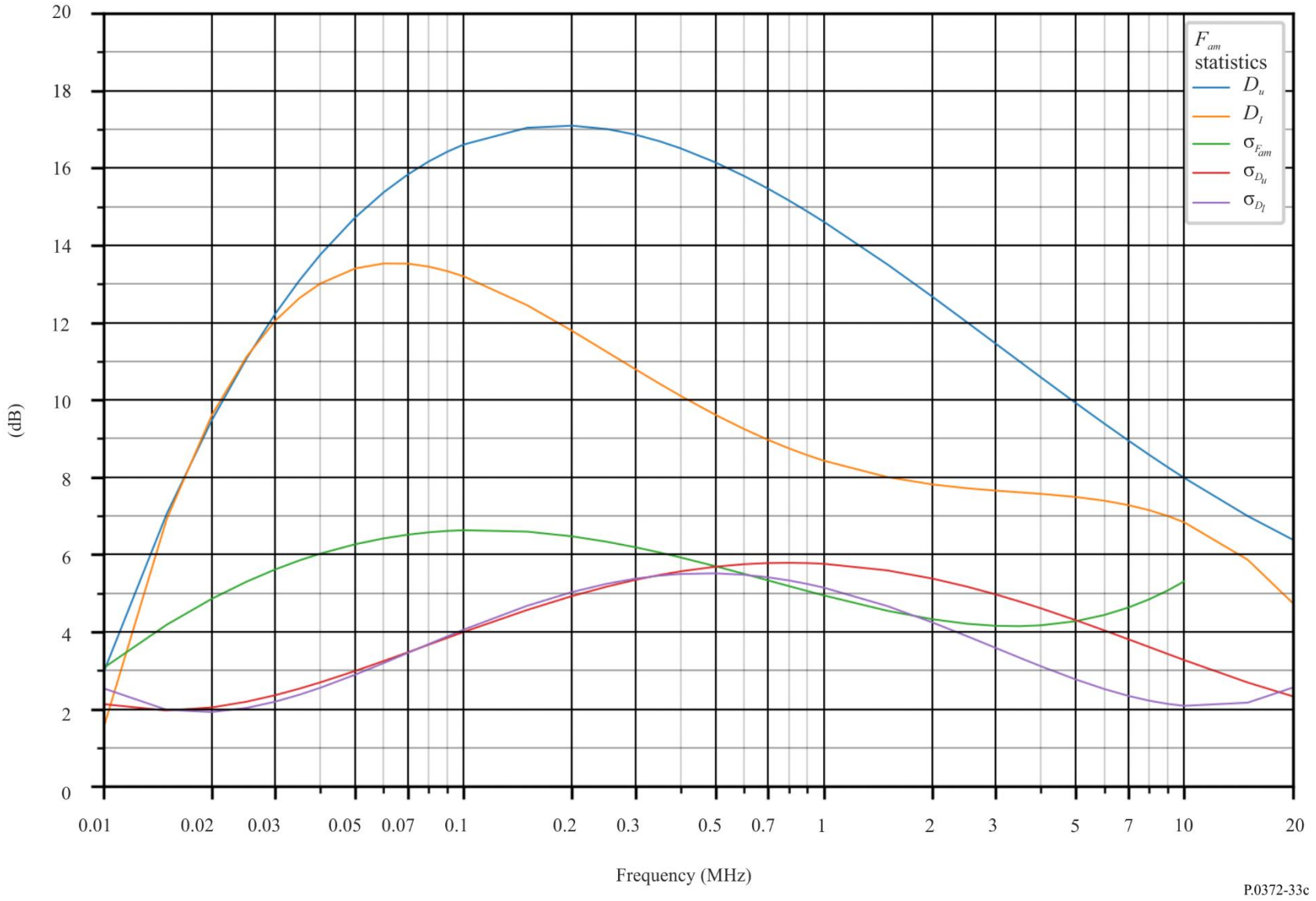

FIGURE 34a

Expected values of atmospheric radio noise, F_{am} (dB above kT_0b at 1 MHz) (Sep-Oct-Nov; 1200-1600 LT)

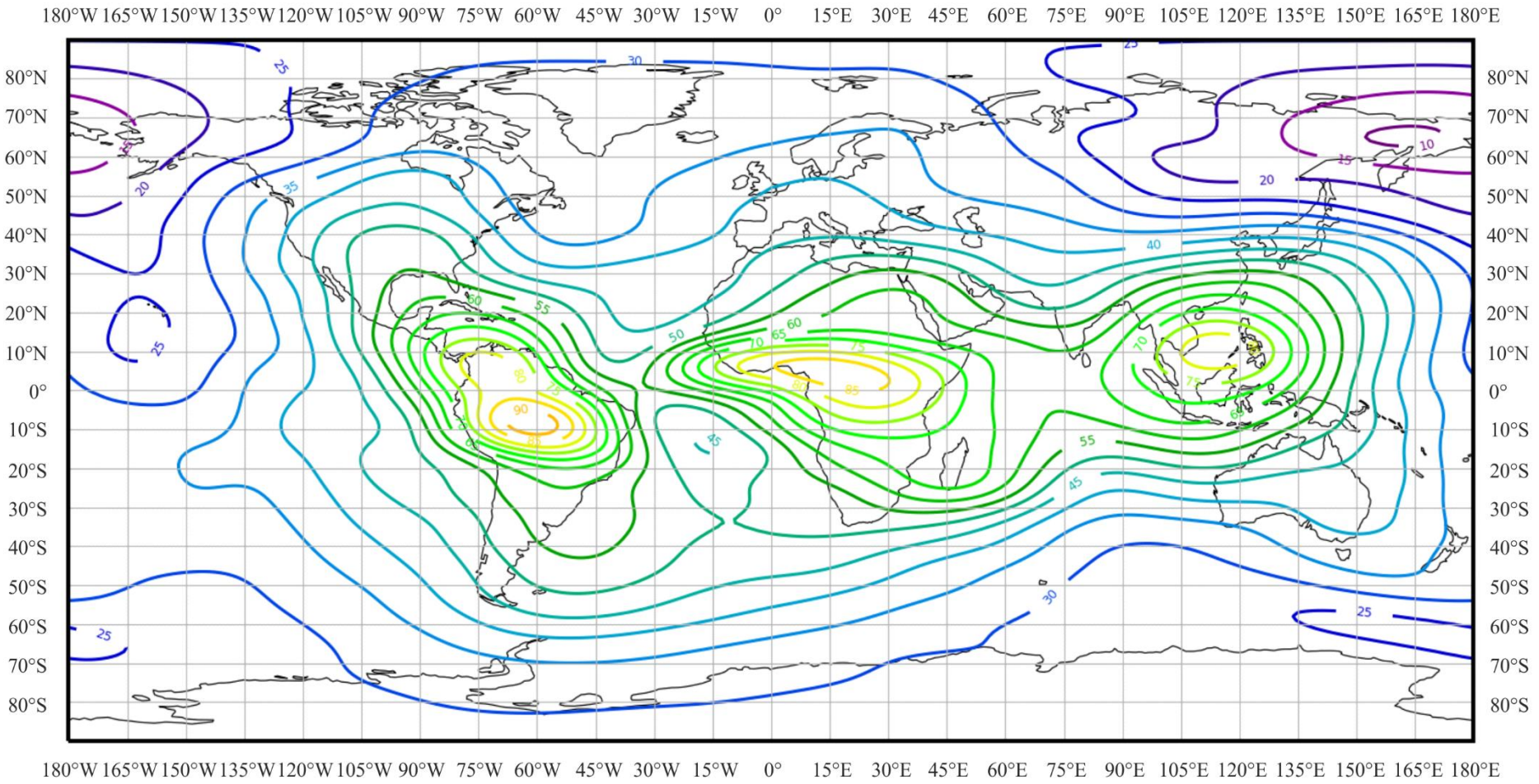

P.0372-34a

FIGURE 34b

Variation of radio noise with frequency (Northern hemisphere: Sep-Oct-Nov; Southern hemisphere: Mar-Apr-May; 1200-1600 LT)

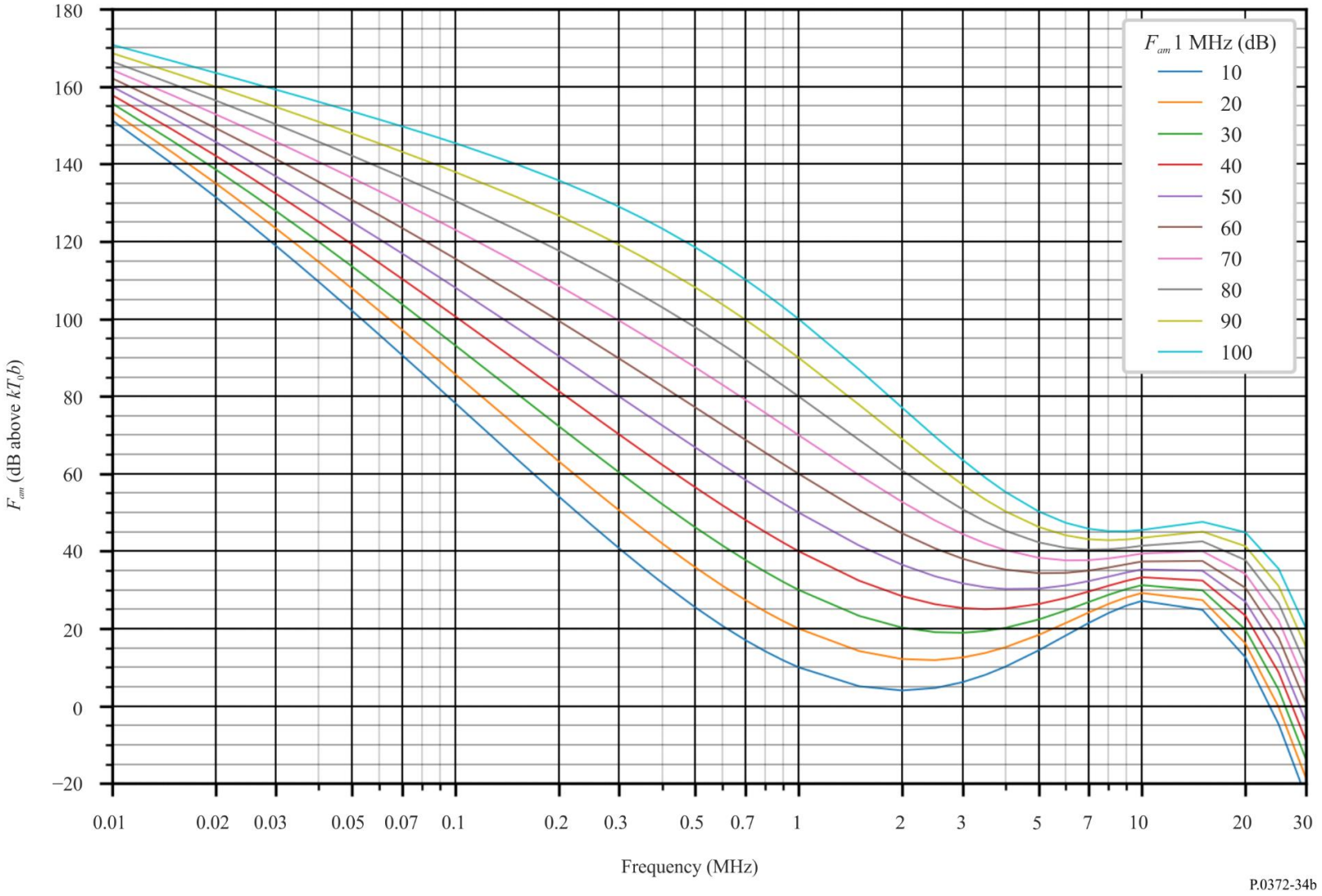

FIGURE 34c

Data on noise variability and character (Northern hemisphere: Sep-Oct-Nov; Southern hemisphere: Mar-Apr-May; 1200-1600 LT)

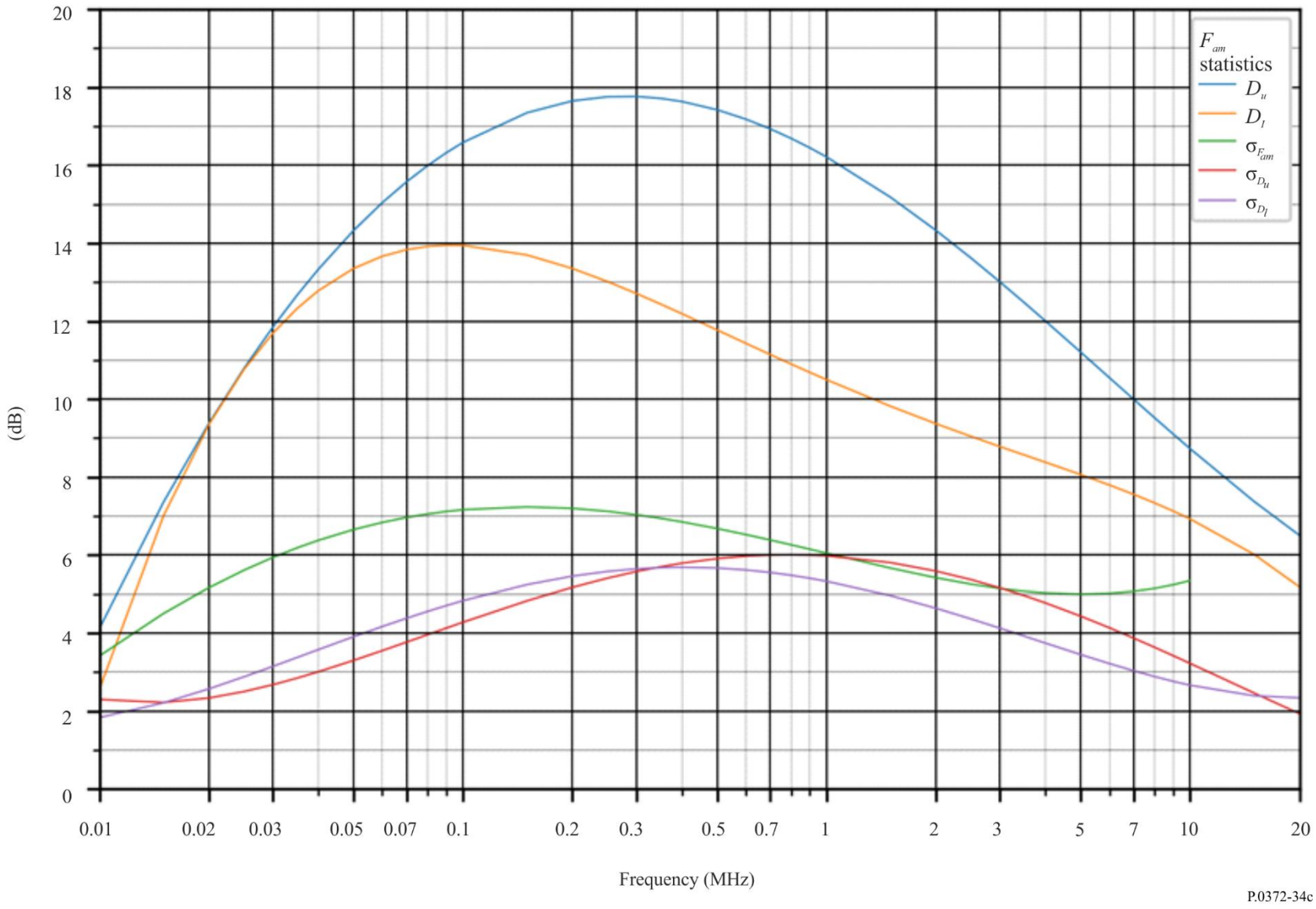

FIGURE 35a

Expected values of atmospheric radio noise, F_{am} (dB above kT_0b at 1 MHz) (Sep-Oct-Nov; 1600-2000 LT)

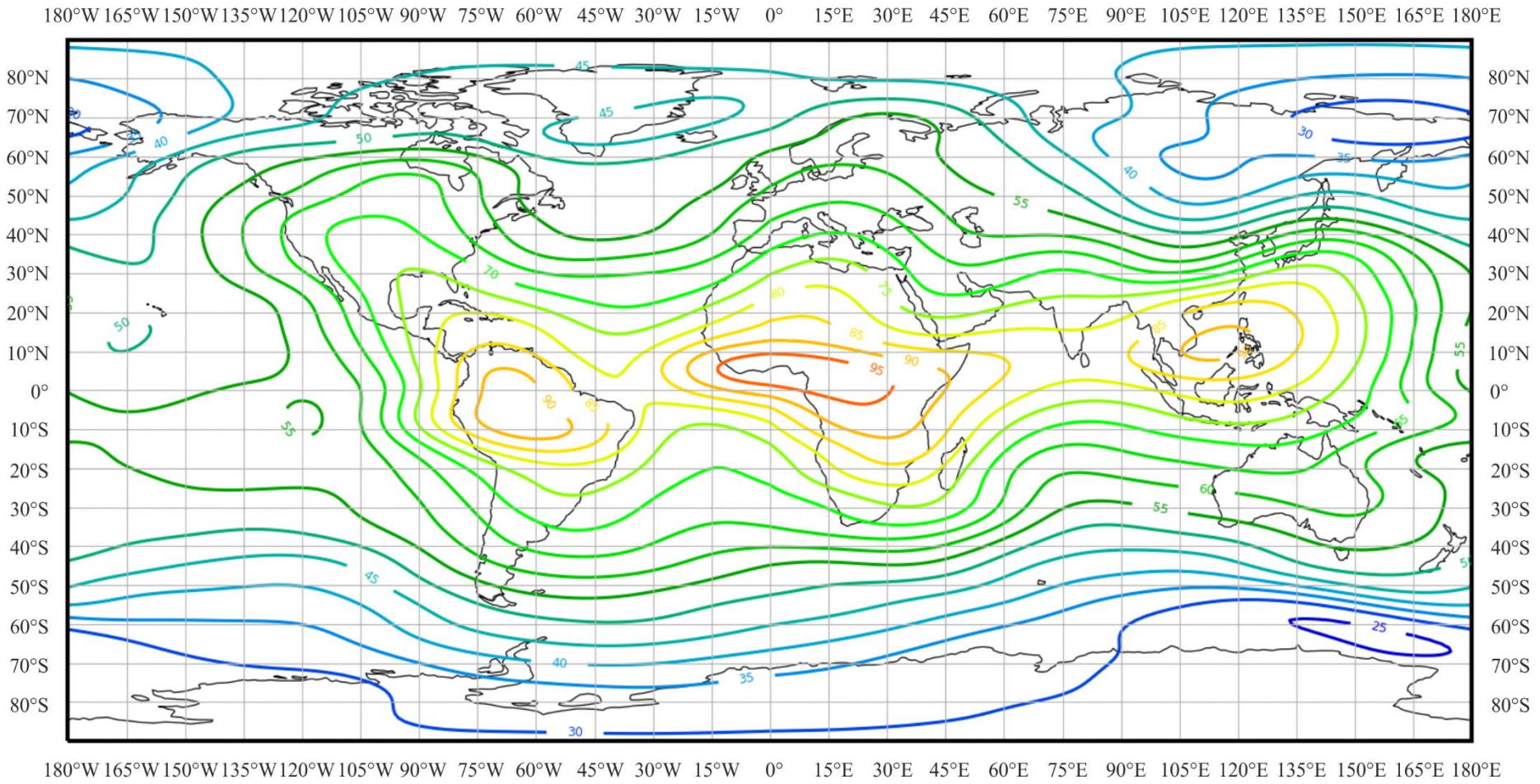

FIGURE 35b

Variation of radio noise with frequency (Northern hemisphere: Sep-Oct-Nov; Southern hemisphere: Mar-Apr-May; 1600-2000 LT)

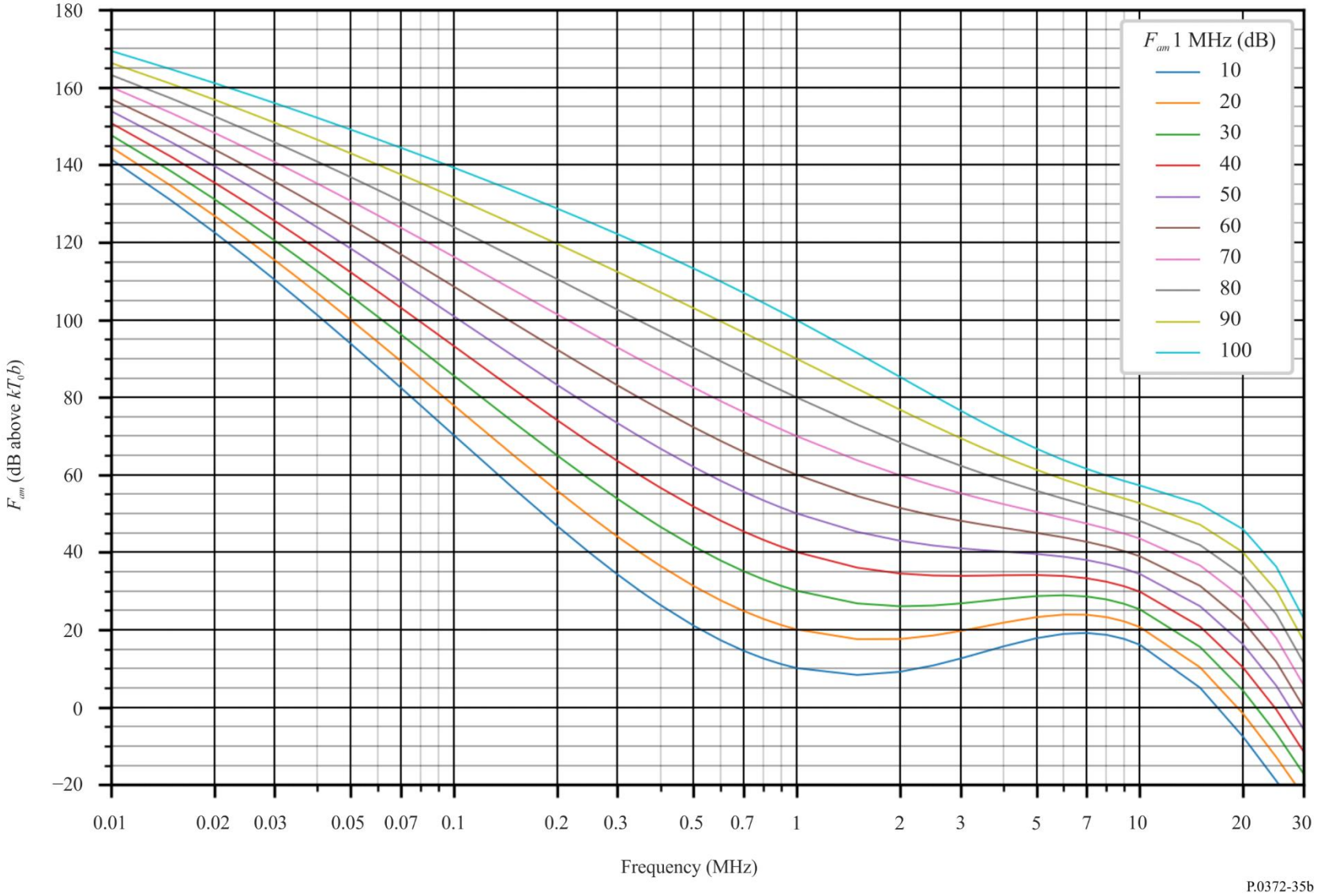

FIGURE 35c

Data on noise variability and character (Northern hemisphere: Sep-Oct-Nov; Southern hemisphere: Mar-Apr-May; 1600-2000 LT)

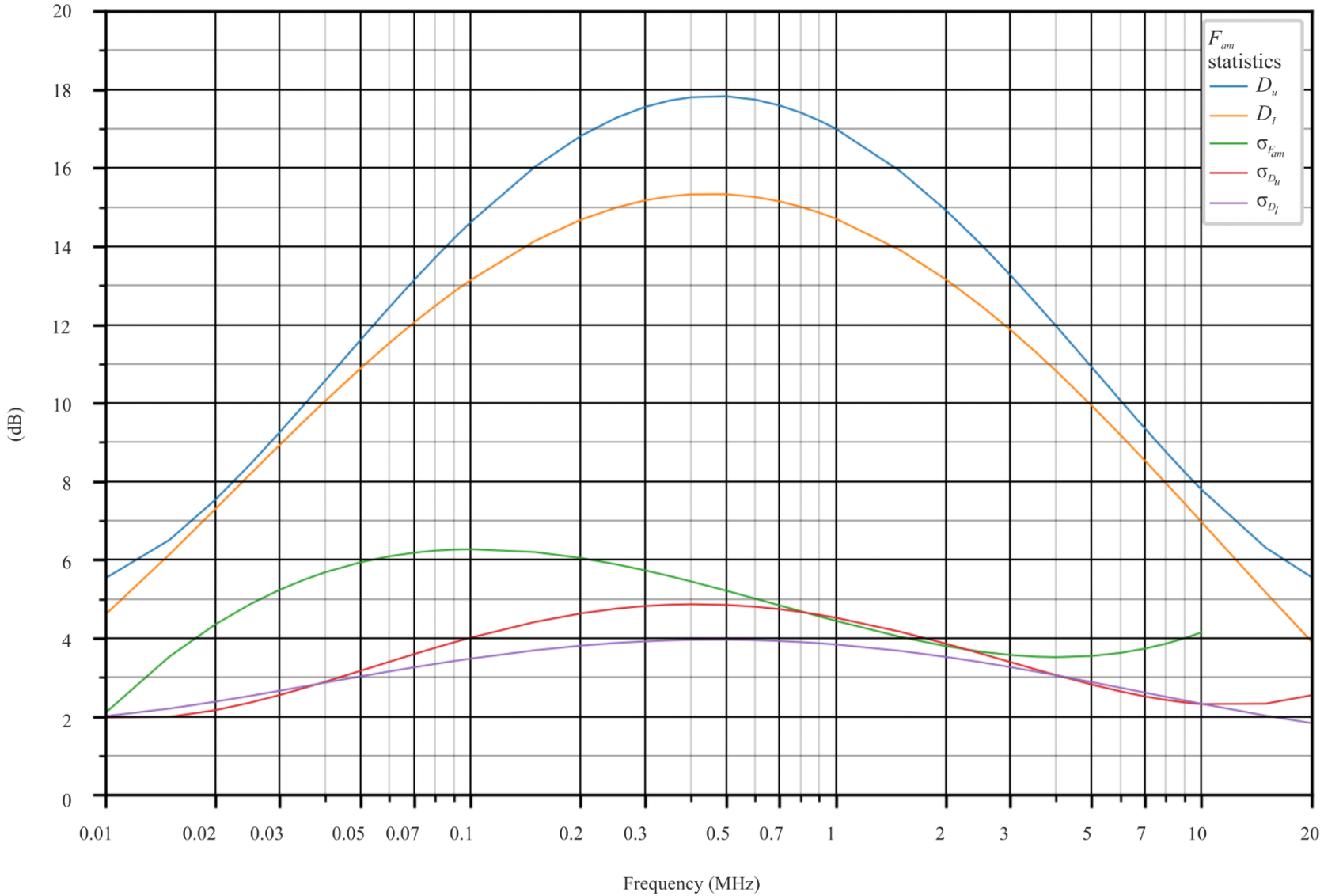

FIGURE 36a

Expected values of atmospheric radio noise, F_{am} (dB above kT_0b at 1 MHz) (Sep-Oct-Nov; 2000-2400 LT)

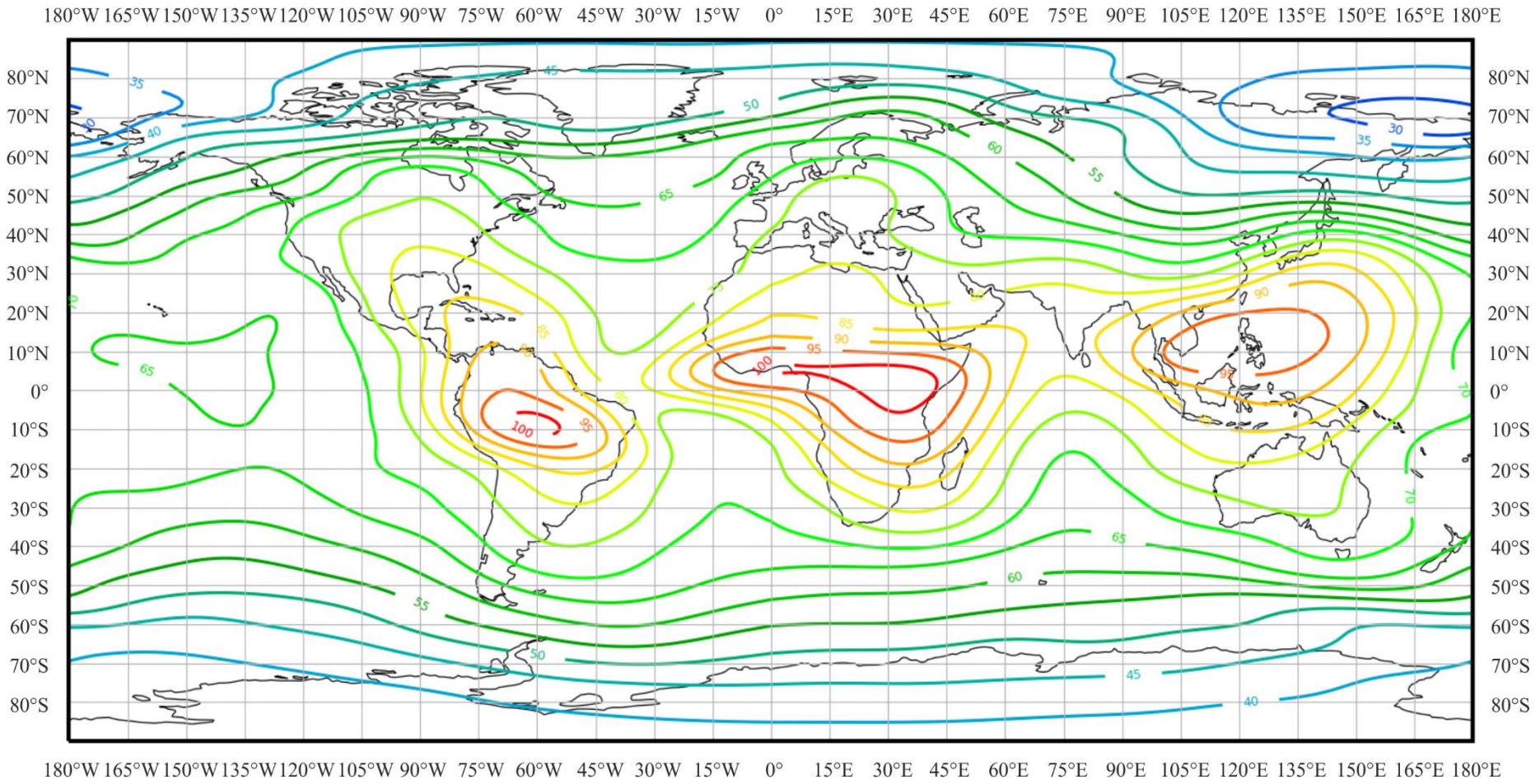

P.0372-36a

FIGURE 36b

Variation of radio noise with frequency (Northern hemisphere: Sep-Oct-Nov; Southern hemisphere: Mar-Apr-May; 2000-2400 LT)

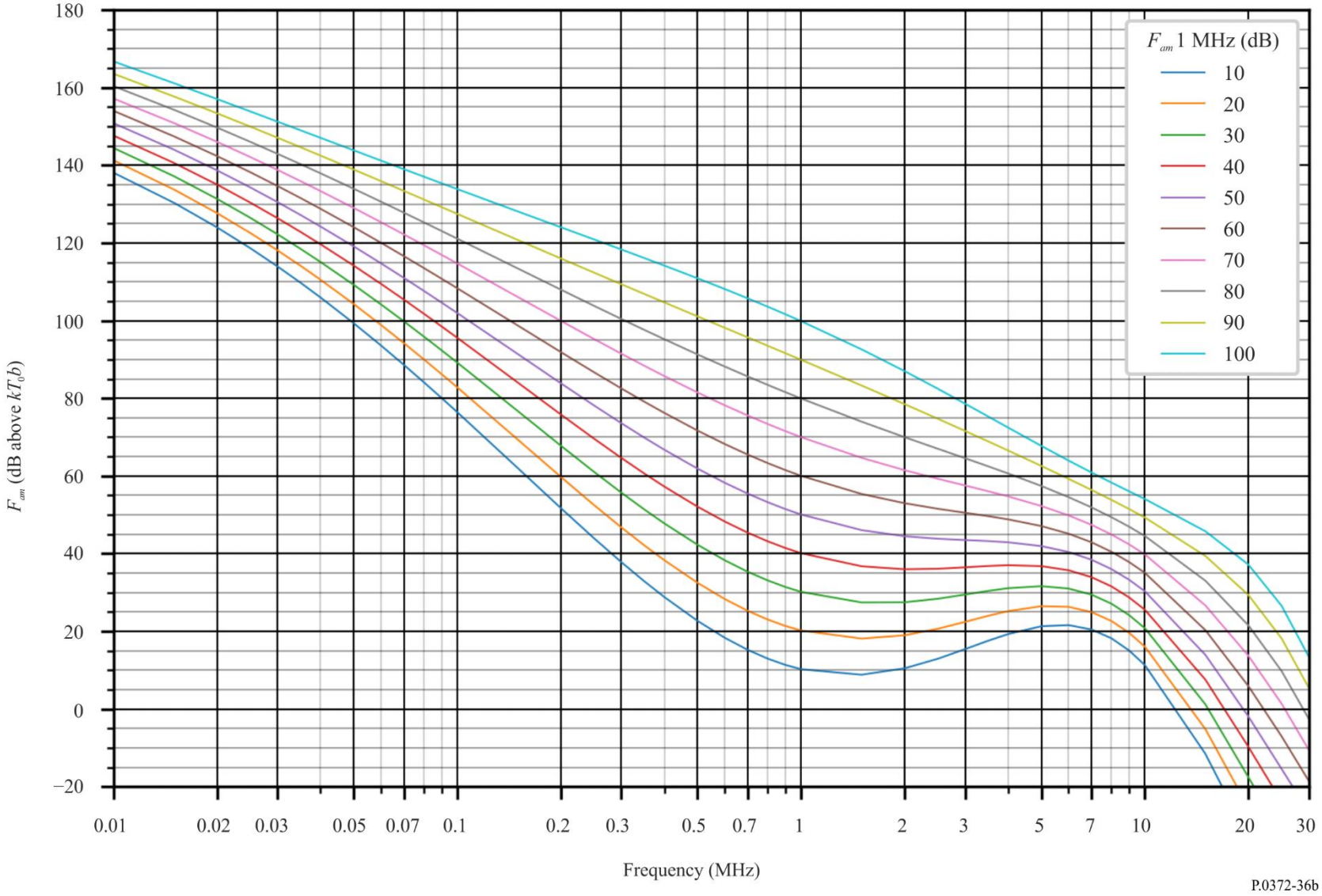

FIGURE 36c

Data on noise variability and character (Northern hemisphere: Sep-Oct-Nov; Southern hemisphere: Mar-Apr-May; 2000-2400 LT)

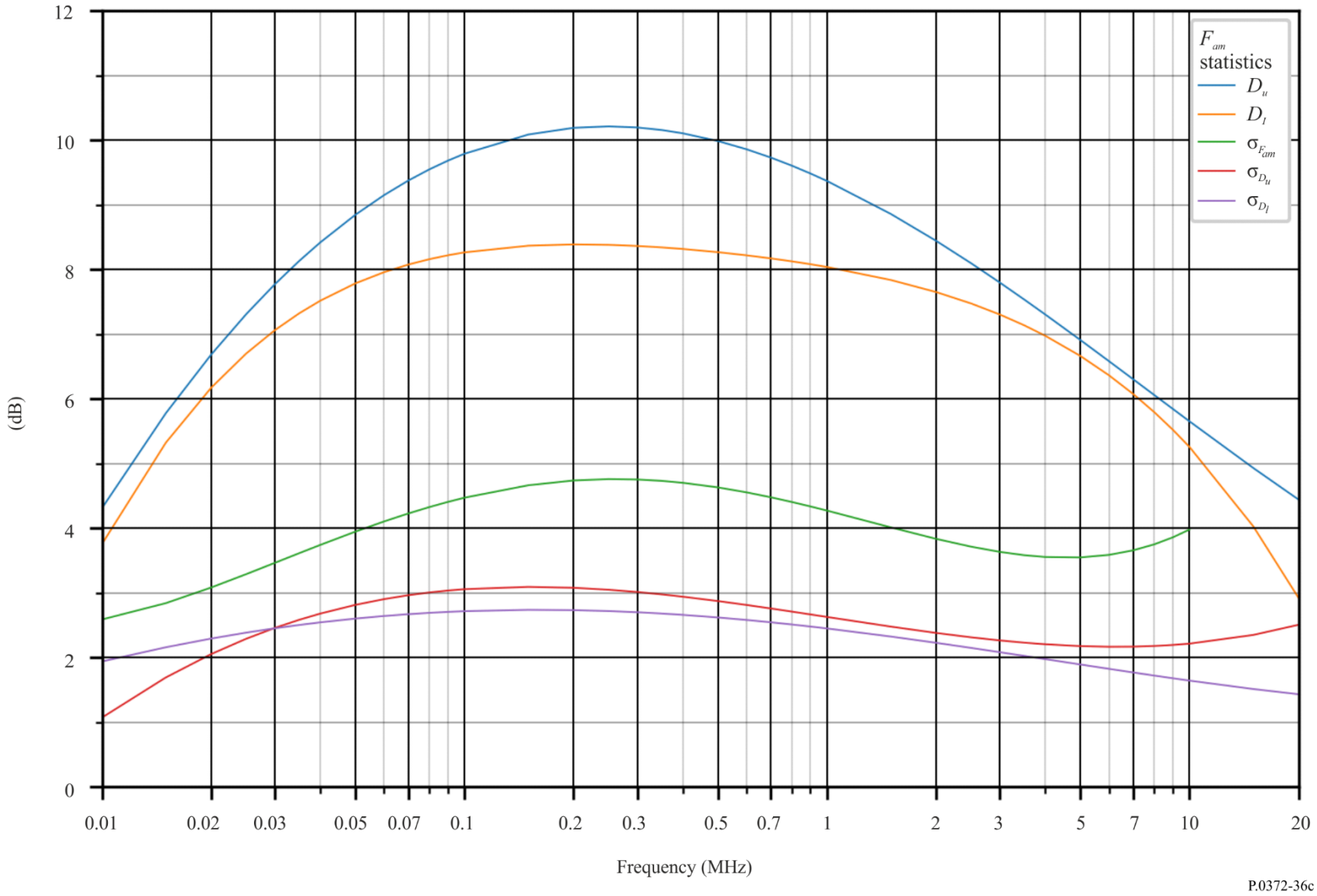

FIGURE 37

Amplitude probability distributions for atmospheric radio noise for various values of V_d

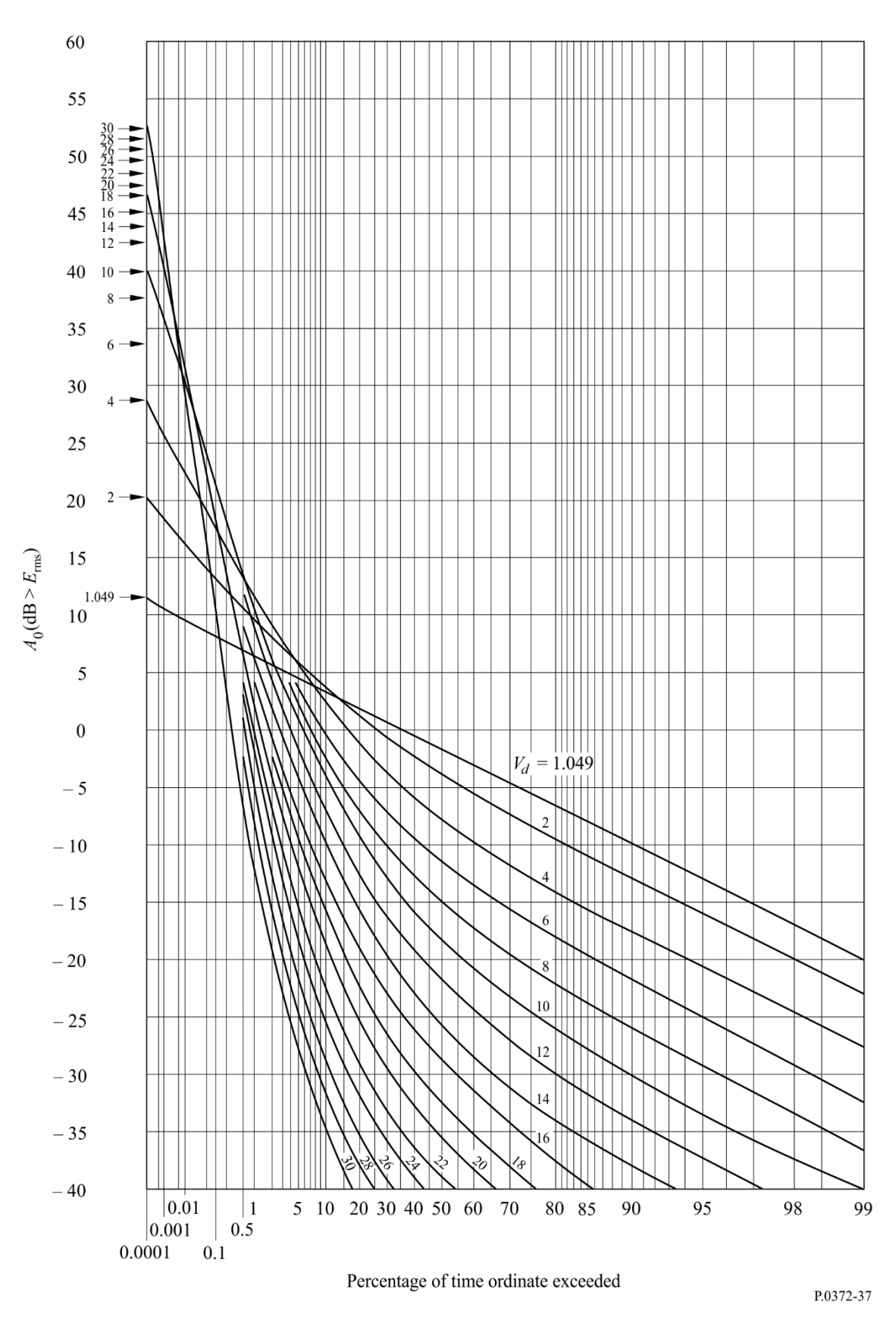

FIGURE 38

Translation of a 200 Hz bandwidth V_d, V_{dm}, to other bandwidths, b

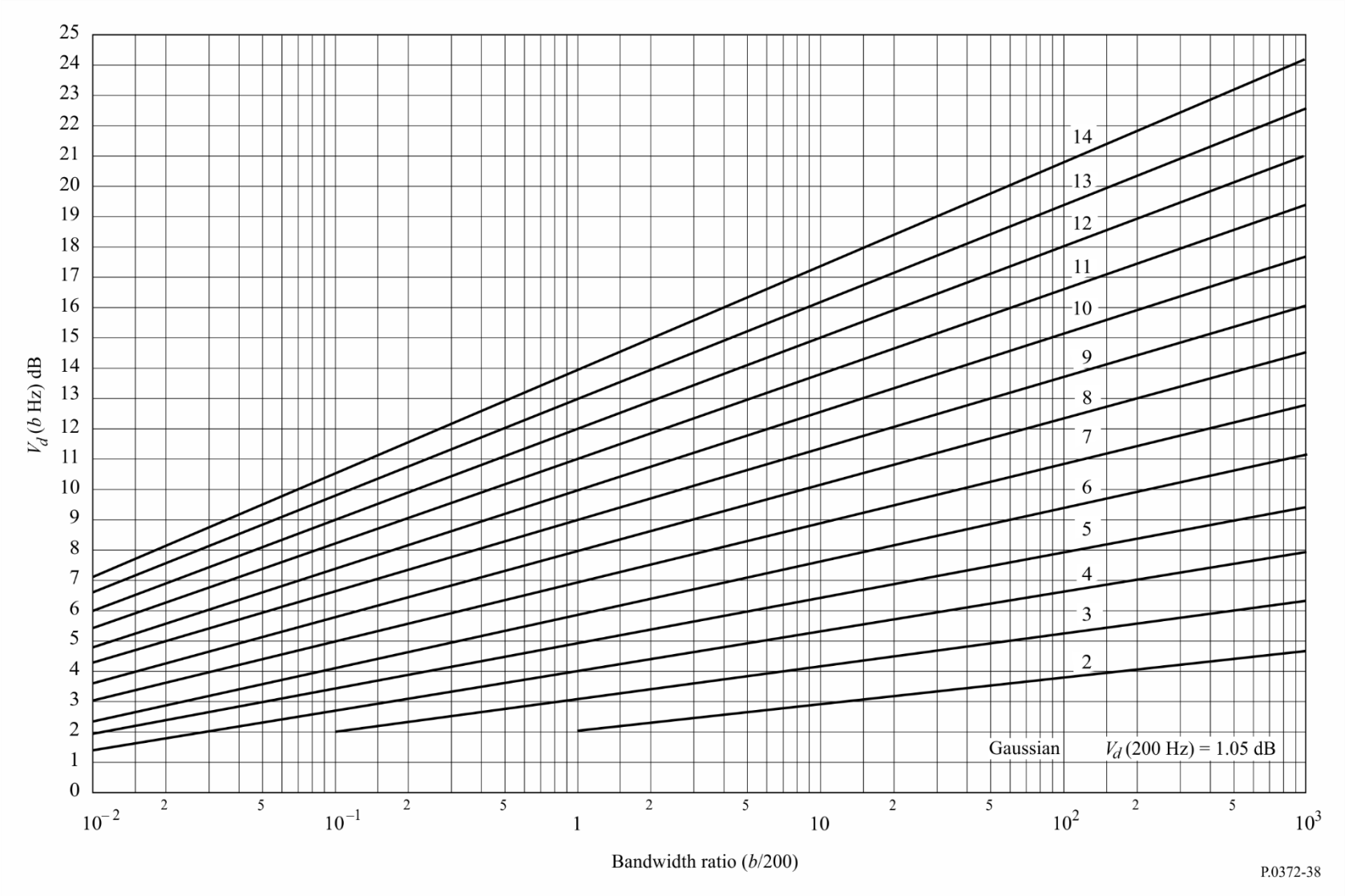

PART 6

Man-made noise

Man-made noise may consist of one of the following categories:

– Wideband noise of which the power spectral density is more or less flat over a large frequency range, with characteristics approaching additive white Gaussian noise (AWGN);

– Impulsive noise (IN);

– Noise that has a frequency dependent character, consisting of a single-carrier, a noisy 'hump' in the frequency spectrum, or a combination of multiple carriers and/or humps. For lack of a better name this type of noise has traditionally been indicated as 'single carrier noise' (SCN).

Observed man-made noise may also consist of a combination of all three categories. The dominance of one category depends on the intensity of the sources and their distance to the observer.

AWGN man-made noise may be observed when a large number of individual sources of comparable intensity and at sufficient distance of the receiver add up. SCN man-made noise indicates the presence of a single nearby source, or a limited number of them. While the former is more likely in an outdoor scenario, the latter is typical for an indoor noise environment.

Methods for the measurement and the representation of man-made noise are given in Recommendation ITU-R SM.1753 (outdoor) and Recommendation ITU-R SM.2093 (indoor).

6.1 Outdoor man-made noise

6.1.1 Additive white Gaussian noise

Median values of the AWGN man-made noise factor for a number of typical outdoor environments are shown in Fig. 39. The Figure also includes a curve for galactic noise (see Part 4).

In all cases results are consistent with a linear variation of the median value, F_{am}, expressed in dB, with frequency f of the form:

$$F_{am} = c - d \log f \quad (17)$$

With f expressed in MHz, c and d take the values given in Table 1. Note that equation (17) is valid in the range 0.3 to 250 MHz for all the environmental categories except those of curves D and E as indicated on the Figure. Man-made noise reflected by the ionosphere (curve D) is observed below the extraordinary-wave critical frequency of the ionosphere (fxF2), which depends on time-of-day, season and sunspot cycle. Above fxF2, the ionosphere gradually becomes transparent and galactic noise becomes dominant (curve E). Although ionosondes do not record fxF2, a proxy for fxF2 under stable ionospheric conditions is the spread F index fxI, which is the maximum F region reflection recorded by an ionosonde during a measurement.

For the business, residential and rural categories, the average over the above frequency range of the decile deviations of noise power with time, D_u and D_l, is given in Table 2. This Table also provides values of the deviation with location. It may be assumed that these variations are uncorrelated and that log-normal half distributions on each side of the median are appropriate.

TABLE 1

Values of the constants *c* and *d*

Environmental category	*c*	*d*
City (curve A)	76.8	27.7
Residential (curve B)	72.5	27.7
Rural (curve C)	67.2	27.7
Quiet rural (curve D)	53.6	28.6
Galactic noise (curve E)	52.0	23.0

TABLE 2

Values of decile deviations of man-made noise

Category	Decile	Variation with time (dB)	Variation with location (dB)
City	Upper Lower	11.0 6.7	8.4 8.4
Residential	Upper Lower	10.6 5.3	5.8 5.8
Rural	Upper Lower	9.2 4.6	6.8 6.8

FIGURE 39

Median values of man-made noise power for a short vertical lossless grounded monopole antenna

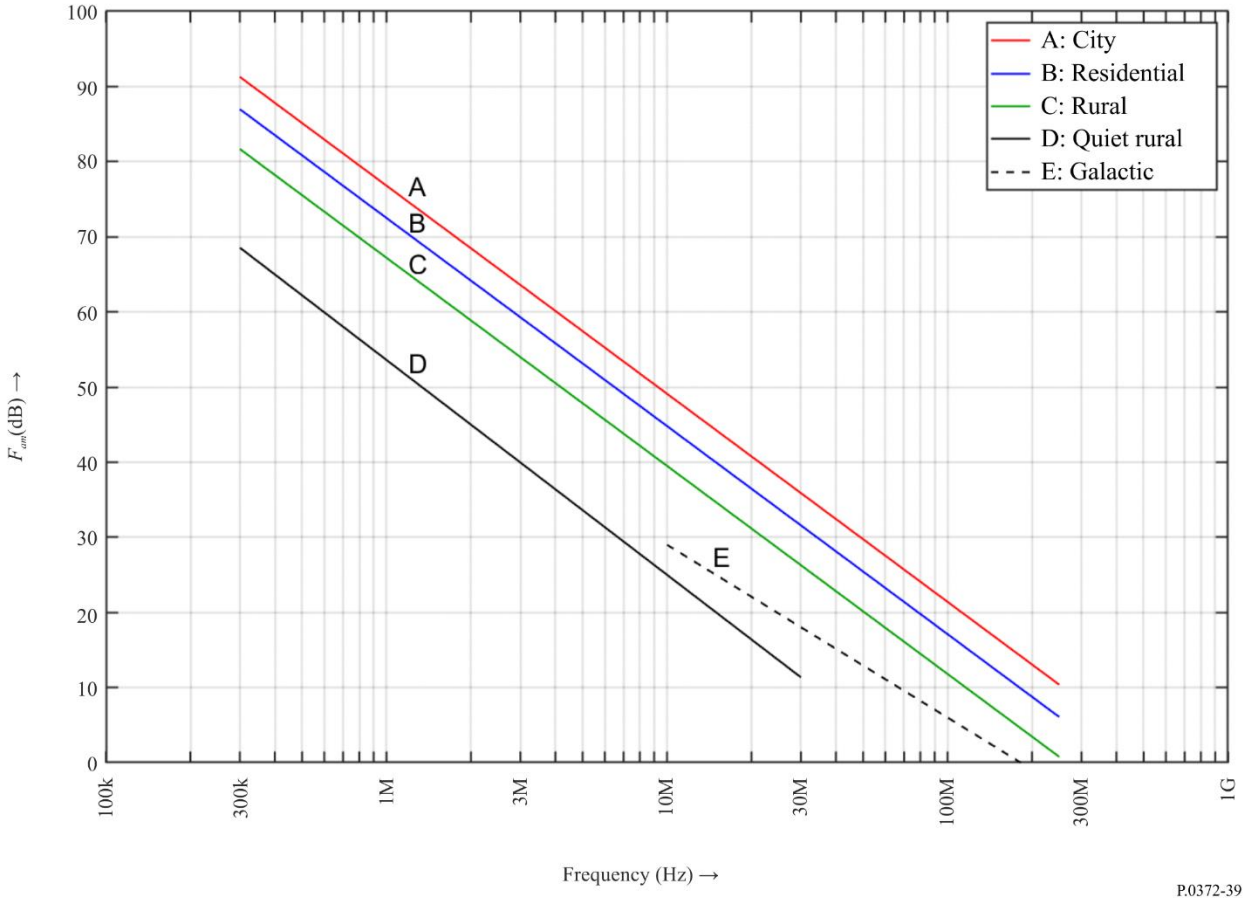

6.2 Indoor man-made noise

6.2.1 Additive white Gaussian noise

At present, insufficient measurement data are available to describe the expected levels of indoor AWGN man-made noise. This section will be updated when such data become available. Table 3 contains measurements in Europe between 2005 and 2007.

TABLE 3

Indoor man-made noise measurements in Europe

Frequency (MHz)	Median noise figure F_a (dB rel kT_0b)		Upper decile deviation		Lower decile deviation	
	City	Residential	City	Residential	City	Residential
210	14	5	3	3	2	1
425	16	3	4	1	1	1

PART 7

The combination of noises from several sources

7.1 The combination of noises from several sources

There are occasions where more than one type of noise needs to be considered because two or more types are of comparable amplitude. This can be true at any frequency, in general, but occurs most often at HF where atmospheric, man-made and galactic noise can be of comparable size (Fig. 2, 10 MHz, for example).

The noise figures for each of the noise sources defined above, F_a (dB) are assumed to have a distribution represented by two half-normal distributions on each side of the median value, F_{am}. The lower half-normal distribution has a standard deviation, $\sigma_l = D_l/1.282$, below the median and the upper half-normal distribution has a standard deviation, $\sigma_u = D_u/1.282$, above the median. The corresponding noise factors, f_a (W), have log-normal distributions on each side of the median.

The median, F_{amT}, and standard deviation, σ_T , of the noise figure for the sum of two or more noise processes are given by:

$$F_{amT} = c\left[\ln(\alpha_T) - \frac{\sigma_T^2}{2c^2}\right] \quad \text{dB} \tag{18}$$

$$\sigma_T = c\sqrt{\ln\left(1 + \frac{\beta_T}{\alpha_T^2}\right)} \quad \text{dB} \tag{19}$$

where:

$$c = 10/\ln(10) = 4.343 \tag{20}$$

$$\alpha_T = \sum_{i=1}^{n}\alpha_i = \sum_{i=1}^{n}\exp\left[\frac{F_{ami}}{c} + \frac{\sigma_i^2}{2c^2}\right] \quad \text{W} \tag{21}$$

$$\beta_T = \sum_{i=1}^{n}\alpha_i^2\left[\exp\left(\frac{\sigma_i^2}{c^2}\right) - 1\right] \quad \text{W}^2 \tag{22}$$

and F_{ami} and σ_i are the median and standard deviation of the noise figures for the component noise sources. For atmospheric noise, these are extracted from Figs 13 to 36. Man-made noise may also be extracted from Fig. 10 and Table 2. For galactic noise, F_{am} is given by equation (15) and σ_i is set at 1.56 dB (= 2/1.282).

The upper decile deviation, D_{uT}, of the noise figure for the sum of two or more noise processes is given by:

$$D_{uT} = 1.282\ \sigma_T \quad \text{dB} \tag{23}$$

where σ_T is calculated by using the upper decile deviations of the noise components to compute the σ_i (= $D_u/1.282$) in equations (21) and (22).

The lower decile deviation, D_{lT}, of the noise figure for the sum of two or more noise processes is given by:

$$D_{lT} = 1.282\ \sigma_T \quad \text{dB} \tag{24}$$

where σ_T is calculated by using the lower decile deviations of the noise components to compute the σ_i (= D_l/1.282) in equations (21) and (22).

When an upper decile deviation of the noise figure for at least one noise component exceeds 12 dB, the σ_T calculated by equations (19) to (22), using the upper decile deviations of the noise components, should be restricted to a maximum value of:

$$\sigma_T = c\sqrt{2\ln\left(\frac{\alpha_T}{\gamma_T}\right)} \quad \text{dB} \tag{25}$$

where γ_T is the noise factor for the simple power sum of the individual median noise factors:

$$\gamma_T = \sum_{i=1}^{n} \exp\left(\frac{F_{ami}}{c}\right) \quad \text{W} \tag{26}$$

Similarly, when a lower decile deviation of the noise figure for at least one noise component exceeds 12 dB, the σ_T calculated by equations (19) to (22), using the lower decile deviations of the noise components, should be restricted to the maximum value given by equation (25).